

11-3-2008

Quantifying the effects of temperature and concentration on variable-density flow in numerical modeling of groundwater systems : implications for predictive uncertainty and data collection

Alyssa Marie Dausman
Florida International University

DOI: 10.25148/etd.FI14062206

Follow this and additional works at: <https://digitalcommons.fiu.edu/etd>

 Part of the [Geology Commons](#)

Recommended Citation

Dausman, Alyssa Marie, "Quantifying the effects of temperature and concentration on variable-density flow in numerical modeling of groundwater systems : implications for predictive uncertainty and data collection" (2008). *FIU Electronic Theses and Dissertations*. 2740.

<https://digitalcommons.fiu.edu/etd/2740>

This work is brought to you for free and open access by the University Graduate School at FIU Digital Commons. It has been accepted for inclusion in FIU Electronic Theses and Dissertations by an authorized administrator of FIU Digital Commons. For more information, please contact dcc@fiu.edu.

FLORIDA INTERNATIONAL UNIVERSITY

Miami, Florida

QUANTIFYING THE EFFECTS OF TEMPERATURE AND CONCENTRATION ON
VARIABLE-DENSITY FLOW IN NUMERICAL MODELING OF GROUNDWATER
SYSTEMS: IMPLICATIONS FOR PREDICTIVE UNCERTAINTY AND DATA
COLLECTION

A dissertation submitted in partial fulfillment of the

requirements for the degree of

DOCTOR OF PHILOSOPHY

in

GEOSCIENCES

by

Alyssa Marie Dausman

2008

To: Dean Kenneth Furton
College of Arts and Sciences

This dissertation, written by Alyssa Marie Dausman, and entitled Quantifying the Effects of Temperature and Concentration on Variable-Density Flow in Numerical Modeling of Groundwater Systems: Implications for Predictive Uncertainty and Data Collection, having been approved in respect to style and intellectual content, is referred to you for judgment.

We have read this dissertation and recommend that it be approved.

Christian Langevin

René M. Price

William T. Anderson

Fernando Miralles-Wilhelm

Michael C. Sukop, Major Professor

Date of Defense: November 3, 2008

The dissertation of Alyssa Marie Dausman is approved.

Dean Kenneth Furton
College of Arts and Sciences

Dean George Walker
University Graduate School

Florida International University, 2008

© Copyright 2008 by Alyssa Marie Dausman

All rights reserved.

DEDICATION

I dedicate this work to my late grandmother, Sylvia Marie Dausman; to my parents, Bob and Ree; my brothers, David and Jason; and my son, Max. Their love and support has enabled me to complete this work.

ACKNOWLEDGMENTS

I would first like to acknowledge my committee members: Christian Langevin, René M. Price, William T. Anderson, Fernando Miralles-Wilhelm, and Michael McClain for their support in my pursuit of this PhD and help and guidance for this dissertation. I would like to give a special thanks to my advisor, Michael C. Sukop; without his help, patience, support, and criticism, this work would not have been possible. He has encouraged me to become a better student, researcher, worker, and person through my education. I also want to thank Florida International University (FIU) and the Department of Earth Sciences for accepting me as a PhD student, even though I have worked full time throughout my education at FIU.

Gratitude is also extended to the scientists who provided me data that was used in parts of this dissertation, including René Price and Jeremy Stalker from FIU, as well as Hector Casanova from FIU and the National Oceanographic and Atmospheric Association (NOAA). Chris Reich and Michael Burns from the U.S. Geological Survey (USGS) were also kind enough to provide me data that aided in my research. I also want to thank USGS employees in the Fort Lauderdale office that aided me in my fourteen month data collection effort. The data was used to calibrate one of the many models developed as part of this research.

I also want to acknowledge the USGS for the financial and professional support in my pursuit of a higher education. Particularly, Barbara Howie and Robert Renken, my supervisors at the USGS who provided me the flexibility I needed to work full time and go to school simultaneously. I also want to acknowledge Chris Langevin, my coworker and colleague at the USGS, my committee member, and most importantly, my friend.

Without his support, I never would have pursued a PhD or finished this dissertation. He has suffered through sharing an office wall with me for eight years while providing me guidance on a daily basis. He has believed in me when I didn't believe in myself, and continued to believe in me until I did.

I also want to recognize my colleagues, fellow students, and friends, Virginia Walsh and Mary Wright. These two women have provided me technical guidance, emotional support, and friendship through the pursuit of this degree. I am indebted to them and I hope to provide them the same support as they pursue their degrees.

I am obliged to my advisor from my M.S. degree at the University of New Orleans, Dale Easley. He was the first person to introduce me to the world of numerical modeling, which has become one of my greatest passions in life. When I started school beneath him 11 years ago, I had no idea that his initial guidance would lead me to the place I am today.

Last, but not least, I owe John Doherty of Watermark Numerical Computing more than can be put into words. Without his brilliant knowledge, guidance, and support, I wouldn't have finished this research or dissertation. Even though my command of the English language has suffered beneath him, my knowledge of modeling highly parameterized systems and predictive uncertainty has increased 10-fold.

ABSTRACT OF THE DISSERTATION

QUANTIFYING THE EFFECTS OF TEMPERATURE AND CONCENTRATION ON
VARIABLE-DENSITY FLOW IN NUMERICAL MODELING OF GROUNDWATER
SYSTEMS: IMPLICATIONS FOR PREDICTIVE UNCERTAINTY AND DATA
COLLECTION

by

Alyssa Marie Dausman

Florida International University, 2008

Miami, Florida

Professor Michael C. Sukop, Major Professor

Groundwater systems of different densities are often mathematically modeled to understand and predict environmental behavior such as seawater intrusion or submarine groundwater discharge. Additional data collection may be justified if it will cost-effectively aid in reducing the uncertainty of a model's prediction. The collection of salinity, as well as, temperature data could aid in reducing predictive uncertainty in a variable-density model. However, before numerical models can be created, rigorous testing of the modeling code needs to be completed. This research documents the benchmark testing of a new modeling code, SEAWAT Version 4. The benchmark problems include various combinations of density-dependent flow resulting from variations in concentration and temperature. The verified code, SEAWAT, was then applied to two different hydrological analyses to explore the capacity of a variable-density model to guide data collection.

The first analysis tested a linear method to guide data collection by quantifying the contribution of different data types and locations toward reducing predictive uncertainty in a nonlinear variable-density flow and transport model. The relative contributions of temperature and concentration measurements, at different locations within a simulated carbonate platform, for predicting movement of the saltwater interface were assessed. Results from the method showed that concentration data had greater worth than temperature data in reducing predictive uncertainty in this case. Results also indicated that a linear method could be used to quantify data worth in a nonlinear model.

The second hydrological analysis utilized a model to identify the transient response of the salinity, temperature, age, and amount of submarine groundwater discharge to changes in tidal ocean stage, seasonal temperature variations, and different types of geology. The model was compared to multiple kinds of data to (1) calibrate and verify the model, and (2) explore the potential for the model to be used to guide the collection of data using techniques such as electromagnetic resistivity, thermal imagery, and seepage meters. Results indicated that the model can be used to give insight to submarine groundwater discharge and be used to guide data collection.

TABLE OF CONTENTS

CHAPTER	PAGE
1	Introduction..... 1
1.1	Preface..... 1
1.2	Problem..... 2
1.3	Objectives 6
1.4	Scientific Contributions of this Dissertation..... 7
1.4.1	Benchmarking the new variable-density flow and transport code SEAWAT Version 4 8
1.4.2	Utilizing a linear method to quantify the worth of salinity and temperature data in a nonlinear variable-density model 9
1.4.3	Utilizing a variable-density flow and transport model to guide data collection by quantifying temperature, salinity, and age of submarine groundwater discharge 9
1.5	Governing equations applied in this dissertation and utilized in SEAWAT Version 4..... 10
1.5.1	Solute and Heat Transport 11
1.5.2	Variable-Density Flow..... 13
1.5.3	Effects of Viscosity..... 15
1.5.4	Simulation of Age..... 16
2	Six benchmark problems for testing heat and solute transport using Seawat Version 4..... 17
2.1	Introduction..... 17
2.2	Dimensionless Numbers 22
2.2.1	Rayleigh Number 25
2.2.2	Darcy Number..... 29
2.2.3	Prandtl Number..... 30
2.2.4	Nusselt Number 31
2.3	Benchmark Problems..... 32
2.3.1	One-Dimensional Flow with Linearly Varying Viscosity Field..... 33
2.3.1.1	Results and Discussion..... 36
2.3.2	Two-Dimensional Oil Convection in Aluminum Foam 37
2.3.2.1	Results and Discussion..... 44
2.3.3	Horton-Rogers-Lapwood (HRL) Convection..... 48
2.3.3.1	Results and Discussion..... 53
2.3.4	Double-Diffusive Finger Convection 55
2.3.4.1	Results and Discussion..... 60
2.3.5	Elder Problem 61
2.3.5.1	Results and Discussion..... 64
2.3.6	Henry-Hilleke 67
2.3.6.1	Results and Discussion..... 71
2.4	Chapter Summary and Conclusions..... 73

3	Quantifying data contributions toward reducing predictive uncertainty in a variable-density flow and solute/heat transport model	75
3.1	Introduction.....	75
3.2	Theory.....	83
3.3	Model Development.....	87
3.3.1	Model Parameterization	89
3.3.2	Observations and Predictions.....	92
3.3.3	Covariance Matrices	93
3.4	Application.....	94
3.4.1	Testing the Effects of Nonlinearity.....	95
3.5	Results and Discussion	97
3.6	Conclusions, Limitations, and Future work.....	103
4	Simulation of submarine groundwater discharge salinity and temperature variations: Implications for data collection.....	108
4.1	Introduction.....	108
4.2	Methods.....	113
4.2.1	Continuous Water-Level and Salinity Data Collection	113
4.2.2	Three-Dimensional Model	115
4.2.3	Two-Dimensional Model	120
4.2.4	Data Collection of Submarine Groundwater Discharge Used to Test Two-Dimensional Model	123
4.3	Results.....	124
4.3.1	Data Collection and Three-Dimensional Model.....	124
4.3.2	Two-Dimensional Model	128
4.3.2.1	Discharge	129
4.3.2.2	Salinity	132
4.3.2.3	Temperature	135
4.3.2.4	Apparent Age	140
4.4	Discussion.....	143
4.4.1	Model Calibration	143
4.4.2	Implications for Data Collection.....	144
4.4.3	Implications for SGD Residence Times and Potential Nutrient Transport	148
4.5	Chapter Summary and Conclusions.....	149
5	Summary and Conclusions.....	150
5.1	Benchmarking of SEAWAT Version 4	151
5.2	Using a linear method to quantify the worth of salinity and temperature data in a nonlinear variable-density model.....	152
5.3	Simulation of submarine groundwater discharge salinity and temperature variations: Implications for data collection	154
	List of References	158
	VITA.....	171

LIST OF TABLES

TABLE	PAGE
Table 1: Identification of variables. L=Length, T=Time, M=Mass, D=Degrees of Temperature.	24
Table 2: Input parameters for problem simulating temperature-dependent viscosity of oil in aluminum foam.	39
Table 3: Input parameters for the Horton-Rogers-Lapwood problem simulated in SEAWAT.	51
Table 4: SEAWAT input parameters for the Hele-Shaw simulation.	59
Table 5: Input parameters for the Elder problem simulated in SEAWAT.	62
Table 6: Input parameters for the Henry-Hilleke problem simulated in SEAWAT.	69
Table 7: Input parameters for the Henry-Hilleke problem.	88
Table 8: Values used to calculate the standard deviation for the parameters used in the predictive uncertainty exercise. The * denotes model parameters that vary spatially.	94
Table 9: Aquifer parameters used in the variable-density 2-D cross-sectional model.	119
Table 10: Approximate amplitude of the tidal fluctuations observed in measured and simulated salinity and water-level data from selected continuous monitoring wells.	128

LIST OF FIGURES

FIGURE	PAGE
<p>Figure 1: Graphs showing the relationships between temperature and salinity effects on density and viscosity published in the literature. (A) Temperature affects on the density of freshwater from five different formulae in the literature. (B) Temperature affects on the dynamic viscosity of freshwater from two published formulae in the literature. (C) Salinity affects on density of water at 20 °C from two published formulae in the literature. (D) Salinity affects on dynamic viscosity of water at 20 °C from two different formulae published in the literature.....</p>	4
<p>Figure 2: Diagram showing map view of model design in SEAWAT.....</p>	36
<p>Figure 3: Results of water-level values with distance in each of the SEAWAT models and the analytical solution.....</p>	37
<p>Figure 4: Schematic diagram for problem simulating temperature-dependent viscosity of oil in aluminum foam.....</p>	39
<p>Figure 5: Graph showing the change in viscosity with temperature according to equation (28) (oil, in black) and equation (29) (water, in pink).....</p>	41
<p>Figure 6: Streamline results for both variable viscosity and constant viscosity (gray/black streamlines) cases from Guo and Zhao (2005) compared with resulting streamlines from SEAWAT (blue streamlines). (a) Results with Darcy numbers of 10^{-4} and Rayleigh* numbers of 10, (b) results with Darcy numbers of 10^{-4} and Rayleigh* numbers of 100, and (c) results with Darcy numbers of 10^{-4} and Rayleigh* numbers of 1000.....</p>	46
<p>Figure 7: Temperature isotherms for both variable viscosity and constant viscosity cases from Guo and Zhao (2005, in gray/black and white) compared with temperature isotherms from SEAWAT (in color). (a) Results with Darcy numbers of 10^{-4} and Rayleigh* numbers of 10, (b) results with Darcy numbers of 10^{-4} and Rayleigh* numbers of 100, and (c) results with Darcy numbers of 10^{-4} and Rayleigh* numbers of 1000.....</p>	47
<p>Figure 8: Simple design of Horton-Rogers-Lapwood benchmark problems where the length of the box is 2 times (or 4 times) the height.....</p>	50
<p>Figure 9: Design of the Horton-Rogers-Lapwood problem in SEAWAT. The colors from blue to red show the initial temperatures for the simulations from 0 °C in blue to 100 °C in red. Height, length, and boundary conditions are also displayed.....</p>	51

Figure 10: Temperature results for the Horton-Rogers-Lapwood convection problem simulated with SEAWAT. (A) Simulation with $Ra^{**}=39$, (B) Simulation with $Ra^{**}=40$, and (C) Simulation with $Ra^{**}=200$. The colors from blue to red show the temperatures for the simulations from 0 °C in blue to 100 °C in red.....	53
Figure 11: Velocity vectors for the second simulation of the Horton-Rogers-Lapwood problem where $Ra^{**}=40$	54
Figure 12: Hele-Shaw cell set up by Pringle and others (2002). Note that the angle of the Hele-Shaw cell from the vertical is the reason that gravity in the simulation is set to 4.14 m/s^2	57
Figure 13: Initial conditions in the Hele-Shaw cell, length and height in meters.....	57
Figure 14: Results from Pringle and others (2002) at (a) $t^*=4.06 \times 10^{-5}$, (b) $t^*=1.29 \times 10^{-4}$, (c) $t^*=3.96 \times 10^{-4}$, (d) $t^*=3.35 \times 10^{-4}$, (e) $t^*=4.35 \times 10^{-4}$, (f) $t^*=5.36 \times 10^{-4}$, (g) $t^*=6.03 \times 10^{-4}$, (h) $t^*=7.37 \times 10^{-4}$, (i) $t^*=8.04 \times 10^{-4}$, (j) $t^*=1.04 \times 10^{-3}$, (k) $t^*=1.78 \times 10^{-3}$, and (l) $t^*=3.19 \times 10^{-3}$. Color sequence is relative concentration of the dye (representative of the NaCl solution).	58
Figure 15: Results from SEAWAT at (a) $t^*=4.06 \times 10^{-5}$, (b) $t^*=1.29 \times 10^{-4}$, (c) $t^*=3.96 \times 10^{-4}$, (d) $t^*=3.35 \times 10^{-4}$, (e) $t^*=4.35 \times 10^{-4}$, (f) $t^*=5.36 \times 10^{-4}$, (g) $t^*=6.03 \times 10^{-4}$, (h) $t^*=7.37 \times 10^{-4}$, (i) $t^*=8.04 \times 10^{-4}$, (j) $t^*=1.04 \times 10^{-3}$, (k) $t^*=1.78 \times 10^{-3}$, and (l) $t^*=3.19 \times 10^{-3}$. Color sequence is relative concentration of the dye (representative of the NaCl solution).	61
Figure 16: Set-up of Elder’s original experiment that is simulated in SEAWAT. The constant-head cells at the bottom left and right-hand side are used in the numerical simulation but do not exist in Elder's original laboratory set-up. NOTE: The height of the model, 150 m, is a measurement of the “active” model domain. The low hydraulic conductivity upper and lower boundaries are not included in the measurement of height, nor are they part of the calculation of the Ra^{**} number.	62
Figure 17: Results of SEAWAT Version 4 compared to the original lab results from Elder, SUTRA (rotated), and an older version of SEAWAT (rotated) (Figure modified from Guo and Langevin, 2002).....	66
Figure 18: The Nusselt number versus time showing the heat flux across the bottom boundary in SEAWAT in black. This is compared to the concentration flux across the top boundary (in the inverted Elder problem) simulated using SUTRA from Prasad and Simmons (2003) in red, and the heat flux across the bottom boundary from the original Elder problem in blue (Elder, 1967).....	67

Figure 19: Set-up of the Henry-Hilleke problem showing the boundary conditions that include: (1) freshwater input, (2) seawater boundary, and (3) temperature boundaries. NOTE: Horizontal scale is exaggerated for comparison with other modeling results.	69
Figure 20: One meter by one meter box showing resulting percent seawater concentrations from (A) SUTRA-MS in color with the solid black lines, Henry and Hilleke numerical solution shown as the 50% contour in the solid red line, and HST3D results shown as the dashed black line (Hughes and Sanford, 2004), and (B) SEAWAT in color with the solid black lines. NOTE: Horizontal scale is exaggerated.	72
Figure 21: One meter by one meter box showing resulting temperatures in degrees Celsius from (A) SUTRA-MS in color with the solid black lines, Henry and Hilleke numerical solution shown as the 27.5 °C contour in the solid red line, and HST3D results shown as the dashed black line (Hughes and Sanford, 2004), and (B) SEAWAT in color with solid black lines. NOTE: Horizontal scale is exaggerated.	72
Figure 22: One meter by one meter box showing resulting velocity vectors for (A) SUTRA-MS (Hughes and Sanford, 2004), and (B) SEAWAT.	73
Figure 23: Floridan Plateau where the Peninsula of Florida is on the eastern part of the plateau (from USGS CMG InfoBank Atlas: Florida EEA regions).	76
Figure 24: Kohout’s conceptualization of convective flow in the Floridan Aquifer (from Kohout, 1965).	76
Figure 25: Set up of the Henry-Hilleke problem showing boundary conditions that include: (1) freshwater input, (2) seawater boundary, and (3) temperature boundaries.	88
Figure 26: Henry-Hilleke problem (a) salinity contour results, 0 kg/m ³ in light gray to 35.7 kg/m ³ in dark gray. Simulated observations: black triangles. Predictions: black squares (labeled 1-6). (b) Temperature contour results from 5 °C in light gray to 50 °C in dark gray. Predictions: white/black squares.	90
Figure 27: Figure showing model domain with pilot points that represent spatially varying parameters.	91
Figure 28: Results from the Henry-Hilleke problem contouring the change in variance of the predictive uncertainty for (a) prediction 2 for the concentration observations (the dashed dark line is 50% seawater), (b) prediction 2 for the temperature observations, (c) prediction 3 for the concentration observations, and (d) prediction 3 for the temperature observations.	98

Figure 29: Contours of change in variance (calculated from equation (40)) of the predictive uncertainty for predictions 2 and 3 in the black contour lines for both salinity and temperature for each of the 5 additional Henry-Hilleke simulations. The stochastic realizations are shown as filled contours in gray to black and correspond to the log of the horizontal hydraulic conductivity. The dark red line shows the 50% seawater line 101

Figure 30: Relative rank of observations (for each of the 6 simulations) that reduce the predictive uncertainty the most for (a) concentration observations for prediction 2, (b) temperature observations for prediction 2, (c) concentration observations for prediction 3, and (d) temperature observations for prediction 3..... 102

Figure 31: Diagram showing groundwater flow lines in a coastal area with a saltwater-freshwater interface. SGD is fresh, brackish, or saline, depending upon the location and source of water. The SGD can carry nutrients or other contaminant from the aquifer to the ocean..... 109

Figure 32: Map of Florida with the 3 counties underlain by the Biscayne aquifer. Broward County is enlarged showing the location of monitoring wells collecting continuous water-level and salinity data. 114

Figure 33: 3-Dimensional model representative of the surficial aquifer system in southeastern Florida. (A) Schematic showing conceptual view of an area where the northern part is symmetrical to the southern part, and (B) map view, and (C) cross-sectional view of model grid showing the boundary conditions and aquifer parameters. 116

Figure 34: Stage measured downstream at structure S-36 (Figure 31) compared to the sine wave used as the ocean stage for the 3-D model. 118

Figure 35: Boundary conditions and finite difference model grid for 2-D model..... 122

Figure 36: (a) The first 6 days of the stage in the ocean boundary, temperature of the ocean boundary, and air temperature used in the recharge and general-head boundary cells in the 2-D model. (b) Recharge applied to the 2-D model. 122

Figure 37: Conceptual models of hydraulic connection between the aquifer and the ocean. 123

Figure 38: Map showing locations where data were collected off the coast of Miami-Dade County in Biscayne Bay used to verify the 2-D model. 125

Figure 39: (A-E) Continuous 15-minute record of water-level and specific conductance data for selected monitoring wells (Figure 32), and (F)

downstream canal stage and rainfall at structure S-36. The continuous 15-minute stage data for S-36 is shown to illustrate tidal effects.	126
Figure 40: 30-day graph of continuous 15-minute record of water levels and specific conductance (converted to TDS) in 2 of the observation wells [(A) G-2270 and (B) G-2900] compared to simulated observation wells in model. (NOTE: The <i>amplitude</i> of the fluctuations between measured and simulated values are intended to be compared, not the actual values of water level and specific conductance.).....	128
Figure 41: (A) The SGD (calculated by summing discharge/recharge to/from all constant-head cells representing the ocean) for each case over time. The first 7 days of the model run are shown. (B) Cumulative discharge to all cells representing the ocean with time (calculated using water into and out of the constant-head cells representing the ocean). (C) Fresh discharge in the model compared to the total discharge to the ocean (these values are not calculated using water entering the model from the ocean, only water being discharged to the ocean).....	130
Figure 42: Model results showing the annual average discharge with distance from the coast.	131
Figure 43: Cross section of three different cases showing salinity contours in g/L of total-dissolved solids.	133
Figure 44: Graphs showing the difference in salinity between the aquifer and ocean (in red, ocean-aquifer salinity) and the ocean stage (in black) with time at the coast for Cases 1, 2, and 3. The difference in salinity and the ocean stage at the submarine spring for Case 3.....	134
Figure 45: Temperature (in degrees Celsius) for the three cases in the winter, summer, and spring.....	135
Figure 46: Graphs showing the difference between the ocean temperature and the groundwater temperature with time. (A) Field data (Figure 38) collected at the coast (A1A and BP1) compared to the difference in temperature at the simulated coast in Cases 1-3 (column 130 minus column 129 in layer 1), and (B) Field data collected at the <i>midbay</i> surf-well (Figure 38) compared with simulated data approximately 3,000 meters from the simulated coast (column 151 in layer 12 minus column 151 in layer 13).	137
Figure 47: Temperature of the ocean showing daily fluctuation in temperature with the temperature of the spring showing tidal fluctuations. (A) Model output from Case 3, and (B) Data collected from spring BBS21 in Biscayne Bay (Proni and others, 2006).....	139

Figure 48: Graph showing discharge, difference in salinity, and difference in temperature versus distance from the coast, at low tide in the winter (differences are calculated by subtracting simulated aquifer salinity/temperatures from ocean/constant-head cell salinity/temperatures). 140

Figure 49: Age of water for each case after 10 years (repeating the one year simulation 10 times) and after 100 years (repeating the one year simulation 100 times)..... 141

1 INTRODUCTION

1.1 Preface

The work for this dissertation was done between 2003 and 2008 in cooperation with the U.S. Geological Survey (USGS). Funding for the work was provided by the USGS. The dissertation is a combination of (1) benchmarking a newly-developed code that simulates variable-density flow resulting from changes in temperature and concentration, and (2) utilizing that code to guide data collection and reduce predictive uncertainty. The dissertation consists of five chapters. An introduction in the first chapter provides background information, innovations of this research, and governing equations for variable-density flow and transport from changes in concentration and temperature. The following three chapters have been derived from peer-reviewed publications or are in the review process for publication by the USGS. These include two USGS Scientific Investigations Reports, a peer-reviewed publication in a refereed symposium book, a USGS Techniques and Methods Report, and a conference paper. A listing of the publications is presented below. Each of the chapters includes background and literature review at the beginning of the chapter that pertains to the research in the chapter. The final chapter contains the discussion and conclusions from the research.

Portions of this dissertation are published in the following:

Dausman, A.M. and Langevin, C.D., 2005, Movement of the saltwater interface in the Surficial Aquifer System in response to hydrologic stresses and water-management practices, Broward County, Florida. USGS Scientific Investigations Report: SIR 2004-5256, 73 p.

Dausman, A.M., Langevin, C.D., and Sukop, M.C., 2007, Simulation of submarine groundwater discharge salinity and temperature variations: implications for remote detection. In Sanford, W., Langevin, C.D., Polemio, M., and Povinec, P.,

eds. A new focus on groundwater-seawater interactions: IAHS Publication 312, Oxfordshire, United Kingdom, p. 272-280.

Dausman, A.M., Doherty, J., Langevin, C.D., and Sukop, M.C., 2008, Quantifying Data Contributions toward Reducing Predictive Uncertainty in a Variable-Density Flow and Solute/Heat Transport Model. Conference proceedings of MODFLOW and More: Ground Water and Public Policy, p. 320-324.

NOTE: Above conference paper has been invited for submission to a theme issue in the journal "Ground Water". The issue will be published in 2009.

Dausman, A.M., Langevin, C.D., Thorne, D.T., Jr., and Sukop, M.C., in review, Six Benchmark Problems for Testing Heat and Solute Transport with Variable Viscosity using SEAWAT Version 4. USGS Scientific Investigations Report.

Langevin, C.D., Thorne, D.T., Jr., Dausman, A.M., Sukop, M.C., and Guo, Weixing, 2008, SEAWAT Version 4: A Computer Program for Simulation of Multi-Species Solute and Heat Transport. U.S. Geological Survey Techniques and Methods Book 6, Chapter A22, 39 p.

1.2 Problem

Numerical modeling of groundwater systems is often undertaken to understand groundwater usage, plan for water supply, or make predictions for the future whether it relates to contaminant transport, water supply, saltwater intrusion, or well field protection. Modeling of groundwater systems that include relatively large changes in concentration requires modeling codes capable of simulating variable-density flow. It is typically assumed that the change in temperature in many groundwater systems is small and will have minimal effect on variable-density flow; therefore, temperature can be ignored in modeling. However, there are environments where ignoring the effects of temperature on flow will have consequences, such as in geothermal convection, deepwell injection, or aquifer storage and recovery (Figure 1A and 1C; Thorne and others, 2006). In fact, temperature effects may be non-negligible in many groundwater systems (Castendyk and Webster, 2004).

Advances in numerical modeling and computing resources have provided to a wider set of users the capability of simulating multiple species related to variable-density flow (Kipp, 1997; Hughes and Sanford, 2004; Langevin and others, 2008).

Mathematically, heat transport can be solved using the same equations used for solute transport with some minor assumptions (Anderson, 2005). Therefore, temperature effects on variable-density flow often can be simulated with modeling codes originally designed for solute transport. Because solute is referred to as a “species” in numerical modeling, heat is typically referred to as a “species” as well when discussed in terms of numerical modeling. When modeling solute or heat transport, heat can be modeled as a single species or an additional species along with other dissolved solutes. However, numerical complications can arise when simulating temperature. Temperature affects water slightly differently than solute; for example, temperature changes have a greater effect on viscosity than differences in salinity over the ranges of interest here (Figure 1B and 1D). Also, the conduction of heat through water/rock is much higher than the diffusion of salinity through water (Anderson, 2005).

The recently published code, SEAWAT Version 4 (Langevin and others, 2008), can simulate the effects of multiple species on variable-density flow, including temperature and salinity. Previous versions of SEAWAT could only simulate the effects of variable-density flow on one species, and did not have options to simulation viscosity variations or multiple diffusion coefficients. The code has been modified to take into account variations in viscosity due to changes in temperature and salinity, as well as include multiple diffusion coefficients. SEAWAT is based on two widely used and

readily available codes, MODFLOW (Harbaugh and others, 2000) and MT3DMS (Zheng and Wang, 1999; Zheng, 2006).

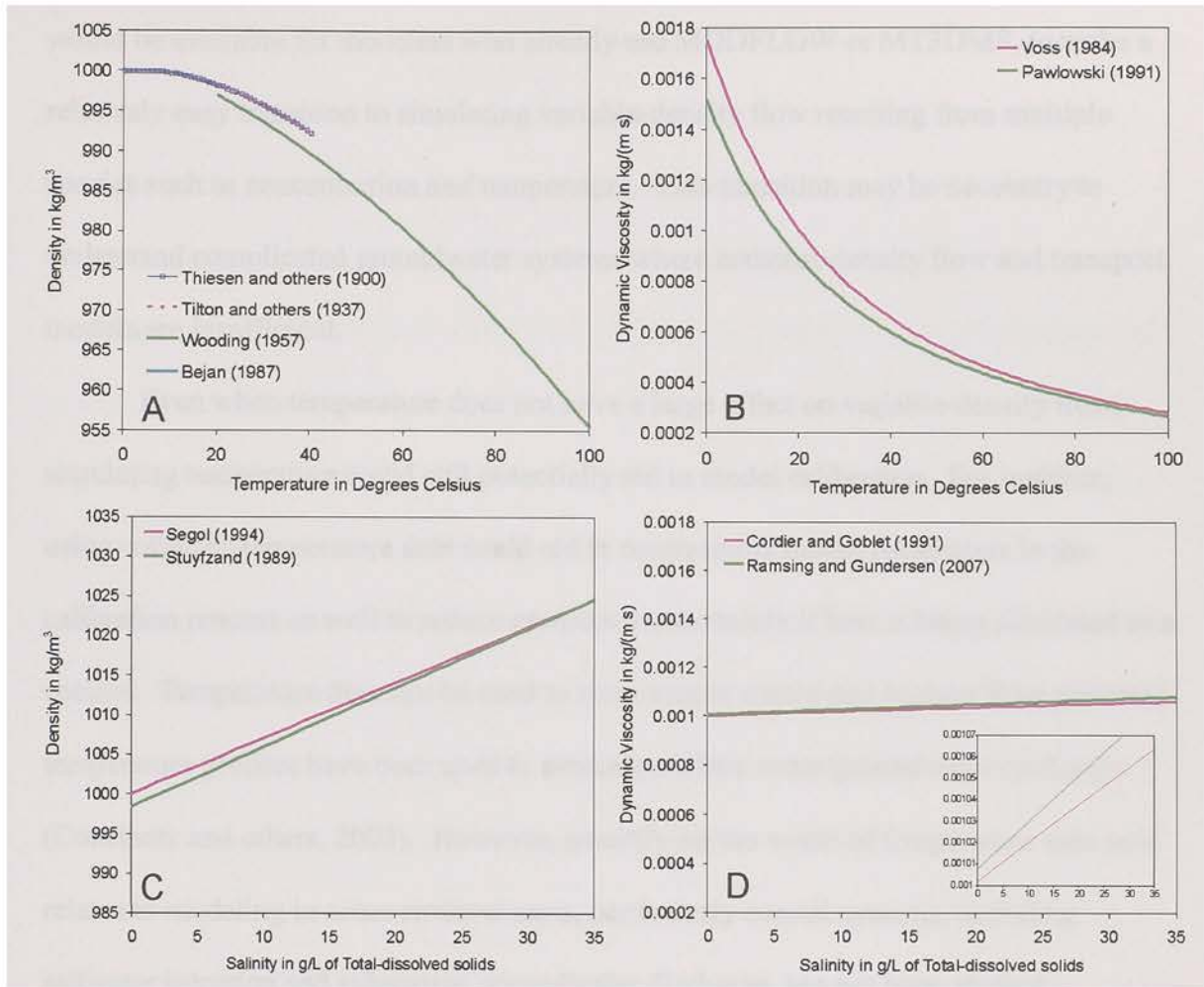


Figure 1: Graphs showing the relationships between temperature and salinity effects on density and viscosity published in the literature. (A) Temperature affects on the density of freshwater from five different formulae in the literature. (B) Temperature affects on the dynamic viscosity of freshwater from two published formulae in the literature. (C) Salinity affects on density of water at 20 °C from two published formulae in the literature. (D) Salinity affects on dynamic viscosity of water at 20 °C from two different formulae published in the literature.

However, for the most recent version of SEAWAT to be broadly accepted for use, thorough benchmarking is essential (Voss and Souza, 1987). In essence, the most recent version of the code needs to be verified against a number of other numerical codes, analytical problems, or laboratory experiments before it can be used with confidence to

solve “real world” problems. Thorough benchmarking of the new version of SEAWAT would then enable the code to be widely accepted by modelers. Therefore, a new tool would be available for modelers who already use MODFLOW or MT3DMS, to make a relatively easy transition to simulating variable-density flow resulting from multiple species such as concentration *and* temperature. This transition may be necessary to understand complicated groundwater systems where constant-density flow and transport models are insufficient.

Even when temperature does not have a large effect on variable-density flow, simulating temperature could still potentially aid in model calibration. For instance, using collected temperature data could aid in constraining model parameters in the calibration process as well as reduce predictive uncertainty if heat is being simulated as a species. Temperature data can be used to trace source waters and analyze flow patterns; temperature profiles have been used to estimate surface water/groundwater exchange (Constantz and others, 2002). However, quantifying the worth of temperature data as it relates to modeling in some environments, particularly coastal systems, including saltwater intrusion and submarine groundwater discharge, has not been studied.

Numerical models of groundwater systems are created to aid in understanding the environment, and often times, to make predictions of the future. However, a well-calibrated model does not necessarily mean that it can make good predictions (Carter and others, 2006). Data are frequently collected to improve the model’s ability to make a prediction. Thorough studies have not been done to see if the data planned to be collected will improve the ability of a model to make a prediction *before* the data are collected. It is hypothesized that a model simulating concentration and temperature could

be used to guide data collection therefore eliminating the costly collection of data that might not aid in understanding the overall groundwater system.

Studies that include the collection of isotope data can be used to determine the age of groundwater and estimate its residence times. These age data could be included in a flow and transport model to estimate parameters if the model has the capability of simulating apparent age (Goode, 1996). Typically, models simulating age use a particle tracking method where advective transport of particles is used; this has proven successful in some studies (Reilly and others, 1994). A particle tracking method to simulate age neglects the affects of diffusion, dispersion, and mixing. However, Walker and Cook (1991) “show how neglecting diffusion can lead to serious underestimates of groundwater ages in unconfined aquifers where recharge rates are...low”. Therefore, calibrating a strictly advective transport model to age data, where groundwater transport is affected by diffusion and dispersion, could result in a misidentification of parameters that affect transport, such as dispersivity. Goode (1996) reveals how the advection-dispersion equation can be modified to include a zero-order source. Zheng (2006) included this in MT3DMS to simulate age; therefore, taking into account both the effects of advection and dispersion when simulating age in a groundwater model. The capability of simulating age in MT3DMS is now available in SEAWAT and has never been tested or applied to a variable-density model simulating a coastal system.

1.3 Objectives

The objectives of the research presented in this dissertation are as follows:

- (1) Benchmark, evaluate, and apply the variable-density flow, solute, and heat transport capabilities of the most recent version of SEAWAT [including the effects of temperature on viscosity].
- (2) Quantify the reduction in uncertainty of a model prediction by determining the worth of different types of data, specifically temperature and salinity data, in a carbonate platform model. This objective includes testing the use of a precalibrated model before any data are collected.
- (3) Quantify the effects of geologic heterogeneity when simulating temperature, salinity, and age of submarine groundwater discharge. This includes simulating long-term seasonal changes and short-term tidal changes in the groundwater system/aquifer. Then, utilize the simulation to guide the collection of aerial imagery data to detect submarine groundwater discharge in a coastal system.

1.4 Scientific Contributions of this Dissertation

The research presented in this dissertation contributes new capabilities and innovative approaches to the field of variable-density numerical modeling, particularly in regard to simulating heat, concentration, and age. The following document benchmarks and verifies a new version of the code SEAWAT, and then utilizes that code to explore the repercussions of ignoring temperature effects on viscosity, as well as presenting innovative techniques for the use of variable-density groundwater models to guide data collection.

1.4.1 Benchmarking the new variable-density flow and transport code SEAWAT

Version 4

Modeling of environmental systems where the change in density of water affects the groundwater flow requires the use of a variable-density modeling code. Typically, variable-density models are developed for isothermal conditions where density is affected solely by the change in concentration. Temperature is often ignored in the process because it is assumed to have negligible effects (Konikow and Reilly, 1999). However, where temperature differences exist, the density and viscosity changes that result in the aquifer system can affect the groundwater flow (Figure 1; Henry and Hilleke, 1972).

This dissertation takes a new code (SEAWAT Version 4; Langevin and others, 2008) capable of simulating variable-density flow from differences in concentration and temperature, and benchmarks it against a number of previously published lab experiments, analytical solutions, and/or numerical solutions. The verified code can be used in a variety of environments, such as groundwater systems affected by saltwater intrusion and/or geothermal convection. In the process of code verification, analyses are also done on the effects of incorporating temperature in variable-density flow modeling. This includes studying the effects of variable viscosity and multiple diffusion coefficients because (1) temperature can have large effects on viscosity (Figure 1), and (2) the conduction of heat in a water/rock system is an order of magnitude greater than the diffusion of solute in a similar system (Anderson, 2005).

1.4.2 Utilizing a linear method to quantify the worth of salinity and temperature data in a nonlinear variable-density model

Environmental models are often developed to make predictions. Data are frequently collected to improve the ability of a calibrated model to make a prediction; however, how can one know that the prediction will be improved by the additional data collected? Calibration of a model does not necessarily mean that it will make accurate predictions (Carter and others, 2006). “The model is considered calibrated when it reproduces historical data within some subjectively acceptable level of coherence—there are no rules other than one’s judgment.” (Konikow and Bredehoeft, 1992).

A new linear technique to quantify the worth of data for making predictions is tested and utilized in a nonlinear variable-density flow and solute/heat transport model (developed using the most recent version of SEAWAT). This research takes the linear method and investigates its applicability to a nonlinear model. The linear technique and its application are innovative in that they (1) take into account the actual heterogeneity determined by aquifer testing and geostatistical analysis, (2) can be used in a model prior to calibration, (3) can be used in a underdetermined model (where there are more parameters than observations), and (4) have never been applied to a nonlinear variable-density flow and transport model to quantify the worth of data.

1.4.3 Utilizing a variable-density flow and transport model to guide data collection by quantifying temperature, salinity, and age of submarine groundwater discharge

A variable-density numerical model representing hydrological conditions in southeastern Florida is used to determine when and where submarine groundwater

discharge (SGD) rates are greatest. The model is then utilized to quantify expected temperature, salinity, and age differences between groundwater and ocean water. The model is innovative in that it uses SEAWAT to demonstrate how a numerical model can (1) simulate estimates of SGD flux, temperature, salinity and age, (2) be used to understand complicated coastal systems by simulating multiple species (heat, salinity, and age) while experimenting with different types of geology, and (3) be used to guide and give insight to data collection efforts in studies of SGD. The model is calibrated to hydrologic conditions in southeastern Florida and is verified against a number of different types of data. The model is unique in that it represents SGD characteristics, including salinity, temperature, and age, at short-term (tidal) and longer-term (seasonal) time scales. The simulation of age is innovative in that it takes into account the effects of not only advection, but also diffusion and dispersion.

1.5 Governing equations applied in this dissertation and utilized in SEAWAT

Version 4

SEAWAT is a coupled version of MODFLOW (Harbaugh and others, 2000) and MT3DMS (Zheng and Wang, 1999; Zheng, 2006) where the flow equation has been modified to include variable-density flow from multiple species, as well as the capability of simulating age. The multiple species discussed herein are solute, heat, and age. SEAWAT is used in all of the numerical modeling in this dissertation; therefore, an overview of the governing equations for solute and heat transport in variable-density flow will be briefly presented. Included in this section are the equations used in calculating the diffusion coefficients, variations in viscosity, and the zeroth-order reaction used in the

advection-dispersion equation to simulate age. These equations were also tested/used as part of the research in this dissertation. A more thorough discussion can be found in Thorne and others (2006), Zheng (2006), and Langevin and others (2008).

1.5.1 Solute and Heat Transport

Heat and solute transport are analogous in many ways (Voss, 1984; Martin and others, 2001; Anderson, 2005; Kim and others, 2005). Mathematically, heat transport can be solved using the same equations for solute transport with some minor assumptions; therefore, MT3DMS (a solute transport code) can be used to solve solute *and* heat transport.

The MT3DMS portion of SEAWAT solves the following solute transport equation

$$\left(1 + \frac{\rho_b K_d^k}{\theta}\right) \frac{\partial(\theta C^k)}{\partial t} = \nabla \cdot \left[\theta \left(D_m^k + \alpha \frac{\mathbf{q}}{\theta} \right) \cdot \nabla C^k \right] - \nabla \cdot (\mathbf{q} C^k) - q'_s C_s^k, \quad (1)$$

where

ρ_b is the bulk density (mass of the solids divided by the total volume) [ML⁻³],

K_d^k is the distribution coefficient of species k [L³M⁻¹],

θ is porosity [-],

C^k is the concentration of species k [ML⁻³],

t is time [T],

D_m^k is the molecular diffusion coefficient [L²T⁻¹] for species k ,

α is the dispersivity tensor [L],

\mathbf{q} is specific discharge [LT⁻¹],

q'_s is a source or sink [T^{-1}] of fluid with density ρ'_s , and

C_s^k is the source or sink concentration [ML^{-3}] of species k .

The dimensions of the variables are expressed using L=Length, T=Time, and M=Mass.

The solute transport equation above was altered by Thorne and others (2006) and Langevin and others (2008) to the heat transport equation

$$\left(1 + \frac{1-\theta}{\theta} \frac{\rho_s c_{Psolid}}{\rho c_{Pfluid}}\right) \frac{\partial(\theta T)}{\partial t} = \nabla \cdot \left[\theta \left(\frac{k_{Tbulk}}{\theta \rho c_{Pfluid}} + \alpha \frac{\mathbf{q}}{\theta} \right) \cdot \nabla T \right] - \nabla \cdot (\mathbf{q}T) - q'_s T_s, \quad (2)$$

where ρ_b , ρ_s , and θ are related by: $\rho_b = \rho_s(1 - \theta)$, and

ρ_s is the density of the solid (mass of the solid divided by the volume of the solid) [ML^{-3}],

ρ is fluid density [ML^{-3}],

c_{Psolid} is the specific heat capacity of the solid [$L^2T^{-2}C^{-1}$],

c_{Pfluid} is the specific heat capacity of the fluid [$L^2T^{-2}C^{-1}$],

T is temperature [$^{\circ}C$],

k_{Tbulk} is the bulk thermal conductivity of the aquifer material [$MLT^{-3}C^{-1}$], and

T_s is the source temperature [$^{\circ}C$].

The similarities between Equations (1) and (2) are evident. Essentially C^* from equation (1) is replaced by temperature (T) in equation (2). A few other assumptions are made for heat to be simulated in MT3DMS. The distribution coefficient, K_d^k , which represents the absorption of solute on solids in equation (1), is replaced by the thermal distribution factor, K_{d_temp} , where

$$K_{d_temp} = \frac{c_{Psolid}}{\rho c_{Pfluid}}. \quad (3)$$

This term assumes thermal equilibration between fluid and solid, and the movement of heat and subsequently the temperature are essentially retarded by heating of the porous media. The thermal distribution factor is represented by the heat capacity of the solid and its relation to the density of the fluid and the heat capacity of the fluid.

The molecular diffusion coefficient, D_m^k , from equation (1) is related to the bulk thermal diffusivity (represented in equation (2)) as

$$D_{m_temp} = \frac{k_{Tbulk}}{\theta \rho c_{Pfluid}}, \quad (4)$$

and the bulk thermal conductivity is frequently approximated by the simple mixing equation as

$$k_{Tbulk} = \theta k_{Tfluid} + (1 - \theta) k_{Tsolid}, \quad (5)$$

with k_{Tfluid} and k_{Tsolid} being the thermal conductivity of the fluid and solid, respectively.

Bulk thermal diffusivity represents how heat is conducted through the water *and* rock (in equation (2)), as opposed to molecular diffusion, where solute diffuses *solely* through the water (in equation (1)).

1.5.2 Variable-Density Flow

The concentration of solute and the temperature can be used to calculate the density of the water. The equation of state for density that includes multiple species (in this example, solute and heat) is

$$\rho = \rho_0 + \frac{\partial \rho}{\partial C}(C - C_0) + \frac{\partial \rho}{\partial T}(T - T_0), \quad (6)$$

where

ρ_0 is the reference fluid density [ML⁻³],

C is salt concentration [ML⁻³],

C_0 is the reference salt concentration [ML⁻³],

T_0 is the reference temperature [°C], with

$$\frac{\partial \rho}{\partial C} = \rho_0 \beta_C, \text{ and} \quad (7)$$

$$\frac{\partial \rho}{\partial T} = \rho_0 \beta_T, \quad (8)$$

where (β_C) and (β_T) are the volumetric expansion coefficients for solute concentration and temperature, respectively (Diersch and Kolditz, 2002). The equation of state (equation (6)) calculates density for any combination of concentration and temperature (other species can be used interchangeably).

The density calculated in equation (6) is used in the variable-density groundwater flow equation in SEAWAT

$$\nabla \cdot \left[\rho \frac{\mu_0}{\mu} \mathbf{K}_0 \left(\nabla h_0 + \frac{\rho - \rho_0}{\rho_0} \nabla z \right) \right] = \rho S_{s,0} \frac{\partial h_0}{\partial t} + \theta \frac{\partial \rho}{\partial C} \frac{\partial C}{\partial t} - \rho'_s q'_s, \quad (9)$$

where

μ is dynamic viscosity [ML⁻¹T⁻¹],

μ_0 is reference dynamic viscosity [ML⁻¹T⁻¹],

\mathbf{K}_0 is the hydraulic conductivity tensor of material saturated with the reference fluid [LT^{-1}] at the reference temperature and concentration,

h_0 is the hydraulic head [L] measured in terms of the reference fluid of a specified concentration and temperature (the reference fluid is commonly freshwater), and

$S_{s,0}$ is the specific storage [L^{-1}], defined as the volume of water released from storage per unit volume per unit decline of h_0 .

The variable-density flow equation in SEAWAT includes the effect of multiple species on density. It has also been altered to utilize multiple diffusion coefficients and the effects of variable viscosity, discussed next.

1.5.3 *Effects of Viscosity*

The effects of solute on viscosity are often considered negligible (unless brine is being simulated); therefore, the viscosity term, $\frac{\mu_0}{\mu}$, in equation (9) is typically assumed to be one when density is calculated solely as a function of solute concentration. However, temperature can have a significant effect on viscosity and naturally should not be ignored in some cases (Holzbecher, 1998; Nield and Bejan, 1999). SEAWAT calculates viscosity as a function of concentration and temperature with one of two equations. The temperature and concentration effects on dynamic viscosity are linear in the first equation

$$\mu = \mu_0 + \sum_{k=1}^{NS} \frac{\partial \mu}{\partial C^k} (C^k - C_0^k) + \frac{\partial \mu}{\partial T} (T - T_0). \quad (10)$$

However, a linear approximation for temperature effects on viscosity is not a valid assumption over many temperature ranges. Therefore, a nonlinear equation is available,

$$\mu = \mu_T(T) + \sum_{k=1}^{NS} \frac{\partial \mu}{\partial C^k} (C^k - C_0^k), \quad (11)$$

where the effects of temperature on viscosity ($\mu_T(T)$) can be calculated by one of two different equations for water,

$$\mu_T(T) = A_1 \cdot A_2^{\left(\frac{A_3}{T+A_4}\right)}, \text{ or} \quad (12)$$

$$\mu_T(T) = A_1 \cdot [A_2 + A_3(T + A_4)]^{A_5}, \quad (13)$$

or one equation that includes the effects of temperature on viscosity in oil,

$$\mu_T(T) = A_1 \cdot T^{A_2}. \quad (14)$$

The values for the constants, A , are specified by the user. These three equations can be found in the literature with typical values given for A depending on the simulation of water or oil and the temperature range in the model (Voss, 1984; Holzbecher, 1998; Nield and Bejan, 1999; Hughes and Sanford, 2004; Guo and Zhao, 2005). The viscosity calculated in either equation (10) or (11) as a result of changes in temperature and concentration is then used in the variable-density flow equation (equation (9)).

1.5.4 *Simulation of Age*

The effects of advection and dispersion on apparent age can be represented in MT3DMS by including a zero-order source, which represents the rate of aging, to the advection-dispersion transport equation (Goode, 1996; Zheng, 2006). A zero-order

reaction increases age at a constant rate, independent of concentrations. The equation is almost identical to equation (1) except for the zeroth-order rate coefficient at the end

$$\left(1 + \frac{\rho_b K_d^k}{\theta}\right) \frac{\partial(\theta C^k)}{\partial t} = \nabla \cdot \left[\theta \left(D_m^k + \alpha \frac{\mathbf{q}}{\theta} \right) \cdot \nabla C^k \right] - \nabla \cdot (\mathbf{q} C^k) - q'_s C_s^k - \gamma_1 \theta, \quad (15)$$

where γ_1 is the zeroth-order rate coefficient for the dissolved phase [$\text{ML}^{-3}\text{T}^{-1}$]. If a negative value is specified for γ_1 , then “production” is occurring in the groundwater, and age is increasing with time.

2 SIX BENCHMARK PROBLEMS FOR TESTING HEAT AND SOLUTE TRANSPORT USING SEAWAT VERSION 4

2.1 Introduction

Groundwater systems are often envisioned as constant-density systems where groundwater flow is mathematically straightforward. However, groundwater systems that have a shallow water table with high evapotranspiration rates, inputs of a highly concentrated contaminant, or saltwater intruding into the fresh groundwater at the coast, will contain increased solute concentrations. The increased concentrations often result in spatial variations of fluid density that affect groundwater flow. Fluid density between freshwater (1000 kg/m^3) and seawater (1025 kg/m^3) increases about 2.5%; this change in density will typically alter the flow field (Guo and Langevin, 2002). Therefore, the mathematical representation of variable-density groundwater systems is more complicated than constant-density systems because the solute concentration affects the density and the density affects the flow.

Mathematically representing groundwater systems affected by variable-density flow can be important for research related to coastal systems such as saltwater intrusion or submarine groundwater discharge. Mathematical models of coastal aquifers were created as early as 1888 by Ghyben and shortly thereafter by Herzberg (1901) to predict the location of the saltwater-freshwater interface. The Ghyben-Herzberg model uses simple hydrostatics to calculate the thickness of a static freshwater lens over a static saltwater wedge. This model assumes a sharp interface. Hubbert (1940) modified the Ghyben-Herzberg model to take into account non-static freshwater where it flows towards the ocean; however, Hubbert still assumed a sharp interface. Glover (1959) extended Hubbert's model to include a gap between the shoreline and the saltwater-freshwater interface with known discharge at the coast. Cooper (1959) created a steady-state mathematical model that accounts for the transition zone across the saltwater-freshwater interface. Cooper's model represents the freshwater discharging at the coast over saltwater that intrudes deep within an aquifer, rises and returns with the freshwater at the coast (simulating a brackish-water zone and a convection cell in the saltwater). Later, Henry (1964) provides a semianalytical solution for a saltwater-freshwater interface in a dynamic coastal system where freshwater is flowing towards an ocean boundary. Numerous variations of the Henry problem have been done since 1964, including a temperature-salinity version developed both numerically and in a laboratory setting by Henry and Hilleke (1972).

A tacit assumption in most groundwater models is that isothermal conditions prevail and that temperature does not affect the density of the water. Therefore, the effects of viscosity variations due to changes in temperature (and often salinity), are also

assumed to be so small they do not influence flow patterns. These assumptions are typically used, even in variable-density models designed to represent saltwater intrusion, wastewater injection, and convection beneath salt lakes. Research has shown, however, that temperature as well as salinity can affect the flow field (Henry and Hilleke, 1972), particularly for deeper aquifer systems. In some deep aquifers, geothermal heating from below can cause the formation of an unstable density profile (Elder, 1967).

The density of water is inversely related to temperature often causing convective flow when warm, less-dense water is overlain by cool, more-dense water. Like fluid density, viscosity is also a function of temperature. Thus, groundwater flow patterns may change in response to a changing temperature distribution because of the effects on density *and* viscosity. Freshwater, with a density of 1000 kg/m^3 , can be decreased to approximately 999.6 kg/m^3 by a 10°C increase in temperature. This is only about $\sim 0.5\%$ reduction in density and can often times be ignored; however, when temperature changes occur over a wider range, the decrease in density can have a significant effect on groundwater flow (Henry and Hilleke, 1972). Therefore, the modeling of some groundwater systems could require simulating the effects of temperature on variable-density flow.

A number of mathematical approaches have been taken to simulate variable-density groundwater flow such as finite-elements in SUTRA (Voss, 1984), analytical elements by Strack (1995), and finite difference approaches such as earlier versions of SEAWAT (Guo and Langevin, 2002; Langevin and others, 2003), MOC DENSE (Sanford and Konikow, 1985), and HST3D (Kipp, 1987). SUTRA was modified by Hughes and Sanford (SUTRA-MS, 2004) to simulate density-dependent flow resulting from multiple

species such as concentration and temperature. HST3D was also modified by Kipp (1997) to include both heat and solute transport effects on variable-density flow.

SEAWAT (Langevin and others, 2003), a combined version of MODFLOW (Harbaugh and others, 2000) and MT3DMS (Zheng, 1990; Zheng and Wang, 1999; Zheng, 2006), is designed to simulate three-dimensional, variable-density groundwater flow. SEAWAT was originally designed to solve variable-density groundwater flow and transport with the assumption that fluid density was a function of only a single solute constituent (Guo and Bennett, 1998; Guo and Langevin, 2002; Langevin and others, 2003). Thus, these previous SEAWAT versions could not be used to simulate simultaneous solute and heat transport. The latest version of SEAWAT, Version 4, was designed in a general fashion so that fluid density and viscosity can be calculated as a function of one or more species, and heat can be represented as one of the species (Langevin and others, 2008). The code can be used to simulate different types of fluids, including oil (as a single phase) or other fluids with variable viscosity, because the effects of viscosity on flow can be included in the simulations. A distinct diffusion coefficient for each species can also be included in this new version of SEAWAT.

For a numerical model to be reliable, the code must be rigorously tested to ensure that it accurately represents physical processes. Voss and Souza (1987) suggested that new modeling codes be tested with benchmark problems. A previous version of SEAWAT (Langevin and others, 2003) has been tested with most of the benchmark problems that are traditionally used to test saltwater intrusion programs. The purpose of this chapter is to document benchmark testing of the new features in SEAWAT (Langevin and others, 2008), including the code's ability to simulate a fluid besides water

(for example, oil as a single phase). In the testing of this new code, the effects of viscosity on convection and conduction are explored, as well as heat/energy transport into and out of modeling systems and the effects of multiple diffusion coefficients. Also included is an analysis of the repercussions of ignoring friction along a model boundary (referred to as a slip boundary) in the simulation of Darcy flow, as opposed to a no-slip boundary when simulating groundwater flow through a porous medium using other equations that include the resistive drag along a model boundary.

Testing of SEAWAT was performed using a suite of six benchmark problems:

- One-dimensional flow through a linearly varying viscosity field (Thorne and others, 2006)
- Two-dimensional oil convection in aluminum foam (Guo and Zhao, 2005)
- Horton-Rogers-Lapwood (HRL) convection (Horton and Rogers, 1945; Lapwood, 1948)
- Double-diffusive finger convection (Pringle and others, 2002)
- Original Elder problem (Elder, 1967)
- Henry-Hilleke problem (Henry and Hilleke, 1972)

These benchmark problems are well-defined and have been represented with laboratory experiments, analytical solutions, or with other modeling programs. Fluid dynamics and dimensionless numbers have been used in coordination with the benchmark problems to enable comparison between SEAWAT and other modeling codes, lab experiments, and systems of different dimensions.

2.2 Dimensionless Numbers

Research concerning temperature effects on the movement of liquids in a system is part of fluid dynamics. Temperature can affect the density and viscosity of liquid; therefore, the flow regime can also be altered by differences in temperature. These temperature changes affect how heat is transferred by means of convection or conduction through the liquids and solids of the system. Dimensionless numbers are often used in the study of fluid dynamics and mass transport to characterize the transfer of heat and solute, as well as movement of fluid. When the equations that govern the behavior of a system are rendered in dimensionless form, a set of dimensionless numbers that characterize the properties of the system emerges. Two systems that are described by the same dimensionless equations (in particular, the same values of the dimensionless numbers) and have the same dimensionless initial and boundary conditions (including geometric similarity) are mathematically equivalent (Bird, Stewart, and Lightfoot, 2006).

The concentration of a solute in a liquid can affect the density and viscosity; and therefore, the flow of a liquid. Because the equations for temperature and concentration effects on a flow regime are analogous (equations (1) and (2); Thorne and others, 2006; Langevin and others, 2008), what we learn from one system with changes in concentration can often be transferred to another system that includes changes in temperature. As long as the dimensionless numbers and dimensionless initial and boundary conditions between the two different systems (one being a system with solute and the other a system with temperature) are equal, a comparison between the two systems can be made.

Benchmark problems from different systems created with different codes can be compared based on the calculation of dimensionless numbers such as the Nusselt or Rayleigh number. Many of the dimensionless numbers used to analyze flow, viscosity, and heat transfer through the liquid in a porous media system are discussed herein because they are used to evaluate and compare the benchmark problems. All variables used in this report are defined in Table 1.

Table 1: Identification of variables. L=Length, T=Time, M=Mass, D=Degrees of Temperature.

Input Parameter	Units	Definition
q	LT ⁻¹	Darcy Flux
Q	L ³ T ⁻¹	Volumetric Flux
H	L	Height of a defined system or cell
L	L	Length of a defined system or cell
W	L	Width of a defined system or cell
h	L	Head
x	L	Distance in x direction
K	LT ⁻¹	Hydraulic conductivity
k	L ²	Permeability
α_L	L	Longitudinal dispersivity
α_T	L	Transverse dispersivity
S _y	-	Specific yield
S	-	Storage
θ	-	Porosity
D*	L ² T ⁻¹	Bulk thermal diffusivity without porosity in the denominator
D**	L ² T ⁻¹	Bulk thermal diffusivity with porosity
ρ_{water}	ML ⁻³	Density of water
ρ_s	ML ⁻³	Density of solids
ρ_b	ML ⁻³	Bulk Density
β_t	D ⁻¹	Thermal Expansion Coefficient
β_c	M ⁻¹ L ³	Solutal Expansion Coefficient
ν	L ² T ⁻¹	Kinematic Viscosity
ν_0	L ² T ⁻¹	Reference Kinematic Viscosity
μ	ML ⁻¹ T ⁻¹	Dynamic Viscosity
μ_0	ML ⁻¹ T ⁻¹	Reference Dynamic Viscosity
T	D	Temperature
T _{ref}	D	Reference Temperature for Reference Dynamic/Kinematic Viscosity
C _{pfluid}	L ² T ⁻² D ⁻¹	Heat Capacity of Fluid
C _{pSolid}	L ² T ⁻² D ⁻¹	Heat Capacity of Solid
k _{TBulk}	LMT ⁻³ D ⁻¹	Bulk Thermal Conductivity
k _{Tfluid}	LMT ⁻³ D ⁻¹	Thermal Conductivity of Fluid
k _{Tsolid}	LMT ⁻³ D ⁻¹	Thermal Conductivity of Solid
g	LT ⁻²	Acceleration due to gravity
Ra	-	Rayleigh Number
Da	-	Darcy Number
Pr	-	Prandtl Number

2.2.1 Rayleigh Number

The Rayleigh number is a dimensionless number that defines the dominance of convection as opposed to conduction of heat (or diffusion of solute). High Rayleigh number systems (above a critical Rayleigh number) are characterized by convective flow and low Rayleigh number systems have stable density profiles where heat/solute is transferred by conduction/diffusion. The critical Rayleigh number is the value above which the change from conduction to convection of the heat/solute through the fluid will occur. All else being equal, systems with equal Rayleigh numbers should have similar solute or heat transport patterns.

The equation used to calculate the Rayleigh number for free thermal convection (when porosity = 1) is

$$Ra = \frac{g\beta\Delta TH^3}{\nu D^*} \quad (16)$$

(Rayleigh, 1916; Holzbecher, 1998; Guo and Zhao, 2005). However, another Rayleigh number, herein referred to as Ra^* , is often used for porous media. $Ra^* = Da \cdot Ra$, where Ra^* is the Darcy number ($Da = \frac{k}{H^2}$) times the Rayleigh number (equation (16)), Ra^* is also called the Darcy-Rayleigh number (the Darcy number is discussed further in the subsequent section). Essentially, the permeability is included in the equation for Ra^* to account for the resistance of fluid flow due to the porous medium. Therefore, the equation is

$$Ra^* = \frac{gk\beta\Delta TH}{\nu D^*} \quad (17)$$

(Lapwood, 1948; Nield and Bejan, 1999), where bulk thermal diffusivity (a physical property that controls the rate at which temperature changes are brought about by conduction) is calculated using the following equation

$$D^* = \frac{k_{Tbulk}}{\rho c_{pfluid}} \quad (18)$$

(Holzbecher, 1998). The bulk thermal conductivity (k_{Tbulk}) is calculated using

$$k_{Tbulk} = \theta k_{Tfluid} + (1 - \theta) k_{Tsolid} \cdot \quad (19)$$

Another version of the Rayleigh number for a porous medium, Ra^{**} , uses the following equation

$$Ra^{**} = \frac{gk\beta\Delta TH}{\theta\nu D^{**}} \quad (20)$$

(Prasad and Simmons, 2003; Weatherhill and others, 2004). Equation (20) uses porosity in the denominator, which is different from Ra^* in equation (17) without porosity. This is because thermal diffusivity is calculated using the following equation

$$D^{**} = \frac{k_{Tbulk}}{\theta\rho c_{pfluid}} \quad (21)$$

(Thorne and others, 2006). Porosity cancels out in the denominator for Ra^{**} , therefore equations (17) and (20) are both correct and equal for a porous medium, depending on how thermal diffusivity is calculated.

Small differences in temperature, such as 1°C, can result in convective flow depending on the aquifer and water properties of the groundwater system. For example, a quartz aquifer system with fresh groundwater, hydraulic conductivity of 100 m/d, porosity of 0.2, a change in density with temperature of -0.375 kg/(m³ °C), and a height

of 100 m, results in a Rayleigh number of 59 (calculated from equation (20), assuming the bulk thermal diffusivity is $0.32 \text{ m}^2/\text{d}$ —from Thorne and others, 2006—and the kinematic viscosity is $0.0864 \text{ m}^2/\text{d}$). If the length of the aquifer system is an exact multiple of the height of the system, 59 is above the critical Rayleigh number of $4\pi^2$ according to Horton and Rogers (1945) and Lapwood (1948). The same aquifer system, but calcite instead of quartz, results in a higher Rayleigh number of 127. This is because the bulk thermal diffusivity of calcite is less at $0.147 \text{ m}^2/\text{d}$ (Thorne and others, 2006). However, if the hydraulic conductivity is decreased to 20 m/d , the calculated Rayleigh numbers for quartz and calcite aquifers, 12 and 25 respectively, fall below the critical Rayleigh number of $4\pi^2$ and would not result in convective flow. These results are expected. Even a small change in temperature would result in convective flow if the aquifer properties were conducive to high Rayleigh numbers.

Thermal Rayleigh numbers are analogous to solutal Rayleigh numbers because they are described by the same dimensionless equations. The coefficients used in calculation of the dimensionless Rayleigh numbers are analogous, such as:

- The thermal and solutal expansion coefficients have a similar overall affect on the Rayleigh number. The thermal expansion coefficient

(equation (8)) is: $\beta_t = \frac{1}{\rho} \left(\frac{\partial \rho}{\partial T} \right)$. $\frac{\partial \rho}{\partial T}$ is negative when simulating

temperature, because as temperature increases, density decreases. When simulating concentrations and calculating the solutal expansion coefficient

(equation (7)), $\frac{\partial \rho}{\partial T}$ is now $\frac{\partial \rho}{\partial C}$, and as concentration increases, density increases (the sign is now positive).

- The change in temperature term, ΔT , in equations (16), (17), or (20) may be substituted with the change in concentration, ΔC , for solute transport problems.
- The molecular diffusion coefficient can be used instead of the bulk thermal diffusivity and it has a similar effect in the solute/heat transport process.

Therefore, the dimensionless Rayleigh numbers in systems with variable-density flow resulting from changes in temperature can be compared to systems with flow affected by changes in concentration.

The different types of Rayleigh numbers presented are used in some of the benchmark problems to compare the results from SEAWAT to previous research. The following benchmark problems use at least one of the different types of Rayleigh numbers discussed:

- Two-dimensional oil convection in aluminum foam (Guo and Zhao, 2005)
- Horton-Rogers-Lapwood (HRL) convection (Horton and Rogers, 1945; Lapwood, 1948)
- Original Elder problem (Elder, 1967)

2.2.2 Darcy Number

Darcy's Law calculates specific discharge in a porous medium with the following equation

$$q = -K \frac{\partial h}{\partial x}. \quad (22)$$

Darcy's Law is generally only valid when assuming flow is through porous media when the pore scale Reynolds number is less than 1; Darcy's Law is not valid for free-fluid flow except under limited circumstances (i.e., Poiseuille-like flow). The Darcy number (Da) is a dimensionless number that tests the validity of Darcy's Law (Nield and Bejan, 1999) where k is the permeability and H is a characteristic length, such as the height of the system being modeled

$$Da = \frac{k}{H^2}. \quad (23)$$

The validity of Darcy's Law, measured by the Darcy number, is important when analyzing the effects of model boundaries on simulations of groundwater flow through a porous medium. A slip boundary condition is assumed when simulating flow based on Darcy's Law, basically meaning that flowing water is not slowed by the presence of a model boundary and slips along the boundary, ignoring friction at the model boundary. A particle flowing through a porous medium is impeded by that medium. The model boundary frictional effect on the flow is considered minimal (almost zero) in comparison to the porous medium effect on the reduction of flow, therefore the model boundary effect is ignored (or considered a slip boundary). However, when simulating free fluid flow or a porous medium with high hydraulic conductivities, the slip boundary condition

is no longer valid and the frictional effects of the model boundary on flow can no longer be ignored. Therefore, a no-slip boundary condition has to be implemented and Darcy's Law cannot be used to simulate flow in this environment.

According to Nield and Bejan (1999), Darcy's Law holds true for Darcy numbers less than 10^{-3} . When Darcy numbers are greater than 10^{-3} , the system is close to an open-channel or free fluid flow system; thus it violates the slip boundary condition assumption in normal applications of Darcy's Law. SEAWAT solves a variable-density flow form of Darcy's Law (Langevin and others, 2008); therefore all model simulations using SEAWAT have to have Darcy numbers less than 10^{-3} .

This research used the Darcy number in a benchmark problem that solves two-dimensional oil convection in aluminum foam (Guo and Zhao, 2005). The problem compares SEAWAT against another modeling method (Lattice Boltzmann). The Lattice Boltzmann method is capable of solving free fluid flow; therefore, it can solve problems with Darcy numbers greater than 10^{-3} . However, for our purpose in comparing the two flow systems in porous media, the Darcy numbers were limited to less than 10^{-3} .

2.2.3 Prandtl Number

The Prandtl number is a dimensionless number used to analyze the hydrodynamic effects on heat transfer from a bounding surface through what is called a boundary layer. The boundary layer is a thin layer of water directly adjacent to the model boundary that is affected by friction, essentially the fluid next the model boundary “sticks” to the boundary surface (i.e., a no-slip boundary). The area of the model that is assumed to be

inviscid, where viscous forces from friction along the wall are assumed to be negligible, is farther from the model boundary outside of the boundary layer.

The Prandtl number

$$\text{Pr} = \frac{\nu}{D^* (\text{or } D^{**})} \quad (24)$$

(Nield and Bejan, 1999; Guo and Zhao, 2005), is a ratio that aids in determining the relative thickness of the momentum boundary layer to the thermal boundary layer.

According to Nield and Bejan, low Prandtl numbers (much less than one) indicate that heat transfer from a wall is dominated by conduction because the diffusive/thermal boundary layer is greater than the momentum (viscous) boundary layer.

The Prandtl number is used in the benchmark problem on two-dimensional oil convection in aluminum foam. Guo and Zhao (2005) compute Prandtl and Darcy numbers, showing mathematically “that for a given Prandtl number, the nonlinear drag force [along a model boundary] becomes negligibly small only for a small Da, or in the Darcy Regime”; and therefore Darcy’s Law applies only for small Darcy numbers (as discussed previously). The Prandtl number is identical for both the model created with the Lattice Boltzmann method and the SEAWAT model; therefore, the two systems are comparable.

2.2.4 Nusselt Number

The Nusselt number is a dimensionless number that enables comparison of the actual heat (or solute) transfer across a boundary into a model layer to the heat (or solute) transfer through the entire system if heat transfer occurred solely via conduction (or diffusion in the case of solute transport). The Nusselt number; defined as

$$Nu = \frac{Q}{\theta D * (\frac{\Delta T}{H}) LW}, \text{ and} \quad (25)$$

is the ratio of the total heat/solute flux through a layer to the steady-state conductive/diffusive flux across the model (Nusselt, 1944; Prasad and Simmons, 2005). Systems where all solute/heat transfer is solely by diffusion or conduction have a Nusselt number of one. Systems that are not stable with respect to their density profiles and heat transfer occurs by free convection in addition to heat conduction, would have Nusselt numbers greater than one. The end result is a dimensionless number representing the energy (or mass) transferred across the system.

The Nusselt number changes with time and is typically analyzed by graphing the Nusselt number vs. time for a system/model. The graphs for different systems are compared to one another to analyze the timing, type of heat transfer (convection or conduction), and the amount of heat transfer. Benchmark problems with similar graphs of the Nusselt number with time are considered analogous. The Nusselt number is used to compare the Elder problem solution from SEAWAT to two other benchmark problems, the original Elder problem (Elder, 1967), and a more recent simulation by Prasad and Simmons (2003).

2.3 Benchmark Problems

A series of benchmark problems were simulated with the newest version of SEAWAT. The benchmark problems have a number of different equations and parameters associated with them. The governing equations for the simulations are presented in Chapter 1 and can also be found in Guo and Langevin (2002), Langevin and

others (2003), and Langevin and others (2008). The dimensionless numbers used to compare the systems were discussed in the previous section. All variables represented in the equations are defined in Table 1.

2.3.1 *One-Dimensional Flow with Linearly Varying Viscosity Field*

This benchmark problem consists of one-dimensional groundwater flow between two constant-head boundaries. The purpose of the problem is to test the implementation of viscosity effects in SEAWAT. The implementation is tested using the premise that simulations with a linearly varying viscosity field and a constant value for reference hydraulic conductivity will give the same result as a simulation with a linearly varying reference hydraulic conductivity field and a constant fluid viscosity. Thorne and others (2006) provide an extensive discussion on the equations used for this benchmark problem.

In the MODFLOW user's guide (Harbaugh and others, 2000), Darcy's law is implemented as: $Q = COND(h_A - h_B)$, where the conductance ($COND$) is multiplied by the difference in hydraulic head ($h_A - h_B$) between two locations, A and B. In SEAWAT, the conductance $COND$ is defined as

$$COND = \frac{\mu_0}{\mu} \frac{KWH}{L}. \quad (26)$$

SEAWAT is formulated using “equivalent freshwater” hydraulic conductivity (Guo and Langevin, 2002). Therefore, K values used in equation (26) represent an aquifer that is saturated with the reference fluid at the reference temperature (normally assumed to be freshwater at 25°C). The ratio $\frac{\mu_0}{\mu}$ reflects the variation in dynamic viscosity $\mu = \mu(C,T)$

from a reference viscosity μ_0 . In SEAWAT, the horizontal conductance between two cells can be averaged by one of three ways: 1) harmonic average, 2) logarithmic average, or 3) arithmetic average. The vertical conductance across two layers with adjacent cells is calculated using the harmonic average.

Conductance between cells in a model can vary by changing either the hydraulic conductivity or the viscosity ratio ($\frac{\mu_0}{\mu}$). Equation (26) reveals that the effects of changing the hydraulic conductivity and the viscosity ratio are inversely related. Therefore, if the viscosity ratio in a cell is increased and hydraulic conductivity in that same cell is proportionally decreased, the conductance between that cell and any adjacent cell will be the same as if no increase/decrease were made in the parameters.

An analytical equation can easily be derived for steady-state, confined, one-dimensional flow through a linearly varying hydraulic conductivity field. Two prescribed head boundaries can arbitrarily be defined as: at $x = x_{\min}$, $h = h_0$; at $x = x_{\max}$, $h = h_1$. A linearly varying hydraulic conductivity field is represented by arbitrarily setting $K = x$ throughout the domain. Thus, Darcy's law is $q = -x(dh/dx)$, where q is flux and dh/dx is the hydraulic gradient. The analytical solution is obtained by setting the derivative of q with respect to x to zero ($dq/dx = 0$; i.e., flux is uniform along the domain) and integrating between x_{\min} and x_{\max} subject to the boundary conditions, resulting in the following equation

$$h = \frac{h_1 - h_0}{\ln(x_{\max}) - \ln(x_{\min})} [\ln(x) - \ln(x_{\min})] + h_0 \quad (27)$$

(Thorne and others, 2006).

The effects of viscosity on groundwater flow are implemented in SEAWAT.

Viscosity can be specified on a cell-by-cell basis, or it can be calculated as a function of one or more MT3DMS species if the simulation includes transport. For the test problem described herein, viscosity is specified as $1/x$ in the cases where hydraulic conductivity is kept constant; this should give the exact same results as a problem where the hydraulic conductivity is equal to x and the viscosity is held constant.

Four simulations were performed with SEAWAT for this test problem. The first three simulations use a constant reference hydraulic conductivity and a prescribed viscosity gradient in (a) the x-direction with 91 columns, 1 row, and 1 layer, (b) the y-direction with 1 column, 91 rows, and 1 layer, and (c) the z-direction with 1 column, 1 row, and 91 layers. The one-dimensional simulations were performed in all three layer, row, and column directions to ensure the implementation was coded correctly in each direction. A fourth simulation with a constant viscosity and a prescribed hydraulic conductivity gradient in the x-direction with 91 columns, 1 row, and 1 layer was also performed. Head results from these simulations should match the analytical solution exactly, with the possible exception of the third case. The analytical solution is based on a linearly varying hydraulic conductivity field. To exactly represent a linearly varying hydraulic conductivity field with SEAWAT, logarithmic averaging should be used to calculate internodal conductances. While logarithmic averaging was used in the first two simulations, harmonic averaging is the only SEAWAT option for calculating internodal conductances in the vertical direction (used in the third case). Results from the third simulation, however, should be very close to the analytical solution.

Figure 2 shows the grid with prescribed water levels on each end, 0 ft to 1 ft (0.3048 m), and the 91 columns (or rows, or layers) with each cell being 1 ft³ (0.02832 m³). $K(x)=1$ ft/day (0.3048 m/day) in the 3 models with a prescribed viscosity gradient where the dynamic viscosity (μ) in each cell is $1/x$. In the fourth case, dynamic viscosity is constant and the hydraulic conductivity in each cell varies with distance where $K(x) = x$. The PCG2 solver from MODFLOW2000 was used to solve for head in each cell. The head change convergence criterion was set to 1×10^{-8} ft (3.048×10^{-9} m).

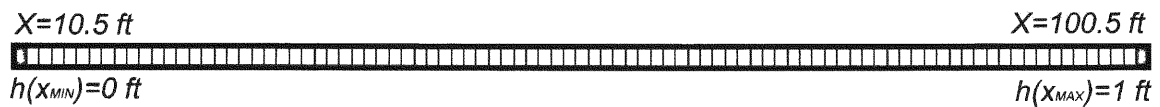


Figure 2: Diagram showing map view of model design in SEAWAT.

2.3.1.1 Results and Discussion

Results indicate that the four SEAWAT simulations are in good agreement with the analytical solution (Figure 3). Although conductance is calculated using the harmonic mean (as opposed to the continuously varying hydraulic conductivity in the analytical solution) in the variable viscosity case with multiple layers, differences between the models are minimal. These results indicate that the effects of viscosity on groundwater flow have been implemented correctly in SEAWAT.

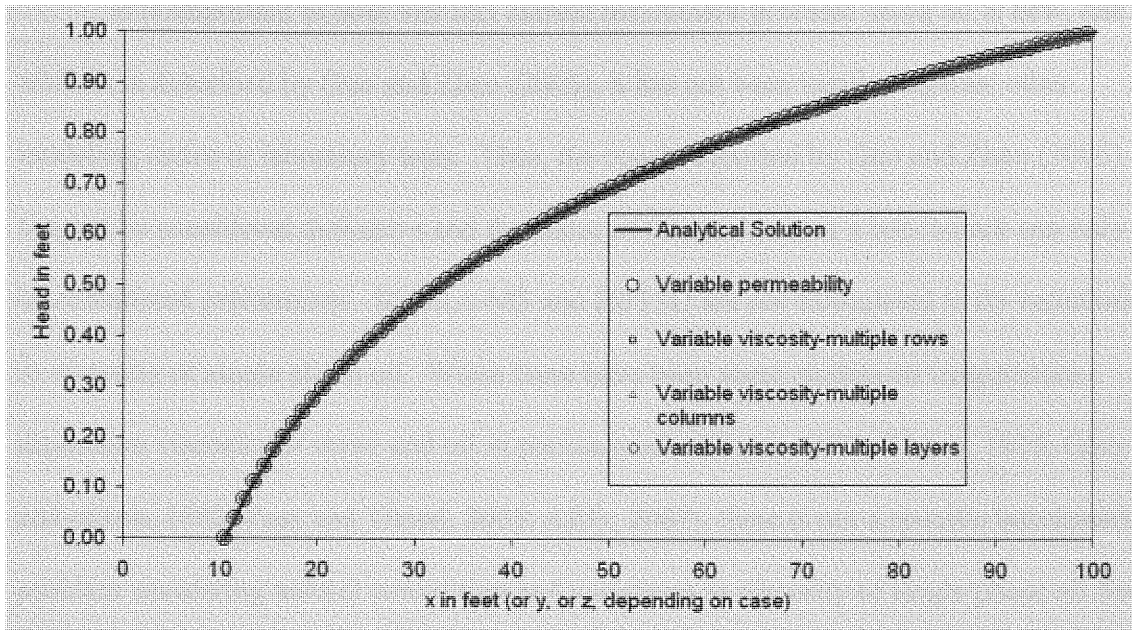


Figure 3: Results of water-level values with distance in each of the SEAWAT models and the analytical solution.

2.3.2 Two-Dimensional Oil Convection in Aluminum Foam

This benchmark problem has never been used as a benchmark before and is believed to be novel. It is a Lattice Boltzmann method simulation of oil convection in aluminum foam. Convection is driven by temperature differences between two vertical walls on opposing sides of a square cross section. Each simulation is run with and without the effects of viscosity variations. The box problem contains oil; therefore there is a relatively strong dependence of viscosity on temperature (as compared to water). The purpose of this benchmark problem is to test the variable viscosity mechanism implemented in SEAWAT (equation (14)), as well as test the capability of SEAWAT to simulate thermally-driven convection in oil. Nield and Bejan (1999) provide an extensive review of these types of problems modeling fluids such as water, but only for constant viscosity.

It is important to note that this current benchmark problem using oil is new, and while it is described by Guo and Zhao (2005), it has not been verified against other modeling codes or laboratory tests. Thus, the results reported by Guo and Zhao (2005) can not be considered definitive and the status of this problem as a benchmark can only be considered preliminary. SUTRA-MS and HST3D are not formulated to do variations in viscosity of single phase oil. While there have been some studies on temperature-dependent viscosity of water and oil in porous media (Horne, 1975; Weber, 1975; Gary and others, 1982; Pasa and Titaud, 2005; Afify, 2007), there is not a specific benchmark problem simulating natural convection and variations in viscosity of single phase oil from changes in temperature in a porous medium, particularly of aluminum foam (aside from Guo and Zhao, 2005). More tests will need to be done to solidify Guo and Zhao's work as a standard benchmark problem.

Guo and Zhao (2005) used Lattice Boltzmann methods to simulate convection of PolyAlphaOlefin (PAO) oil in aluminum foam. The authors conducted a series of simulations with different Rayleigh (equation (16)) and Darcy (equation (23)) numbers, and also tested the effects of viscosity. The design of the problem is shown in Figure 4 with the model parameters, grid dimensions, and solution schemes given in Table 2.

The viscosity (μ) of a saturating fluid is often assumed to be constant if the viscosity of the fluid is only weakly dependent upon temperature. However, when simulating some environments with large temperature differences or environments that contain fluids with strong temperature dependent viscosities (such as oil), variations in viscosity cannot be ignored. The change in viscosity will affect heat transfer and fluid

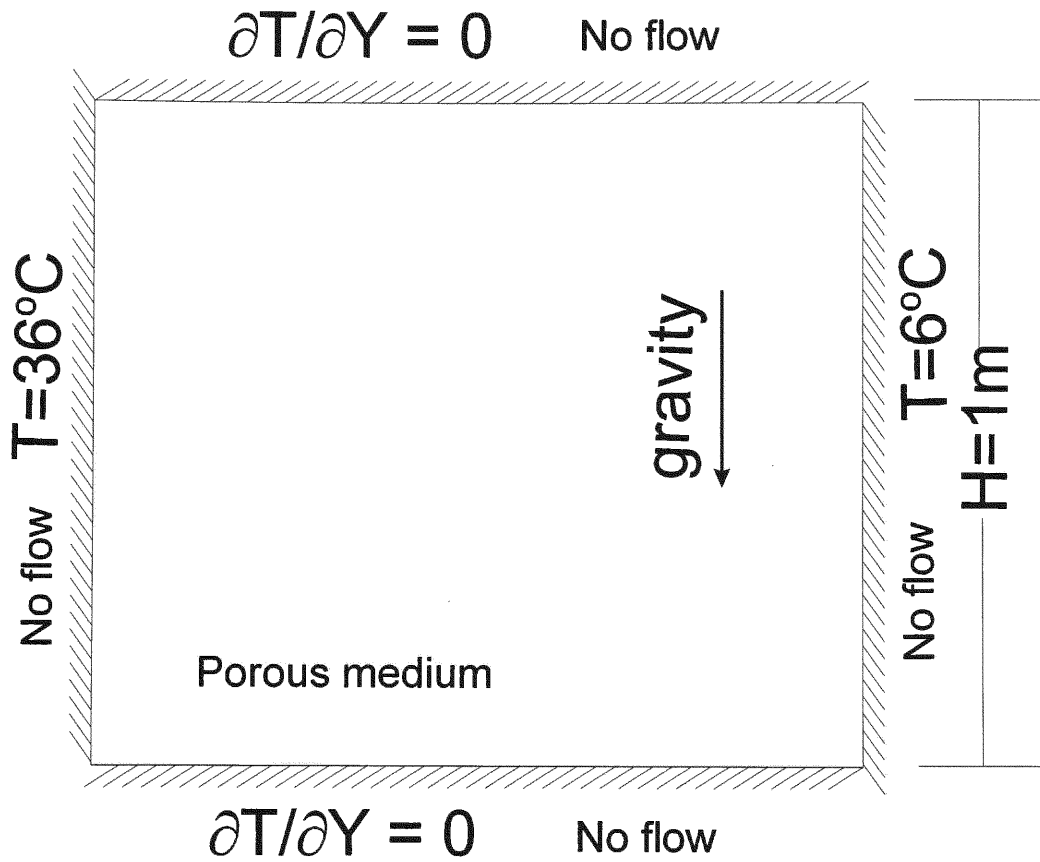


Figure 4: Schematic diagram for problem simulating temperature-dependent viscosity of oil in aluminum foam.

Table 2: Input parameters for problem simulating temperature-dependent viscosity of oil in aluminum foam.

Input Parameter	Value	Units	Comments
Number of columns	130	-	Assigned
Number of rows	1	-	Assigned
Number of layers	128	-	Assigned
$\Delta x(\text{DELR})$	0.0078125	m	Assigned
$\Delta y(\text{DELC})$	0.0078125	m	Assigned
$\Delta z(\text{DELZ})$	0.0078125	m	Assigned
H	1	m	Length and Height of "active" model domain
K, $Da = 10^4$	127	m/s	Hydraulic conductivity
K, $Da = 10^2$	12658	m/s	Hydraulic conductivity
k, $Da = 10^4$	1.0×10^4	m^2	Permeability
k, $Da = 10^2$	1.0×10^2	m^2	Permeability
α_L	0	m	Longitudinal dispersivity
α_T	0	m	Transverse dispersivity
S_y	0.01	-	Specific yield

S	0.01	-	Storage
θ	0.58	-	Porosity
D^*	4.7184×10^{-5}	m^2/s	Thermal diffusivity
ρ_{water}	768.5	kg/m^3	Density of water at 21 °C (reference temperature)
$\frac{\partial \rho}{\partial T}, \text{Ra} = 1 \times 10^5$	-9.55×10^{-5}	$\text{kg}/(\text{m}^3 \text{ } ^\circ\text{C})$	Density change with temperature
$\frac{\partial \rho}{\partial T}, \text{Ra} = 1 \times 10^6$	-9.55×10^{-4}	$\text{kg}/(\text{m}^3 \text{ } ^\circ\text{C})$	Density change with temperature
$\frac{\partial \rho}{\partial T}, \text{Ra} = 1 \times 10^7$	-9.55×10^{-3}	$\text{kg}/(\text{m}^3 \text{ } ^\circ\text{C})$	Density change with temperature
$\beta_t, \text{Ra} = 1 \times 10^5$	1.24×10^{-7}	$1/^\circ\text{C}$	Thermal Expansion Coefficient
$\beta_t, \text{Ra} = 1 \times 10^6$	1.24×10^{-6}	$1/^\circ\text{C}$	Thermal Expansion Coefficient
$\beta_t, \text{Ra} = 1 \times 10^7$	1.24×10^{-5}	$1/^\circ\text{C}$	Thermal Expansion Coefficient
ν_0	7.74×10^{-6}	m^2/s	Reference Kinematic Viscosity
μ_0	0.00595	$\text{kg}/(\text{m s})$	Reference Dynamic Viscosity
T_{ref}	21	$^\circ\text{C}$	Reference Temperature for Reference Dynamic Viscosity
c_{pfluid}	1971.35	$\text{m}^2/(\text{s}^2 \text{ } ^\circ\text{C})$	Heat Capacity of Fluid
k_{fluid}	0.1424	$\text{m kg}/(\text{s}^3 \text{ } ^\circ\text{C})$	Thermal Conductivity of Fluid
k_{solid}	170	$\text{m kg}/(\text{s}^3 \text{ } ^\circ\text{C})$	Thermal Conductivity of Solid
g	9.8	m/s^2	Acceleration due to gravity
Cool Temperature Boundary	6	$^\circ\text{C}$	Assigned
Hot Temperature Boundary	36	$^\circ\text{C}$	Assigned
Matrix solution technique for flow	PCG2	-	Assigned
Head convergence value	0.001	m	Assigned
Flow convergence value	1	kg/s	Assigned
Advection term	TVD	-	Assigned
Dispersion and source terms	Implicit finite difference; GCG, SSOR	-	Assigned
Time-step length	1-10000	s	Varies between models for different Rayleigh numbers
Temperature convergence value	1×10^{-12} to 1×10^{-13}	$^\circ\text{C}$	Varies between models for different Rayleigh numbers

flow. Viscosity varies with temperature in PAO oil according to the equation

$$\mu(T) = 0.168 \cdot T^{-1.0868} . \quad (28)$$

This equation and its parameters come from Guo and Zhao (2005) and is an optional equation for temperature dependent viscosity implemented in SEAWAT (equation (14)).

Another equation from SEAWAT that can be used for viscosity variations with temperature when simulating water is

$$\mu(T) = 0.00002394 \cdot 10^{\left(\frac{248.37}{T+133.15}\right)} \quad (29)$$

(from equation (12)). The values for this equation come from SUTRA-MS (Hughes and Sanford, 2004). A graph showing the change in viscosity with temperature according to equation (28) and equation (29) is shown in Figure 5. This figure reveals that viscosity variations with temperature are much higher when simulating oil as opposed to simulating water.

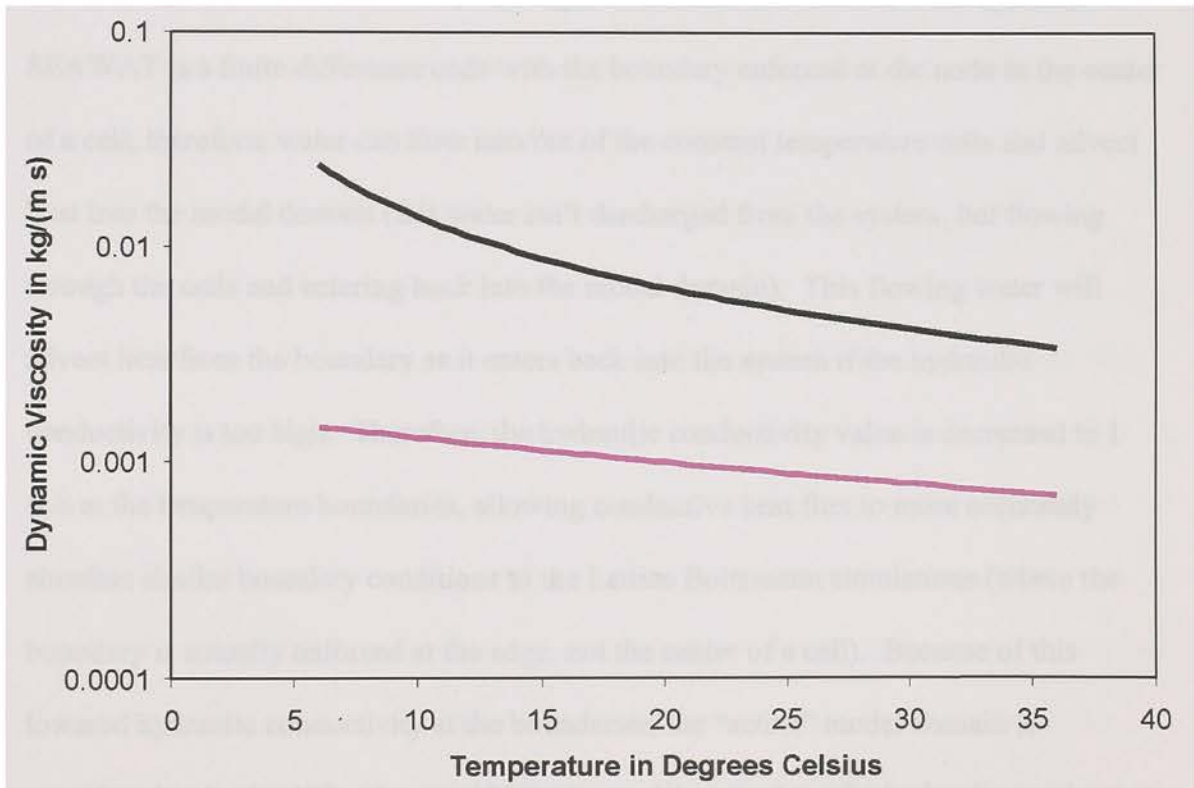


Figure 5: Graph showing the change in viscosity with temperature according to equation (28) (oil, in black) and equation (29) (water, in pink).

The simulation uses a finite difference grid of 130 columns by 128 layers by 1 row to discretize the cross section that is 1 m high by 1.015625 m long (Figure 4). An

insulated (i.e., zero-temperature gradient) no-flow boundary is assigned across the top and bottom of the box. There is a no-flow, constant “cool” boundary (T_c) of 6°C along the right-hand side and a no-flow, constant “hot” temperature boundary (T_h) of 36°C along the left-hand side. The columns containing the constant cool/hot temperature boundaries have a lowered hydraulic conductivity to minimize the convective heat flux from the temperature boundaries; by definition, conduction should be the sole heat transport mechanism at the boundary. Even though there is no water entering the model from the left and right boundaries, water flowing inside the modeled system can actually flow into and out of the cells at left and right boundaries (but not leave the system). SEAWAT is a finite difference code with the boundary enforced at the node in the center of a cell; therefore, water can flow into/out of the constant temperature cells and advect heat into the model domain (this water isn’t discharged from the system, but flowing through the cells and entering back into the model domain). This flowing water will advect heat from the boundary as it enters back into the system if the hydraulic conductivity is too high. Therefore, the hydraulic conductivity value is decreased to 1 m/s at the temperature boundaries, allowing conductive heat flux to more accurately simulate similar boundary conditions to the Lattice Boltzmann simulations (where the boundary is actually enforced at the edge, not the center of a cell). Because of this lowered hydraulic conductivity at the boundaries, the “active” model domain is considered to be the 128 columns, 128 layers, and 1 row where the hydraulic conductivity is uniform at 127 m/s (in a 1 m by 1 m cross section). All dimensionless numbers are calculated based on a 1 m by 1 m domain and a hydraulic conductivity of 127 m/s.

The Lattice Boltzmann simulations conducted by Guo and Zhao (2005) simulated oil in a homogeneous isotropic porous medium and used a generalized version of the Navier-Stokes equation that accounts for all fluid forces, including the resistive drag along a boundary (a no-slip boundary). Therefore, they can simulate flow with larger Darcy numbers (see discussion under “Dimensionless Numbers”, equation (22)). The SEAWAT simulations presented here are only valid for conditions with relatively small Darcy numbers (less than 10^{-3}) because of the slip boundary condition. Table 2 lists the calculated hydraulic conductivities using two different Darcy numbers. The hydraulic conductivity for a Darcy number of 10^{-2} is extremely high (2,658 m/s), suggesting that explicit representation of boundary friction (such as that provided by the Lattice Boltzmann method) would be required. Therefore, to compare SEAWAT to the simulations by Guo and Zhao (2005), a Darcy number of 10^{-4} is used in all the simulations so Darcy’s Law remains valid.

Guo and Zhao (2005) performed a series of Lattice Boltzmann simulations with and without the effects of viscosity variations and multiple Rayleigh numbers between 10^3 and 10^7 (see equation (16)). They also presented Rayleigh* numbers for the same benchmark problems (see equation (17)). Guo and Zhao (2005) likely used both equations (16) and (17) because they experiment with porous media simulations with low to high hydraulic conductivities; therefore, as hydraulic conductivity is increased, the simulations moved toward simulating free fluid flow. Thermal diffusivity, used in the Rayleigh number, is calculated using equation (18), resulting in a Prandtl number (equation (24)) of 0.164. (See discussion under “Dimensionless Numbers” for more details.)

A total of six simulations were performed with SEAWAT for comparison with Guo and Zhao (2005). The Darcy number for these simulations was 10^{-4} . Three different Rayleigh numbers were explored: 10^5 , 10^6 , and 10^7 . The parameter $\frac{\partial \rho}{\partial T}$ was altered to adjust the Rayleigh number (Table 2). This parameter affects the calculated thermal expansion coefficient β_t ($\beta_t = \frac{1}{\rho} \left(\frac{\partial \rho}{\partial T} \right)$) used in the Rayleigh number. Therefore, by increasing the change in density with the change in temperature, the Rayleigh number is also increased. Two cases were run with each Rayleigh number: (1) a constant viscosity case using the reference viscosity of 0.00595 kg/(m s) (Table 2), and (2) a variable viscosity case using equation (28). Solvers and time step options for the models are shown in Table 2. Models were run until temperatures reached an equilibrium configuration.

2.3.2.1 Results and Discussion

Results from SEAWAT are compared with the results from Guo and Zhao (2005) as shown in Figure 6 and Figure 7. The differences between the SEAWAT and the Lattice Boltzmann simulations are likely caused from the differences in boundary conditions (i.e., slip vs. no-slip boundaries and the decreased hydraulic conductivity boundary in SEAWAT to reduce advective heat flux). The difference in streamline patterns (Figure 6) between the Lattice Boltzmann and SEAWAT simulations could also result from the SEAWAT figures being created for a qualitative visual comparison to Guo and Zhao (2005). Quantitative values for the streamlines (or temperature contours) were not provided in the paper by Guo and Zhao (2005).

However, the overall streamline and temperature patterns are similar, particularly in the constant viscosity cases. What is also important is how each of the simulations results in flow patterns that differ between the variable and constant viscosity cases. When viscosity variations are included, the flow patterns are asymmetric (Figure 6) for the SEAWAT simulations, where the center of the convection cell shifts toward the warmer wall. This shift results from the decrease in viscosity near the warmer wall and increase in viscosity near the cooler wall. In other words, the center of the convection cell tends to move toward the warmer wall because the overall resistance to flow is less in the warmer parts of the domain. The asymmetry in the streamlines is discussed in Guo and Zhao (2005); however, it is visually more difficult to see in their published figures, which are the only results available.

The temperature contours between the Lattice Boltzmann and SEAWAT simulations appear very close (Figure 7). Also evident is the change in temperature contours between the variable and constant viscosity cases, as well as, a difference in temperature contours among the different Ra^* numbers. The constant viscosity cases have slightly more vertical contours when compared to the variable viscosity cases with the same Rayleigh number. In Figure 7, for the model with a $Ra^*=10$, the temperature contours are nearly vertical for the both the constant and variable viscosity cases, revealing that the simulation is close to the critical Ra^* number (the reference viscosity used in the calculation of the Ra^* is from Table 2, which is the viscosity at the reference temperature, 21°C, the average of the end temperatures). For the variable viscosity cases, the temperature contours are slightly less vertical, suggesting there is more heat transfer via convection than the similar constant viscosity case with the same Ra^* . This

No variable viscosity

Variable viscosity

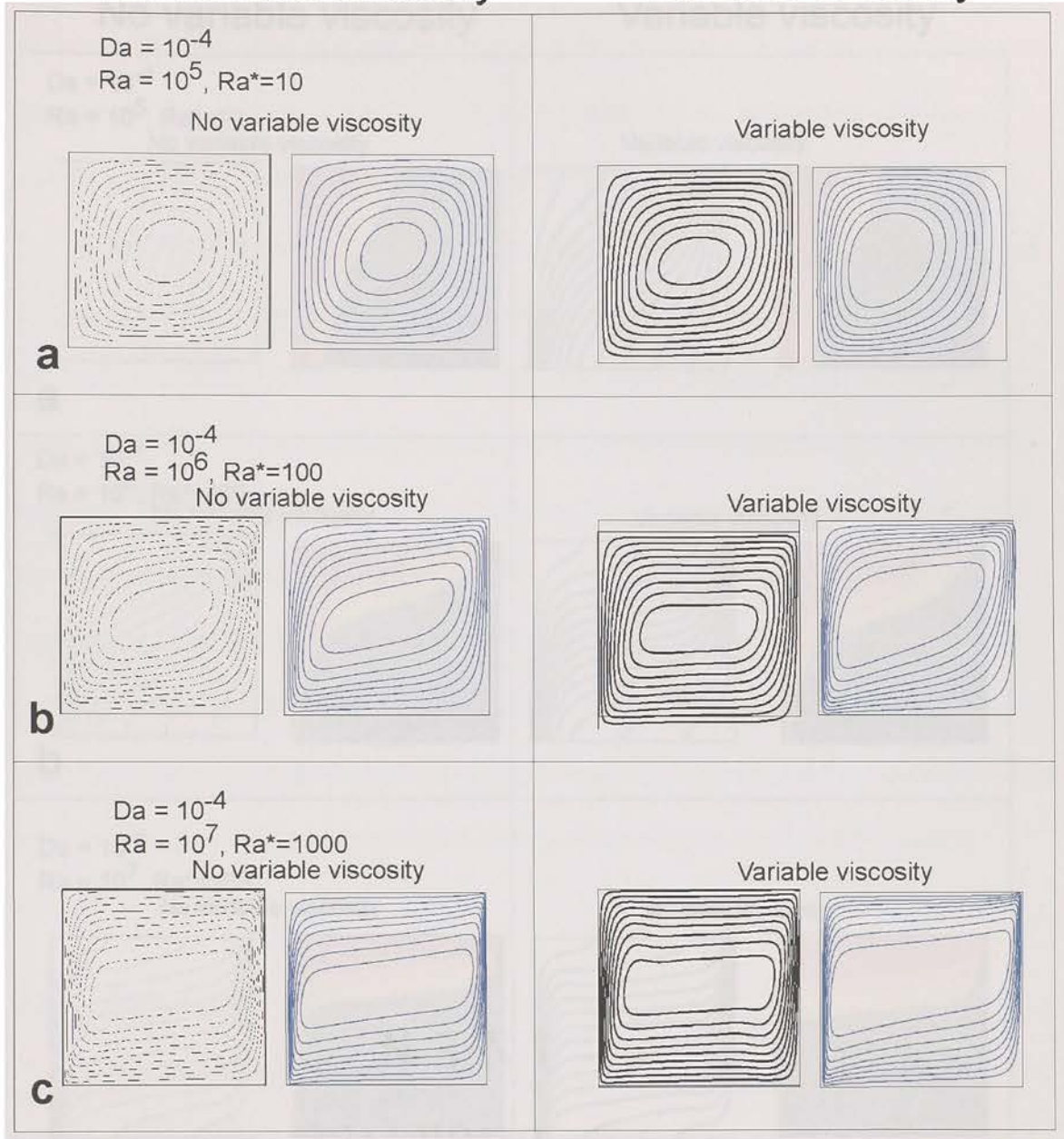


Figure 6: Streamline results for both variable viscosity and constant viscosity (gray/black streamlines) cases from Guo and Zhao (2005) compared with resulting streamlines from SEAWAT (blue streamlines). (a) Results with Darcy numbers of 10^{-4} and Rayleigh* numbers of 10, (b) results with Darcy numbers of 10^{-4} and Rayleigh* numbers of 100, and (c) results with Darcy numbers of 10^{-4} and Rayleigh* numbers of 1000.

No variable viscosity

Variable viscosity

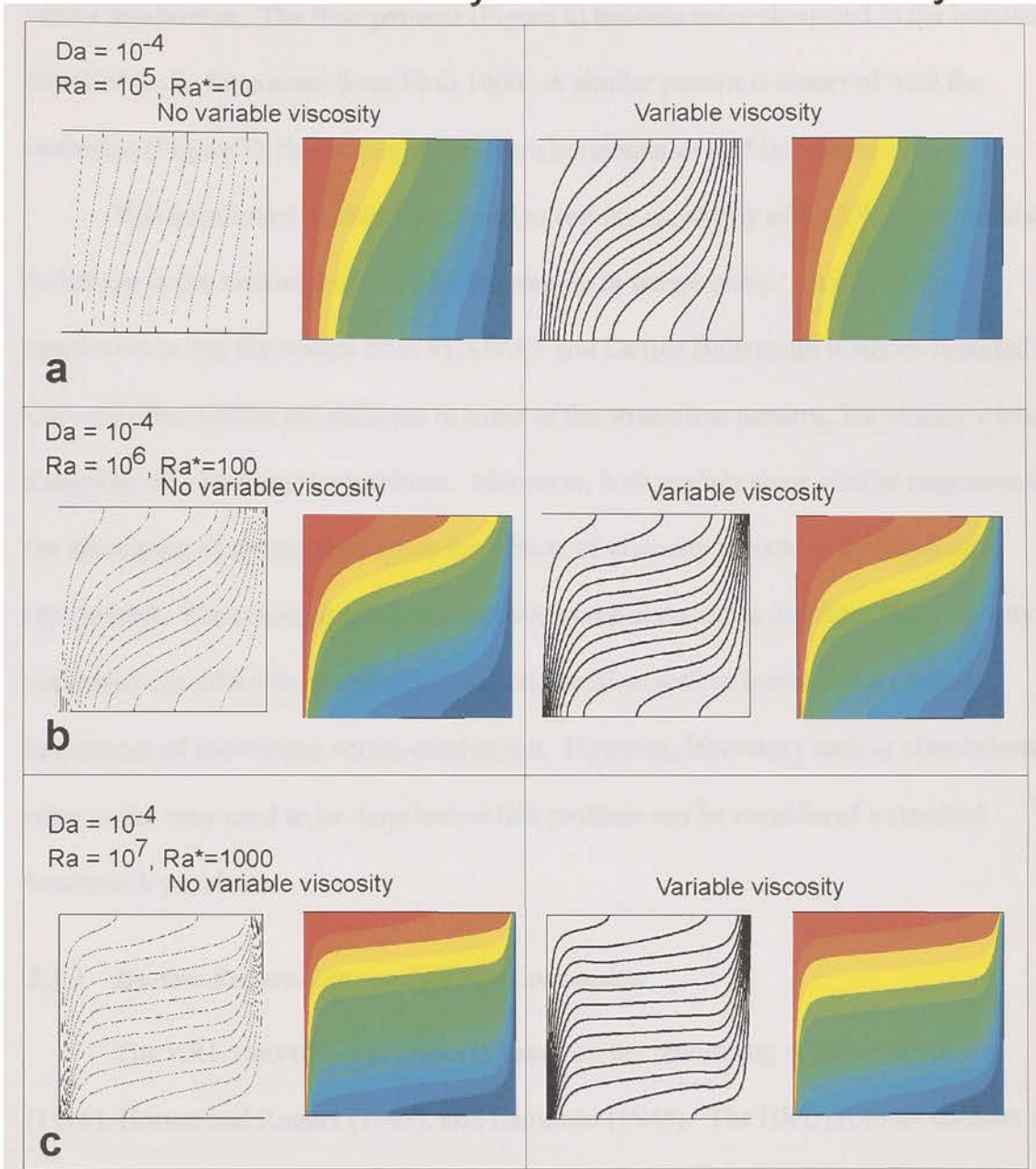


Figure 7: Temperature isotherms for both variable viscosity and constant viscosity cases from Guo and Zhao (2005, in gray/black and white) compared with temperature isotherms from SEAWAT (in color). (a) Results with Darcy numbers of 10^{-4} and Rayleigh* numbers of 10, (b) results with Darcy numbers of 10^{-4} and Rayleigh* numbers of 100, and (c) results with Darcy numbers of 10^{-4} and Rayleigh* numbers of 1000.

pattern is most clearly seen where $Ra^* = 1000$, suggesting that the critical Ra^* is lower when viscosity variations with temperature are represented in these problems. An

increase in the Ra^* with each simulation reveals the increased tendency for convection versus conduction. The flow patterns (Figure 6) become more elongated in the horizontal direction as Ra^* increases from 10 to 1000. A similar pattern is observed with the isotherms (Figure 7); the isotherms are more horizontal as Ra^* increases.

This benchmark problem was used to test the capability of SEAWAT to simulate variations in the viscosity of oil from differences in temperature. An important conclusion is that the results from SEAWAT and Lattice Boltzmann methods reported by Guo and Zhao (2005) are different in some of the streamline patterns, but similar when analyzing the resulting temperatures. Moreover, both models show similar responses in the simulation of temperature when the effects of viscosity variations are explicitly represented. The consistent response between both approaches indicates that viscosity variations can affect the shape of a convection cell as well as increase the relative importance of convection versus conduction. However, laboratory tests or simulations by other codes may need to be done before this problem can be considered a standard benchmark problem.

2.3.3 Horton-Rogers-Lapwood (HRL) Convection

The HRL convection problem is based on the pioneering work of Rayleigh (1916), Horton and Rogers (1945), and Lapwood (1948). The HRL problem consists of an infinitely long layer of a fully saturated porous medium with a specified height of H . The temperature assigned to the lower boundary is fixed at a value higher than the temperature assigned for the upper boundary. Thus, there is lighter water underlying denser water. For the HRL problem, one of two things will occur depending on the

values used to define the system. The fluid may remain stationary, and heat will conduct from the lower boundary to the upper boundary. Under this condition, the entire layer is characterized by a linear vertical temperature gradient. The other possibility is that convection cells will form. Horton and Rogers (1945) showed that convection will occur when Ra^{**} (equation (20)) is greater than $4\pi^2$ (a value of approximately 39.48), this value is referred to as the critical Ra^{**} number.

Weatherhill and others (2004) conducted a series of simulations using SUTRA and showed that the onset of convection will occur when Ra^{**} is greater than $4\pi^2$. If the values were assigned so that the resulting Ra^{**} value was less than $4\pi^2$, then convection did not occur, and all heat transport was through conduction. Instead of trying to approximate an infinitely long layer, Weatherhill and others (2004) showed that the HRL problem can be represented as rectangular box provided that the length of the box, L , is an integer multiple of the height of the box, H (Figure 8). Or, for simplification, the aspect ratio, A , defined as

$$A = \frac{L}{H} \quad (30)$$

(Weatherhill and others, 2004) must be an integer if $4\pi^2$ is to apply as the critical Ra^{**} value. If A is an integer, then the center between zones of upwelling and downwelling will occur exactly at the boundary and the critical Ra^{**} value is $4\pi^2$. This characterization applies because the areas of upwelling and downwelling are related to the height of the box. If A is not an integer, convective flow will still occur, but the critical Ra^{**} number will not be $4\pi^2$ because the center zones of upwelling/downwelling will not be at the boundary.

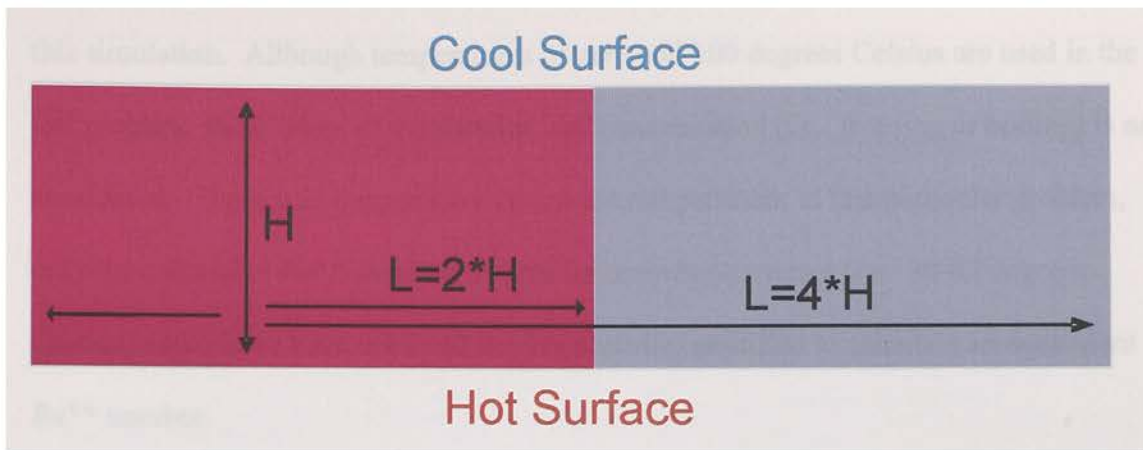


Figure 8: Simple design of Horton-Rogers-Lapwood benchmark problems where the length of the box is 2 times (or 4 times) the height.

The HRL convection problem was simulated with SEAWAT to test the ability of the code to represent thermally-driven convection. The basic design of the problem is shown in Figure 9 with the model parameters, grid dimensions, and solution schemes given in Table 3. The model simulates freshwater with a domain of 1 row, 416 columns, and 54 layers. The top and bottom boundaries were set as constant temperature boundaries with a decreased hydraulic conductivity of 1×10^{-6} m/d. This low hydraulic conductivity value was assigned only to the top and bottom layers in order to minimize the advective heat flux across the temperature boundaries; by definition, conduction should be the sole heat transport mechanism at the boundary.

Because of the decreased hydraulic conductivity in the top and bottom layers, H is calculated as the distance between the bottom of layer 1 and the top of layer 54 (156 m). Constant-head boundary cells, with an arbitrary value, were placed at the upper left and upper right corners (Figure 9) to facilitate efficient solution of the flow equation. The left and right hand side of the model are no-flow, insulated (i.e., zero-temperature-gradient), boundaries. The model only simulates heat transfer; solute transport is not included in

this simulation. Although temperatures of zero and 100 degrees Celsius are used in the test problem, the process of evaporation and condensation (i.e., freezing or boiling) is not considered. The actual temperature values are not pertinent to this particular problem, only the calculated Ra^{**} number. A smaller temperature range (i.e., 30-40 degrees Celsius) could have been used and the permeability modified to calculate an equivalent Ra^{**} number.

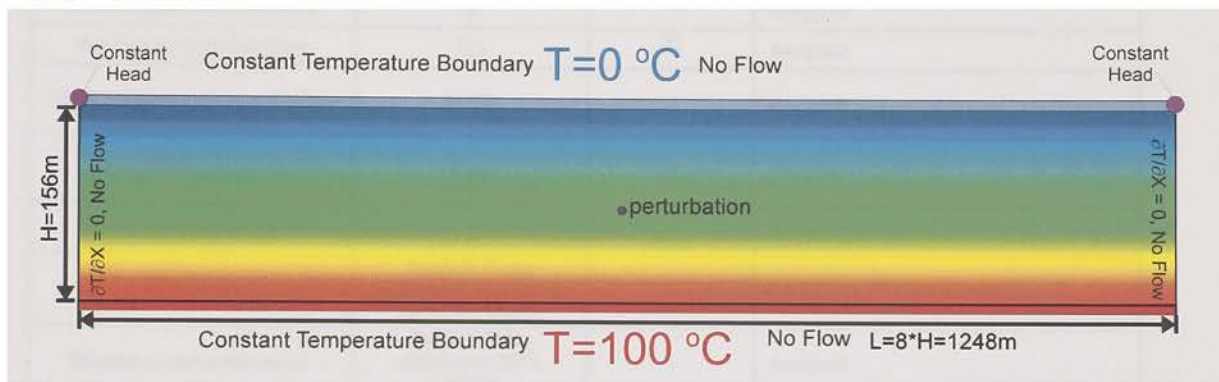


Figure 9: Design of the Horton-Rogers-Lapwood problem in SEAWAT. The colors from blue to red show the initial temperatures for the simulations from 0 °C in blue to 100 °C in red. Height, length, and boundary conditions are also displayed.

Table 3: Input parameters for the Horton-Rogers-Lapwood problem simulated in SEAWAT.

Input Parameter	Value	Units	Comments
Number of columns	416	-	Assigned
Number of rows	1	-	Assigned
Number of layers	54	-	Assigned
Δx (DELR)	3	m	Assigned
Δy (DELC)	3	m	Assigned
Δz (DELZ)	3	m	Assigned
K, where $Ra^{**} = 39$	0.0385	m/d	Hydraulic conductivity
K, where $Ra^{**} = 40$	0.03949	m/d	Hydraulic conductivity
K, where $Ra^{**} = 200$	0.19744	m/d	Hydraulic conductivity
k, where $Ra^{**} = 39$	4.54×10^{-14}	m^2	Permeability
k, where $Ra^{**} = 40$	4.66×10^{-14}	m^2	Permeability
k, where $Ra^{**} = 200$	2.33×10^{-13}	m^2	Permeability
α_L	0	m	Longitudinal dispersivity
α_T	0	m	Transverse dispersivity
S_y	None-steady state	-	Specific yield
S	None-steady state	-	Storage

θ	0.1	-	Porosity
D^*	0.308	m^2/d	Thermal diffusivity
ρ_{water}	1000	kg/m^3	Density of water at 4 °C
$\frac{\partial \rho}{\partial T}$	-2	$kg/(m^3 \text{ } ^\circ C)$	Density change with temperature
β	0.002	$1/^\circ C$	Thermal Expansion Coefficient
ν_o	0.0864	m^2/d	Reference Kinematic Viscosity
μ_o	86.4	$kg/(m \text{ } d)$	Reference Dynamic Viscosity
T_{ref}	4	$^\circ C$	Reference Temperature for Reference Dynamic Viscosity
g	7.32×10^{10}	m/d^2	Acceleration due to gravity
Cool Temperature Boundary	0	$^\circ C$	Assigned
Hot Temperature Boundary	100	$^\circ C$	Assigned
Matrix solution technique for flow	PCG2	-	Assigned
Head convergence value	1×10^{-10}	m	Assigned
Flow convergence value	1	kg/d	Assigned
Advection term	Implicit Finite Difference-Central in Space Weighting	-	Assigned
Dispersion and source terms	Implicit finite difference; GCG, SSOR	-	Assigned
Time-step length	Calculated using Courant of 0.01	s	Assigned
Temperature convergence value	1×10^{-12}	$^\circ C$	Assigned

Three simulations were performed with SEAWAT using Ra^{**} values of 39, 40, and 200. The simulations were identical except (1) the hydraulic conductivity was adjusted in order to achieve the desired Ra^{**} number (Table 3), and (2) the initial temperatures for the $Ra^{**} = 200$ simulation were set from the temperatures resulting from the $Ra^{**} = 40$ simulation. For the $Ra^{**} = 40$ simulation, the temperature at a single node was slightly perturbed to initiate convection in the model.

2.3.3.1 Results and Discussion

Results show that for the first simulation ($Ra^{**} = 39$) there is no convection, and all heat transport is solely through conduction (Figure 10A). (A perturbation was included for the simulation where $Ra^{**}=39$ to test the potential for convection. The density configuration remained stable at the end of the simulation). As the Rayleigh number increases (Figure 10B and C), convection cells form. Convection can clearly be seen in the velocity field, as shown in Figure 11 for the $Ra^{**} = 40$ simulation. Upwelling brings the warmer water closer to the top boundary; downwelling occurs and brings cooler water closer to the bottom boundary (Figure 10). According to Weatherhill and others (2004) the wavelength, λ , of the convection cells is $2H$ and the number of convection cells should equal L/H (the aspect ratio). Thus, for the values used here, there should be 8 convection cells, which is the number observed in Figure 10B and C and in Figure 11.

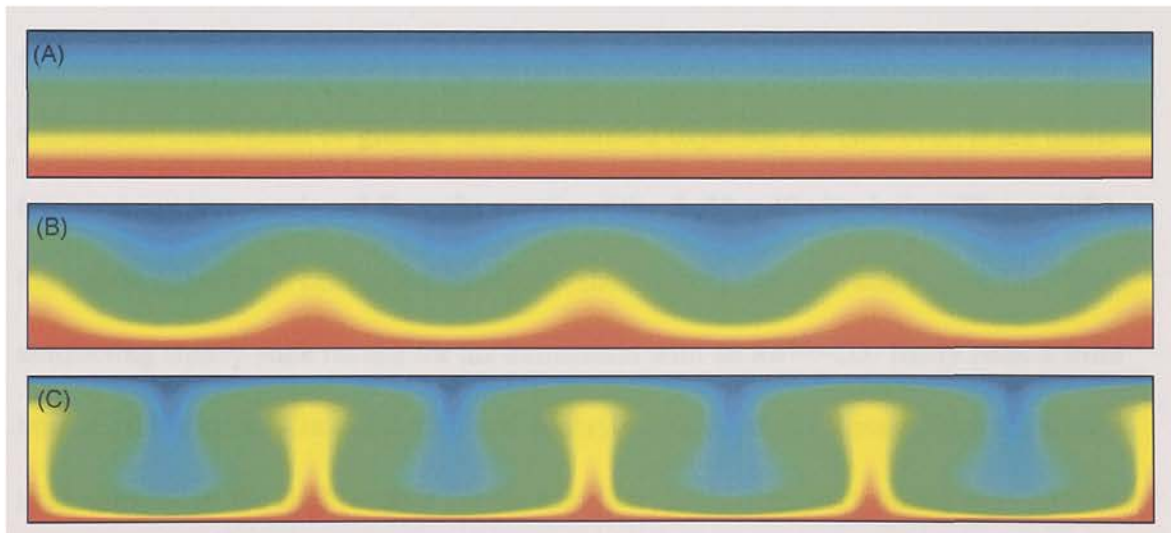


Figure 10: Temperature results for the Horton-Rogers-Lapwood convection problem simulated with SEAWAT. (A) Simulation with $Ra^{}=39$, (B) Simulation with $Ra^{**}=40$, and (C) Simulation with $Ra^{**}=200$. The colors from blue to red show the temperatures for the simulations from $0\text{ }^{\circ}\text{C}$ in blue to $100\text{ }^{\circ}\text{C}$ in red.**

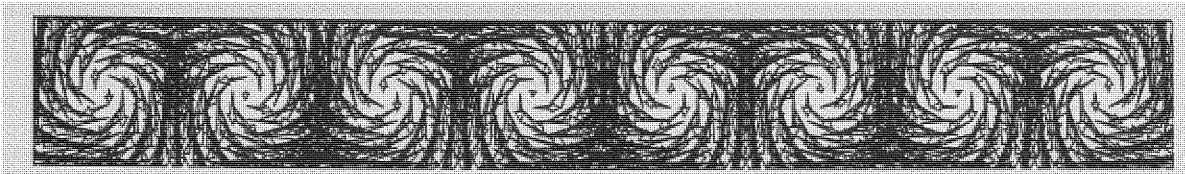


Figure 11: Velocity vectors for the second simulation of the Horton-Rogers-Lapwood problem where $Ra^{}=40$.**

Ataie-Ashtiani and Aghayi (2006) analyzed the suitability of the HRL convection problem for testing variable-density modeling codes. According to Ataie-Ashtiani and Aghayi (2006), the critical Ra^{**} number of $4\pi^2$ may be useful for benchmarking a code; however, the wavelength test ($\lambda = 2H$) does not apply if calculated Ra^{**} numbers are significantly higher than $4\pi^2$. The significantly larger Ra^{**} numbers can cause more convection cells to develop in the model (greater than the aspect ratio, A). Similar results to Ataie-Ashtiani and Aghayi (2006) were also observed with SEAWAT simulations of the HRL problem; however, the research here revealed that initial temperatures affected the number of convection cells. Results from our simulation with a Ra^{**} number of 200 revealed that if initial temperatures were stable such as in Figure 10A, the number of convection cells would be greater than the number expected, 8. However, if the initial temperatures were assigned from the results of the $Ra^{**} = 40$ simulation (Figure 10B), then eight convection cells would result (as shown in Figure 10C and Figure 11). The conflicting steady-state results for the simulation with an $Ra^{**}=200$ likely results from numerical errors, as Ataie-Ashtiani and Aghayi (2006) stated, “It seems that the steady state solution of the IHB [Infinite Horizontal Box] problem is very sensitive to numerical errors (including truncation and round off errors). So even when steady-state solutions of the IHB problem converge to a specific solution... still it cannot be assured that this

stationary solution is unique. Such a phenomenon is observed in some other numerical problems which were based on formation of convective instabilities in porous media.”

The results shown indicate that SEAWAT can correctly simulate conduction versus convection according to results from an analytical solution. However, when simulating density-dependent flow systems with high Ra^{**} numbers, it is important to note that initial temperatures can potentially alter the results. Regardless, results from this benchmark problem lend further confidence in the application of SEAWAT to problems that involve thermally-driven conduction and convection.

2.3.4 Double-Diffusive Finger Convection

Double-diffusive finger convection is an interesting mixing process because density-driven fingering can occur from an initially stable density configuration (a less-dense fluid on top of a more-dense fluid). Consider a case where two miscible solutions with different viscosities are separated by a sharp interface. The solute in the overlying fluid has a molecular diffusion coefficient that is less than the molecular diffusion coefficient of the solute in the underlying fluid. Under these conditions, double-diffusive finger convection can occur in response to small perturbations along the interface, even though the overlying fluid is less dense than the fluid on the bottom. As explained by Hughes and others (2005), "a parcel of fluid perturbed downward across the interface takes on solute mass from the surrounding fluid faster than it diffuses solute mass so the parcel continues to fall."

Pringle and others (2002) documented the process of double-diffusive finger convection in the laboratory using a Hele-Shaw cell. Prior to convection, the cell

consisted of a less-dense sucrose solution overlying a more-dense sodium-chloride (NaCl) solution. The sucrose solution was about 4 kg/m^3 less dense than the underlying NaCl solution. The Hele-Shaw cell was tilted to an angle of 25 degrees from a horizontal plane (Figure 12 and Figure 13). A conservative dye was mixed with the NaCl solution to allow for visual observation of the finger formation and convection. The dye was assumed to have a minimal effect on the density of the NaCl solution. A sequence of laboratory photographs clearly documents the formation and convection of fingers (Figure 14). Actual times, t , are related to the dimensionless times, t^* , listed in Figure 14 by the following equation

$$t^* = \frac{tD^*_{NaCl}}{H^2}, \quad (31)$$

where t is elapsed time in seconds and H is the height of the cell, 0.1625m. By the end of the experiment, the dye is almost entirely mixed throughout the cell.

This double-diffusive finger convection observed in the laboratory experiment was simulated using a modified version of the SUTRA program, SUTRA-MS (Hughes and Sanford, 2004; Hughes and others, 2005). A similar approach is used here to test SEAWAT and its ability to simulate finger convection with multiple diffusion coefficients and variable viscosity. The input parameters, grid dimensions, and solution schemes for the numerical simulation are shown in Table 4. These parameters correspond with those listed by Pringle and others (2002). The simulation domain is the same size as the Hele-Shaw cell (0.2541 m long by 0.1625 m high). The model domain is surrounded on all four sides by no-flow and zero diffusive flux conditions (Figure 13). Constant-head cells with an arbitrary head value of 0.1625 m were placed at the top left

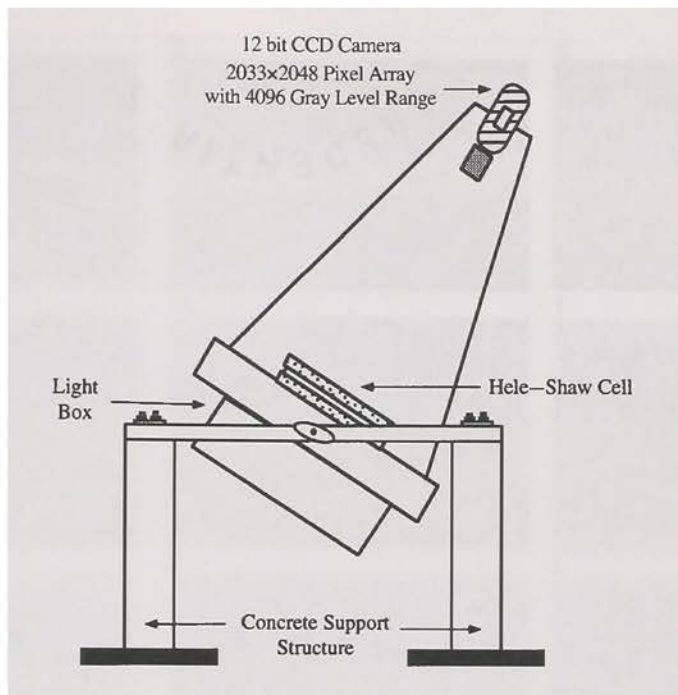


Figure 12: Hele-Shaw cell set up by Pringle and others (2002). Note that the angle of the Hele-Shaw cell from the vertical is the reason that gravity in the simulation is set to 4.14 m/s^2 .

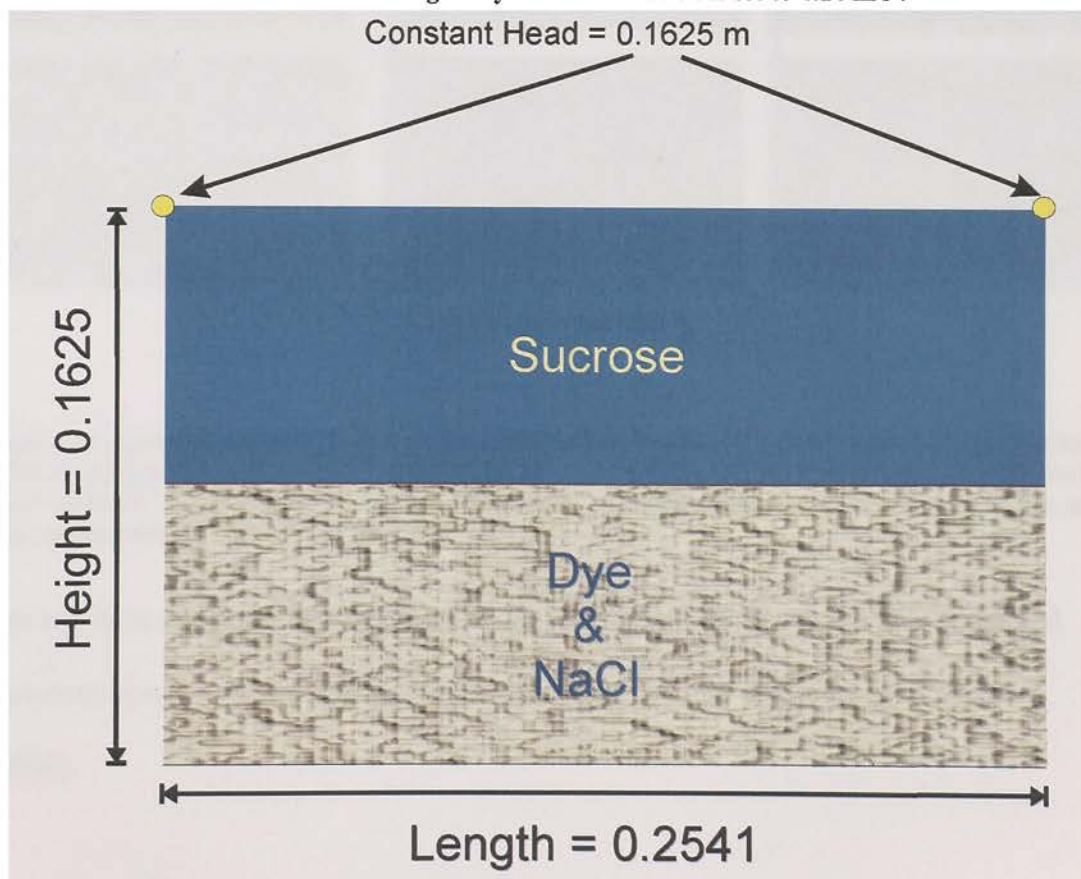


Figure 13: Initial conditions in the Hele-Shaw cell, length and height in meters.

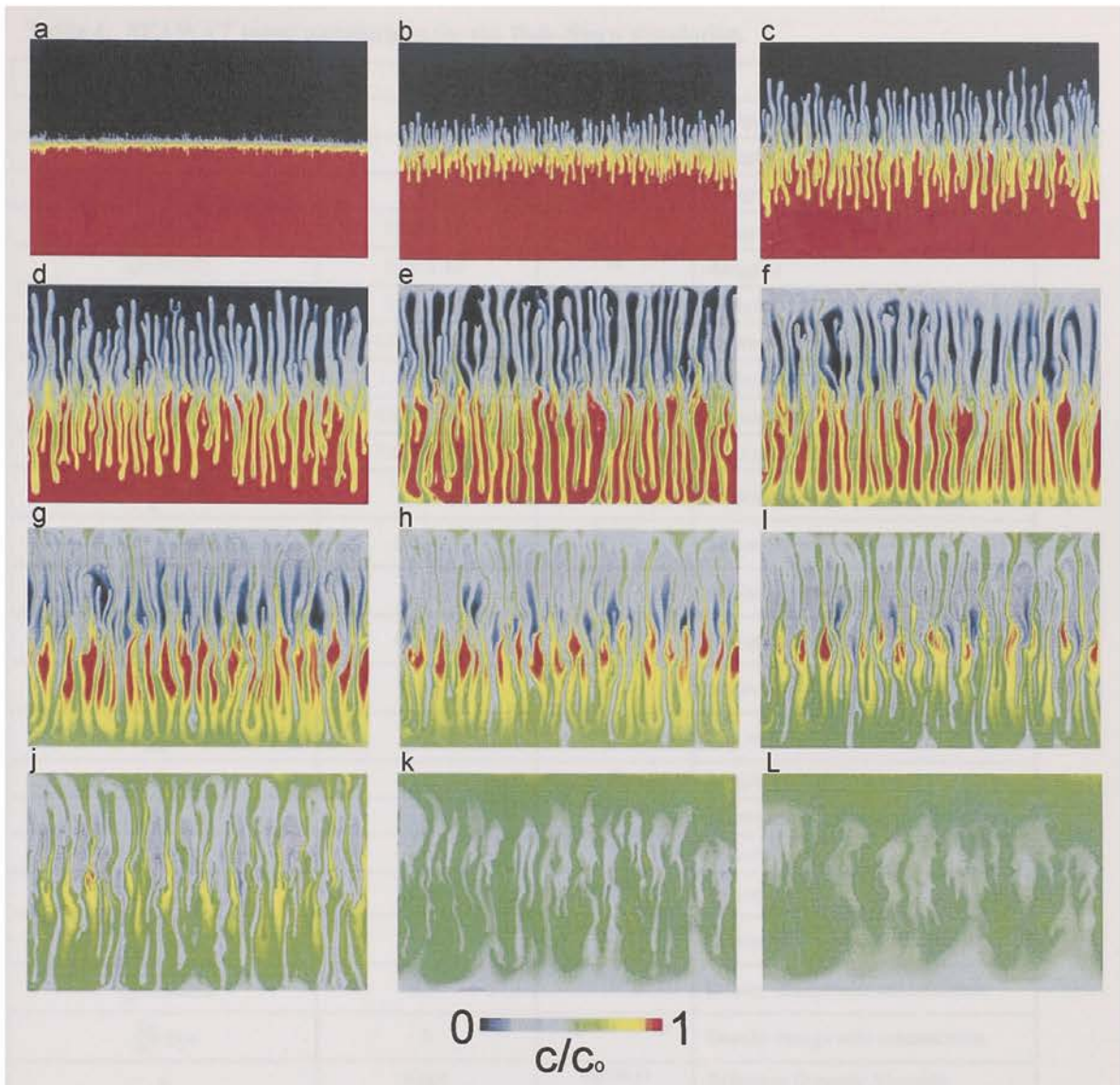


Figure 14: Results from Pringle and others (2002) at (a) $t^*=4.06 \times 10^{-5}$, (b) $t^*=1.29 \times 10^{-4}$, (c) $t^*=3.96 \times 10^{-4}$, (d) $t^*=3.35 \times 10^{-4}$, (e) $t^*=4.35 \times 10^{-4}$, (f) $t^*=5.36 \times 10^{-4}$, (g) $t^*=6.03 \times 10^{-4}$, (h) $t^*=7.37 \times 10^{-4}$, (i) $t^*=8.04 \times 10^{-4}$, (j) $t^*=1.04 \times 10^{-3}$, (k) $t^*=1.78 \times 10^{-3}$, and (l) $t^*=3.19 \times 10^{-3}$. Color sequence is relative concentration of the dye (representative of the NaCl solution).

and top right corners of the model. Random perturbations were applied to the initial concentrations along the interface following the procedure of Hughes and Sanford (2004).

Table 4: SEAWAT input parameters for the Hele-Shaw simulation.

Input Parameter	Value	Units	Comments
Number of columns	1024	-	Assigned
Number of rows	1	-	Assigned
Number of layers	656	-	Assigned
$\Delta x(\text{DELR})$	2.48×10^{-4}	m	Assigned
$\Delta y(\text{DELC})$	2.48×10^{-4}	m	Assigned
$\Delta z(\text{DELZ})$	2.48×10^{-4}	m	Assigned
K	1.0784×10^{-2}	m/s	Hydraulic conductivity
D^* NaCl	1.477×10^{-9}	m^2/s	Molecular diffusion
D^* Sucrose	4.878×10^{-10}	m^2/s	Molecular diffusion
D^* Dye	5.670×10^{-10}	m^2/s	Molecular diffusion
C_o NaCl	0.0	kg/m^3	Minimum concentration
C_{MAX} NaCl	0.03463	kg/m^3	Maximum concentration
C_o Sucrose	0	kg/m^3	Minimum concentration
C_{MAX} Sucrose	0.05234	kg/m^3	Maximum concentration
C_o Dye	0.0	kg/m^3	Minimum concentration
C_{MAX} Dye	1	kg/m^3	Maximum concentration
α_L	0	m	Longitudinal dispersivity
α_T	0	m	Transverse dispersivity
θ	1.0	-	Porosity
ρ_{water}	998	kg/m^3	Density of freshwater
$\frac{\partial \rho}{\partial C}$ NaCl	689	-	Density change with concentration
$\frac{\partial \rho}{\partial C}$ Sucrose	371	-	Density change with concentration
$\frac{\partial \rho}{\partial C}$ Dye	0	-	Density change with concentration
μ	0.001	$\text{kg}/(\text{m s})$	Reference Dynamic Viscosity
$\frac{\partial \mu}{\partial C}$ NaCl	1.59×10^{-3}	m^2/s	Viscosity change with concentration
$\frac{\partial \mu}{\partial C}$ Sucrose	2.75×10^{-3}	m^2/s	Viscosity change with concentration
$\frac{\partial \mu}{\partial C}$ Dye	0	m^2/s	Viscosity change with concentration
G	4.14	m/s^2	Acceleration due to gravity
Matrix solution technique for flow	PCG2	-	Assigned
Head convergence value	1.0×10^{-6}	m	Assigned
Flow convergence value	1	kg/s	Assigned
Length of stress period	57600	s	Steady-state model, one stress period
Advection term	Implicit Finite Difference-Central in Space Weighting	-	Assigned

Dispersion and source terms	Implicit finite difference; GCG	-	Assigned
Maximum transport step length	10	s	Assigned
Concentration convergence value	1×10^{-10}	kg/m ³	Assigned

2.3.4.1 Results and Discussion

The laboratory photographs shown in Figure 14 can be directly compared to the dye concentrations from the SEAWAT simulation shown in Figure 15. The close comparison between the laboratory experiment and results from SEAWAT reveal that SEAWAT is capable of representing the complex process of double-diffusive finger convection. This is an additional demonstration of the correct implementation of multiple diffusion coefficients, variable viscosity, and variable-density flow in the SEAWAT code.

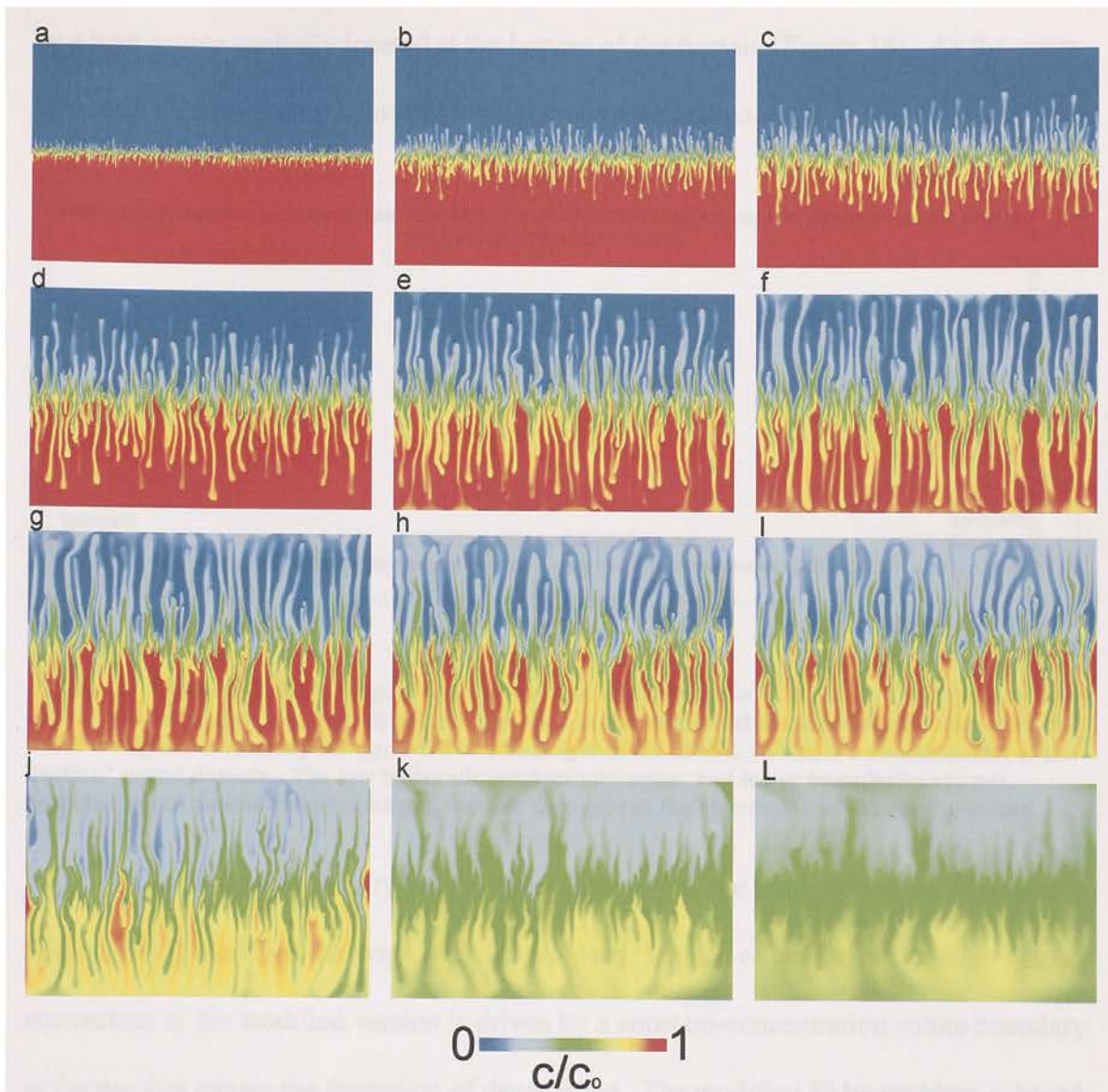


Figure 15: Results from SEAWAT at (a) $t^*=4.06 \times 10^{-5}$, (b) $t^*=1.29 \times 10^{-4}$, (c) $t^*=3.96 \times 10^{-4}$, (d) $t^*=3.35 \times 10^{-4}$, (e) $t^*=4.35 \times 10^{-4}$, (f) $t^*=5.36 \times 10^{-4}$, (g) $t^*=6.03 \times 10^{-4}$, (h) $t^*=7.37 \times 10^{-4}$, (i) $t^*=8.04 \times 10^{-4}$, (j) $t^*=1.04 \times 10^{-3}$, (k) $t^*=1.78 \times 10^{-3}$, and (l) $t^*=3.19 \times 10^{-3}$. Color sequence is relative concentration of the dye (representative of the NaCl solution).

2.3.5 Elder Problem

The classic laboratory experiment reported by Elder (1967) has been widely used to test numerical codes (i.e., Voss and Souza, 1987; Guo and Langevin, 2002). The original Elder problem consists of two-dimensional, thermally-driven convection caused

by a heat source centrally located at the bottom of the domain (Figure 16). As the water is heated, it rises causing convection within the cross section.

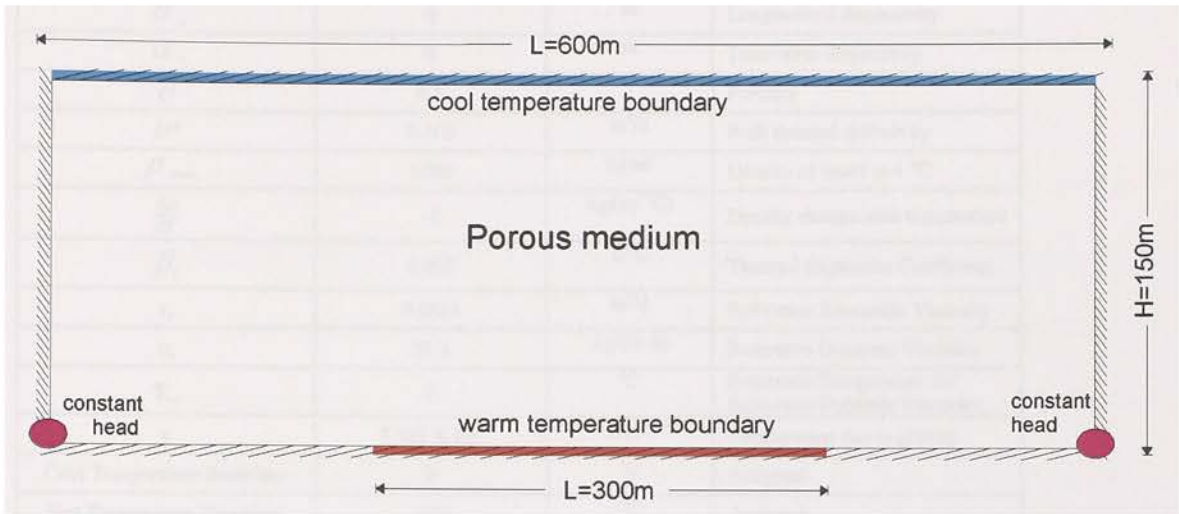


Figure 16: Set-up of Elder’s original experiment that is simulated in SEAWAT. The constant-head cells at the bottom left and right-hand side are used in the numerical simulation but do not exist in Elder’s original laboratory set-up. NOTE: The height of the model, 150 m, is a measurement of the “active” model domain. The low hydraulic conductivity upper and lower boundaries are not included in the measurement of height, nor are they part of the calculation of the Ra^{} number.**

To test variable-density groundwater flow and solute transport codes, Voss and Souza (1987) modified the original Elder problem. Instead of heating water from below, convection in the modified version is driven by a constant-concentration solute boundary at the top that causes the formation of dense brine. The modified Elder problem is based on a set of parameters (Table 5) that result in an identical Rayleigh** number to that used in the original experiment.

Table 5: Input parameters for the Elder problem simulated in SEAWAT.

Input Parameter	Value	Units	Comments
Number of columns	88	-	Assigned
Number of rows	1	-	Assigned
Number of layers	52	-	Assigned
$\Delta x(\text{DELR})$	6.818	m	Assigned
$\Delta y(\text{DELC})$	6.818	m	Assigned

$\Delta z(\text{DELZ})$	3	m	Assigned
K	0.411	m/d	Hydraulic conductivity
k	4.85×10^{-13}	m ²	Permeability
α_L	0	m	Longitudinal dispersivity
α_T	0	m	Transverse dispersivity
θ	0.1	-	Porosity
D^*	0.308	m ² /d	Bulk thermal diffusivity
ρ_{water}	1000	kg/m ³	Density of water at 4 °C
$\frac{\partial \rho}{\partial T}$	-2	kg/(m ³ °C)	Density change with temperature
β_t	0.002	1/°C	Thermal Expansion Coefficient
ν_o	0.0864	m ² /d	Reference Kinematic Viscosity
μ_o	86.4	kg/(m d)	Reference Dynamic Viscosity
T_{ref}	0	°C	Reference Temperature for Reference Dynamic Viscosity
g	7.323×10^{10}	m/d ²	Acceleration due to gravity
Cool Temperature Boundary	0	°C	Assigned
Hot Temperature Boundary	100	°C	Assigned
Matrix solution technique for flow	PCG2	-	Assigned
Head convergence value	1×10^{-7}	m	Assigned
Flow convergence value	1000	kg/d	Assigned
Flow time-step length	60 time steps with time step multiplier of 5	d	Assigned
Advection term	Implicit Finite Difference: upstream weighting	-	Assigned
Dispersion and source terms	Implicit finite difference; GCG, SSOR	-	Assigned
Transport time-step length	Calculated using Courant of 0.1	d	Assigned
Temperature convergence value	1×10^{-10}	°C	Assigned

The original Elder problem is used here to further test the ability of SEAWAT to simulate thermally-driven convection. There is no analytical solution therefore SEAWAT results are compared with (1) the original numerical results from Elder (1967), (2) results from a previous version of SEAWAT (Guo and Langevin, 2002), and (3) results from SUTRA (Voss, 1984; Voss and Souza, 1987; Prasad and Simmons, 2005).

The design of the Elder problem simulated in SEAWAT is shown in Figure 16 with the model parameters, grid dimensions, and solution schemes given in Table 5. This numerical model simulates freshwater with variations in temperature for 7300 days (or 20 years). The top boundary was set at a constant temperature boundary of zero. A relatively low hydraulic conductivity value of 1×10^{-5} m/d was also assigned to the top layer to minimize the advective heat flux from the boundary. The bottom boundary has a constant temperature of 100°C from columns 23 to 66 and also has a relatively low hydraulic conductivity value. Constant-head boundary cells of zero are placed at the bottom left and bottom right corners to ensure convergence of the flow solution. The initial temperature is set everywhere to zero. The temperature values of zero and 100°C are arbitrary in this case; the value for $\frac{\partial \rho}{\partial T}$ was calculated such that the Ra^{**} number is equal to 400, the value for the original Elder problem. (As stated previously, the actual temperature values are not important for certain benchmark problems. What is pertinent is that the correct Ra^{**} of 400 is calculated for the “active” model domain in Figure 16. Different temperature values could have been used with the values for $\frac{\partial \rho}{\partial T}$ or the permeability modified to calculate a Ra^{**} number equal to 400.)

2.3.5.1 Results and Discussion

Results from SEAWAT compare reasonably well to the original Elder (1967) results, SUTRA results from Voss and Souza (1987), and results from a previous version of SEAWAT (Figure 17). There are visual differences in the isotherm (or isochlor) contours and timing of the maximum penetration depth of the 60% isotherm. The

discrepancy in results is likely due to differences in grid dimensions, time step length, or solution schemes. Variations in discretization and solution schemes have been shown to affect simulation results for the Elder problem (Frolkovic and Schepper, 2000; Diersch and Kolditz, 2002; Simpson and Clement, 2004; Thorne and Sukop, 2004; Al-Maktoumi and others, 2007).

Prasad and Simmons (2003, 2005) and Elder (1967) calculated the Nusselt number (equation (25)) with time for their Elder simulations. The temporal variation in the Nusselt number is shown in Figure 18 for SEAWAT, the SUTRA results from Prasad and Simmons (2003), and the numerical results from Elder (1967). The results are similar between the three models, particularly the results from SUTRA and SEAWAT, however some differences are evident. These differences could be due to using different modeling codes, numerical discretization, temporal discretization, or solution schemes. The similarities between the graphs reveal how the simulations are alike in the timing and amount of the transfer of energy (or solute in Prasad and Simmons, 2003), as well as the energy transfer mechanism. Overall, the three different models have a similar total flux compared to the expected conductive or diffusive flux. (For more details, see the discussion of the Nusselt number in the section “Dimensionless Numbers”.)

Favorable comparisons of SEAWAT Version 4 results with the results from other programs suggest that SEAWAT is capable of simulating the complex convective flow patterns that result from temperature variations as shown by the Elder problem. The results from Elder, in conjunction with results from the HRL benchmark problem, reveal that SEAWAT accurately simulates thermally-driven convection, conduction, and heat transport.

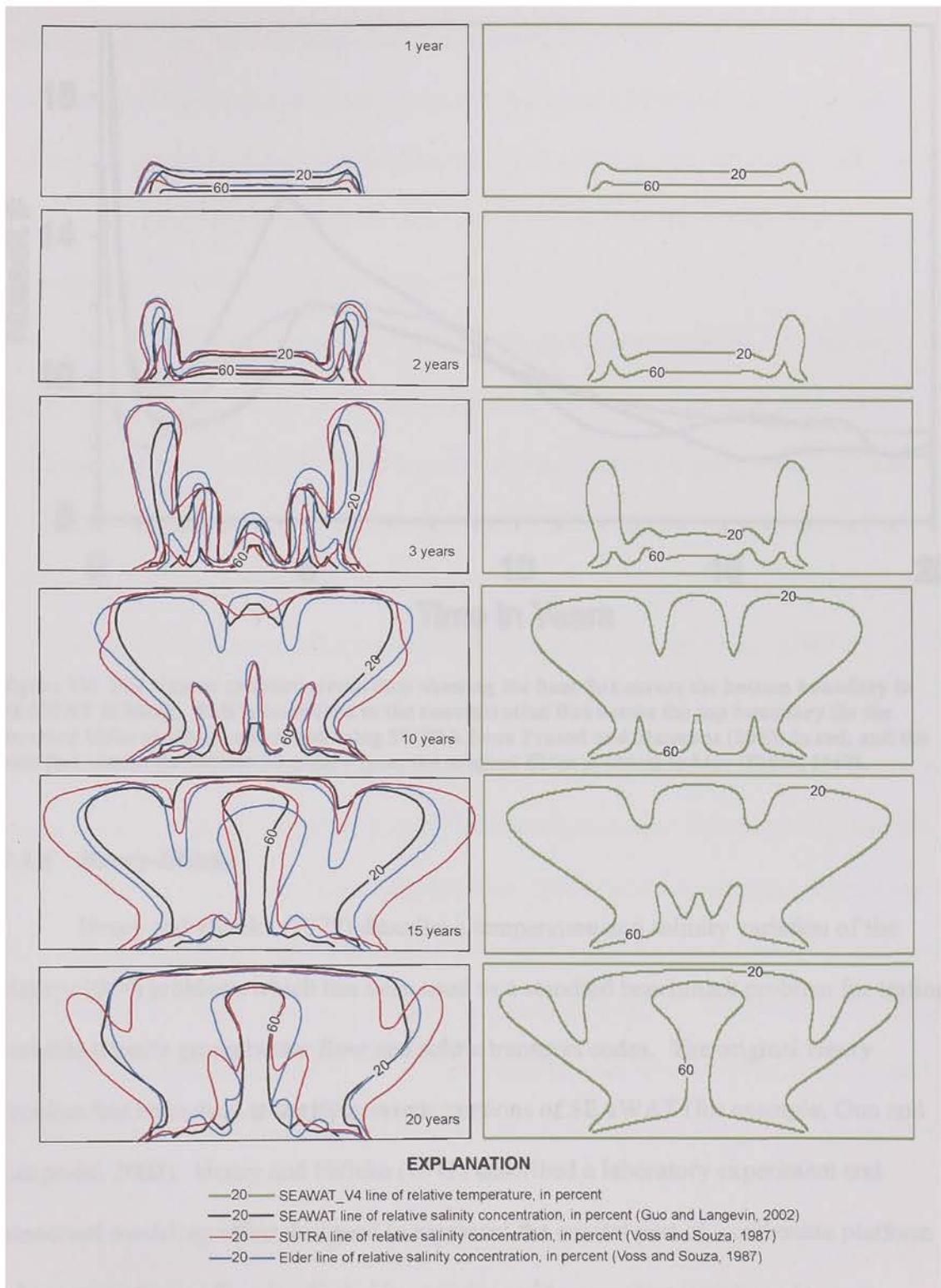


Figure 17: Results of SEAWAT Version 4 compared to the original lab results from Elder, SUTRA (rotated), and an older version of SEAWAT (rotated) (Figure modified from Guo and Langevin, 2002).

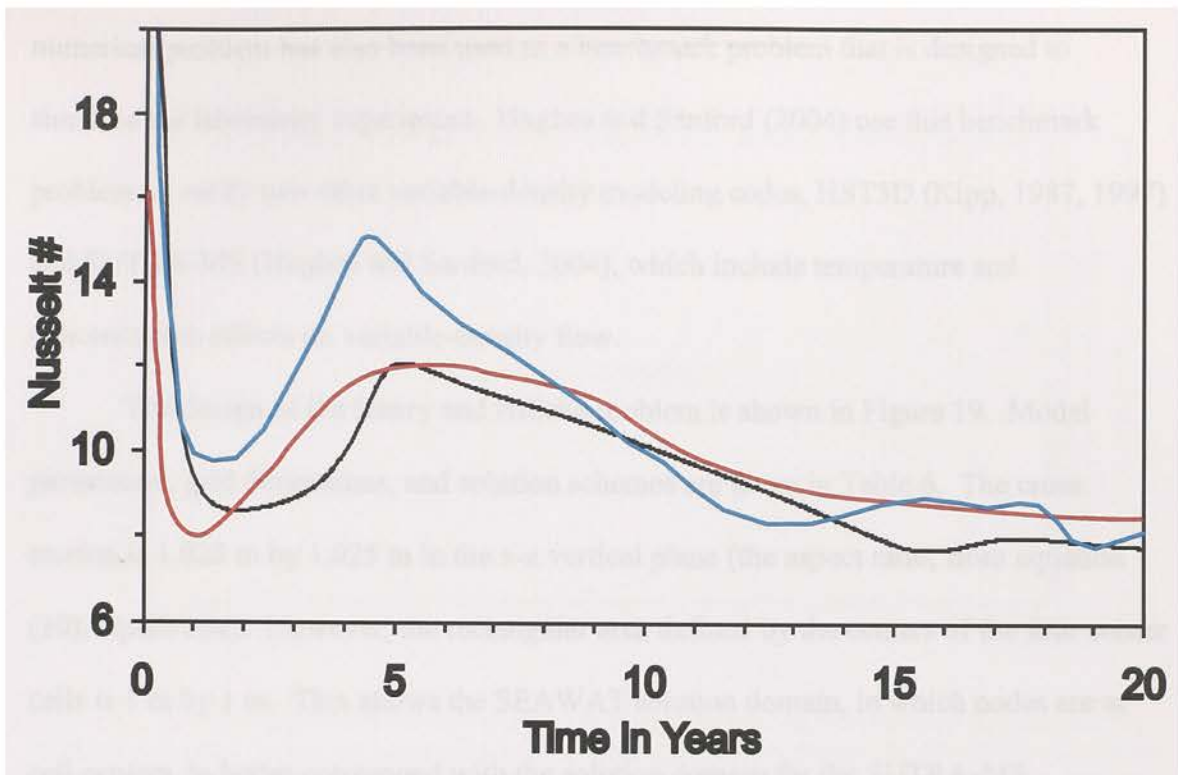


Figure 18: The Nusselt number versus time showing the heat flux across the bottom boundary in SEAWAT in black. This is compared to the concentration flux across the top boundary (in the inverted Elder problem) simulated using SUTRA from Prasad and Simmons (2003) in red, and the heat flux across the bottom boundary from the original Elder problem in blue (Elder, 1967).

2.3.6 Henry-Hilleke

Henry and Hilleke (1972) describe a temperature and salinity variation of the Henry (1964) problem, which has been used as a standard benchmark problem for testing variable-density groundwater flow and solute transport codes. The original Henry problem has been used to verify previous versions of SEAWAT (for example, Guo and Langevin, 2002). Henry and Hilleke (1972) described a laboratory experiment and numerical modeling effort designed to represent the coastal part of a carbonate platform where groundwater flow is affected by salinity and temperature variations (a more thorough discussion will be presented in Chapter 3). The Henry and Hilleke (1972)

numerical problem has also been used as a benchmark problem that is designed to simulate the laboratory experiment. Hughes and Sanford (2004) use this benchmark problem to verify two other variable-density modeling codes, HST3D (Kipp, 1987, 1997) and SUTRA-MS (Hughes and Sanford, 2004), which include temperature and concentration effects on variable-density flow.

The design of the Henry and Hilleke problem is shown in Figure 19. Model parameters, grid dimensions, and solution schemes are given in Table 6. The cross section is 1.025 m by 1.025 m in the x-z vertical plane (the aspect ratio, from equation (30), equals one). However, the rectangular area defined by the centers of the four corner cells is 1 m by 1 m. This allows the SEAWAT solution domain, in which nodes are at cell centers, to better correspond with the solution domain for the SUTRA-MS representation, in which nodes are at the corners of elements. SUTRA-MS is a finite-element code and allows for elements to be placed along boundaries. The right boundary has seawater concentrations of 35.7 kg/m^3 with a constant-head flow boundary, and the left boundary has a constant influx of freshwater. The model has constant temperature cells surrounding the domain (Figure 19). The right boundary has a constant temperature of 5°C , the lower left corner has a constant temperature of 50°C , and the upper left corner has a constant temperature of 38.75°C . Temperatures vary linearly along the boundary. Equations used to calculate the constant temperature at each cell along the boundary are shown in Figure 19.

As discussed earlier, an exception to the hydraulic conductivity is along the layers of the top and bottom boundaries (which are constant temperature cells with a lower hydraulic conductivity of 432 m/d as compared to the bulk of the domain, 864 m/d). This

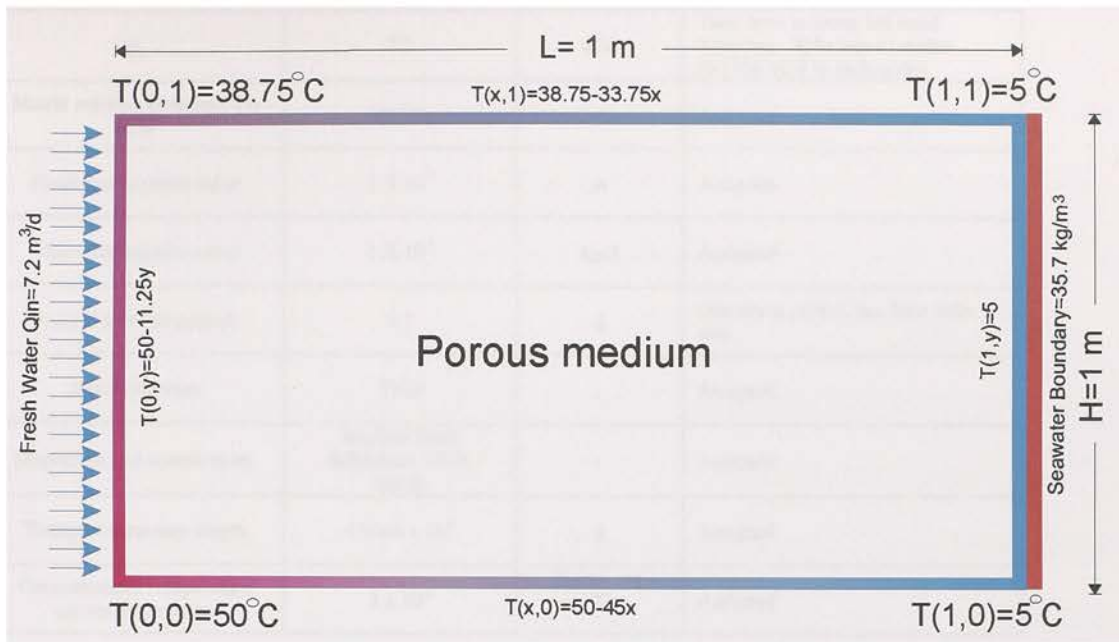


Figure 19: Set-up of the Henry-Hilleke problem showing the boundary conditions that include: (1) freshwater input, (2) seawater boundary, and (3) temperature boundaries. NOTE: Horizontal scale is exaggerated for comparison with other modeling results.

Table 6: Input parameters for the Henry-Hilleke problem simulated in SEAWAT.

Input Parameter	Value	Units	Comments
Number of columns	41	-	Assigned
Number of rows	1	-	Assigned
Number of layers	41	-	Assigned
$\Delta x(\text{DELR})$	0.025	m	Assigned
$\Delta y(\text{DELC})$	1	m	Assigned
$\Delta z(\text{DELZ})$	0.025	m	Assigned
K	864	m/d	Hydraulic conductivity
α_L	0	m	Longitudinal dispersivity
α_T	0	m	Transverse dispersivity
θ	0.35	-	Porosity
D_m^*	2.0571	m ² /d	Molecular diffusivity
D^*	20.571	m ² /d	Thermal diffusivity
ρ_f	1000	kg/m ³	Density of freshwater
ρ_s	1025	kg/m ³	Density of seawater
$\frac{\partial \rho}{\partial C}$	0.7	-	Density change with concentration
$\frac{\partial \rho}{\partial T}$	-0.375	kg/(m ³ °C)	Density change with temperature
ν_o	0.0864	m ² /d	Reference Kinematic Viscosity
μ_o	86.4	kg/(m d)	Reference Dynamic Viscosity
T_{ref}	0	°C	Reference Temperature for Reference Dynamic Viscosity

Q_{in}	7.2	m ³ /d	Total flow in along left hand boundary. Split into 41 nodes (0.1756 m ³ /d in each node)
Matrix solution technique for flow	PCG2	-	Assigned
Head convergence value	1 X 10 ⁻⁷	m	Assigned
Flow convergence value	1 X 10 ⁻⁷	kg/d	Assigned
Length of stress period	0.2	d	One stress period, one flow time step
Advection term	TVD	-	Assigned
Dispersion and source terms	Implicit finite difference; GCG, SSOR	-	Assigned
Transport time-step length	6.9444 x 10 ⁻⁴	d	Assigned
Concentration/Temperature convergence value	1 x 10 ⁻⁶	kg/m ³ , or °C	Assigned

lowered hydraulic conductivity is to minimize the convective heat flux from the temperature boundaries. Even though there is no water entering the model from the top and bottom boundaries, water that enters and leaves the system from the ocean and freshwater boundaries, along the sides, can actually flow up or down through the top and bottom cells along the boundary. This water isn't discharged from the system at the top and bottom boundaries, but flowing through the cells and entering back into the model domain. This flowing water advects heat from the boundary as it enters back into the system if the hydraulic conductivity is too high at 864 m/d. The numerical Henry-Hilleke problem simulated in SUTRA-MS (a finite difference code), does not have advective heat flux from these boundaries (only diffusive) because the boundary is enforced right at a node at the bounding surface.

2.3.6.1 Results and Discussion

SEAWAT successfully simulates the Henry and Hilleke problem and results are compared to SUTRA-MS and HST3D (Hughes and Sanford, 2004; Thorne and others, 2006), as well as the original Henry and Hilleke problem (1972). Results from SUTRA-MS, HST3D, Henry-Hilleke, and SEAWAT are shown in Figure 20, Figure 21, and Figure 22. Velocity vectors for SUTRA-MS and SEAWAT compare favorably with same observed pattern in both models (Figure 22). Concentration and temperature contours between SUTRA-MS and SEAWAT are almost identical (Figure 20 and Figure 21), and compare well with HST3D. There are slight differences between concentration contours for HST3D and contours for SUTRA-MS and SEAWAT, but these differences are minimal.

Concentration and temperature results from SEAWAT, SUTRA-MS, and HST3D do not compare particularly well to the numerical solution from Henry-Hilleke, although the general shape of the contours is the same. The differences are likely because the Henry and Hilleke (1972) numerical solution is a “simplified form of the variable-density flow and transport equation” (Hughes and Sanford, 2004) as compared to the equations used in SUTRA-MS and SEAWAT. When the aspect ratio (equation (30)) is much smaller than one however, results from Henry and Hilleke (1972) are similar to SUTRA-MS (Hughes and Sanford, 2004). Hughes and Sanford (2004) give a more detailed discussion of the effects of grid and mesh resolution on the numerical simulation of the Henry and Hilleke problem. Their results show that the smaller the aspect ratio, the more similar the results are from Henry and Hilleke (1972) and SUTRA-MS.

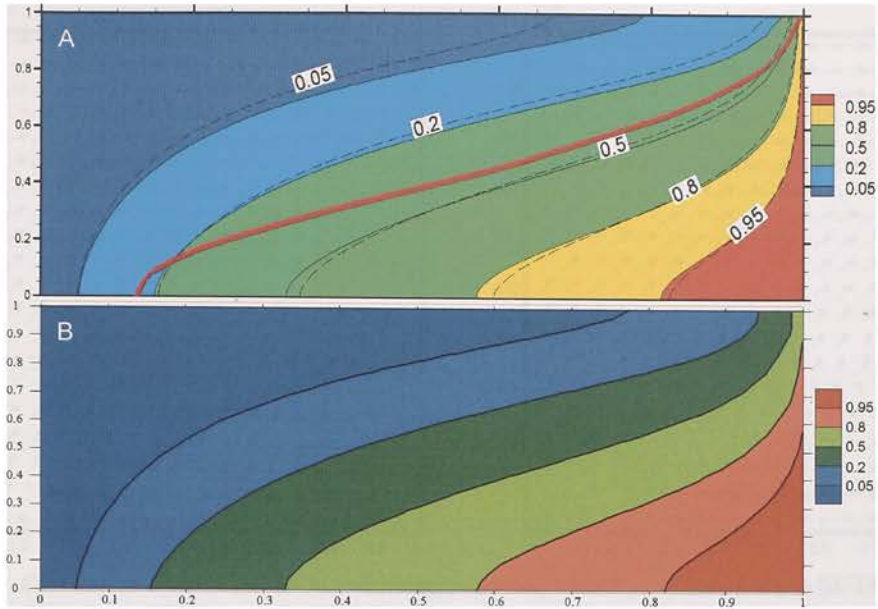


Figure 20: One meter by one meter box showing resulting percent seawater concentrations from (A) SUTRA-MS in color with the solid black lines, Henry and Hilleke numerical solution shown as the 50% contour in the solid red line, and HST3D results shown as the dashed black line (Hughes and Sanford, 2004), and (B) SEAWAT in color with the solid black lines. NOTE: Horizontal scale is exaggerated.

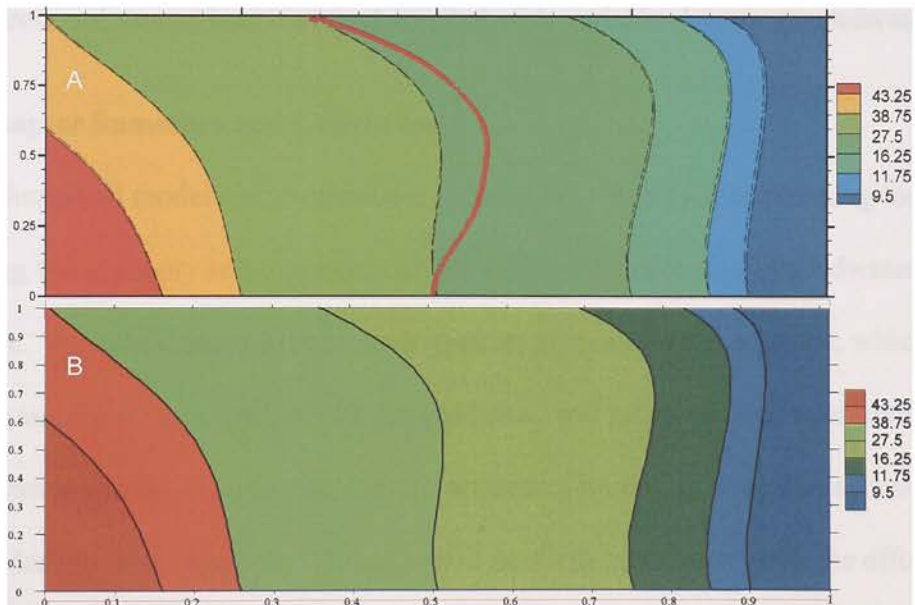


Figure 21: One meter by one meter box showing resulting temperatures in degrees Celsius from (A) SUTRA-MS in color with the solid black lines, Henry and Hilleke numerical solution shown as the 27.5 °C contour in the solid red line, and HST3D results shown as the dashed black line (Hughes and Sanford, 2004), and (B) SEAWAT in color with solid black lines. NOTE: Horizontal scale is exaggerated.

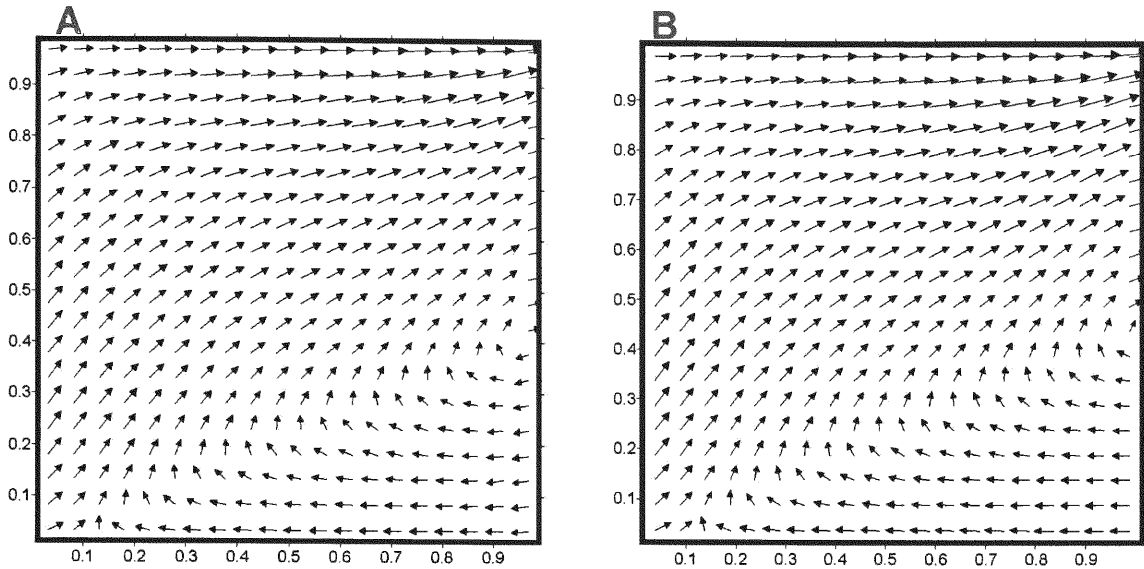


Figure 22: One meter by one meter box showing resulting velocity vectors for (A) SUTRA-MS (Hughes and Sanford, 2004), and (B) SEAWAT.

SEAWAT reasonably simulates the Henry and Hilleke problem as compared to other variable-density modeling codes that have successfully simulated this benchmark problem. This is additional confirmation that SEAWAT can successfully simulate simultaneous solute and heat transport coupled with variable-density groundwater flow.

2.4 Chapter Summary and Conclusions

Numerical models of groundwater systems are often used as planning tools for improving water supply and management, as well as understanding groundwater flow processes. Variable-density groundwater systems such as coastal aquifers, which include saltwater and freshwater, wastewater disposal sites, salt lakes, or deep aquifers affected by geothermal heating, require the use of a numerical modeling code that solves the variable-density flow equation. This equation needs to include not only the effects of concentration on density, but also temperature.

Depending on the temperature or concentration of the water, their effects on viscosity and molecular diffusion may need to be included as well. The most recent

published version of the SEAWAT program, SEAWAT Version 4, supports equations of state for fluid density and viscosity. The code can be used to simultaneously simulate salinity and temperature effects on variable-density flow in water, as well as, in oil (as a single phase). Variations in viscosity from changes in temperature or concentration have also been included, as well as the ability to implement distinct diffusion coefficients to accommodate multiple species. Because thermal diffusivity can be an order of magnitude higher than molecular diffusion, the capacity to include multiple diffusion coefficients is pertinent when simulating salinity and temperature concurrently.

This chapter documents the first thorough verification of SEAWAT by benchmarking the code against six previously published numerical modeling, analytical, or laboratory problems. Results from the benchmark problems reveal that the following equations and/or processes have been implemented correctly in the code: (1) density-dependent flow due to changes in temperature and/or concentration of one or more species, (2) temperature or concentration dependent fluid viscosity, and (3) molecular diffusion of multiple species (including solute and heat). Results from the benchmark problems also reveal that SEAWAT can correctly simulate convective versus conductive transport of heat/energy through a porous medium. In the process of exploring the effects of viscosity on convection versus conduction, it is apparent that the critical Rayleigh number is different in a variable viscosity model.

In summary, the newest version of SEAWAT, SEAWAT Version 4, has been expanded to simulate single phase liquids with concentrations from fresh to brine. Included in the new version is the ability to simulate temperature and concentration effects on density and viscosity. This expanded version of the code could be used to aid

in solving multiple field problems such as water supply and waste disposal. This dissertation is the first verification of this new modeling code's capabilities.

3 QUANTIFYING DATA CONTRIBUTIONS TOWARD REDUCING PREDICTIVE UNCERTAINTY IN A VARIABLE-DENSITY FLOW AND SOLUTE/HEAT TRANSPORT MODEL

3.1 Introduction

In deeper aquifer systems, such as the Floridan aquifer, it is theorized that heat as well as salinity, affects flow in the aquifer (Kohout, 1965). Kohout offered a conceptual model for groundwater flow in the Floridan Plateau (Figure 23), wherein cold seawater enters the base of the Floridan aquifer and is warmed by geothermal heating as the water nears the center of the platform. Then, the less-dense warm water circulates upward toward the surface (Figure 24). In an environment such as this, it is thought that large difference in temperature could affect overall movement of the saltwater-freshwater interface as displayed in the laboratory experiments of Henry and Hilleke (1972).

In coastal areas, interface movement and saltwater intrusion are topics of concern to water supply managers and scientists, primarily because saltwater in the aquifer can contaminate coastal well fields and damage freshwater aquifer systems (Dausman and Langevin, 2005). It is difficult to quantify movement of the interface however, because spatial variations in recharge, aquifer hydraulic properties, tides, geothermal heating and other complicating factors can affect patterns and rates of variable-density groundwater flow (Henry and Hilleke, 1972), such as in the Floridan Plateau. Therefore, variable-density numerical models are often used for management purposes to simulate

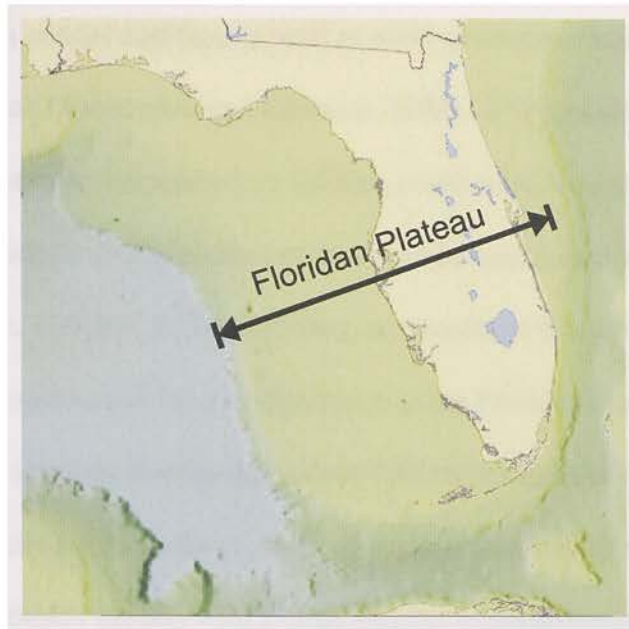


Figure 23: Floridan Plateau where the Peninsula of Florida is on the eastern part of the plateau (from USGS CMG InfoBank Atlas: Florida EEA regions).

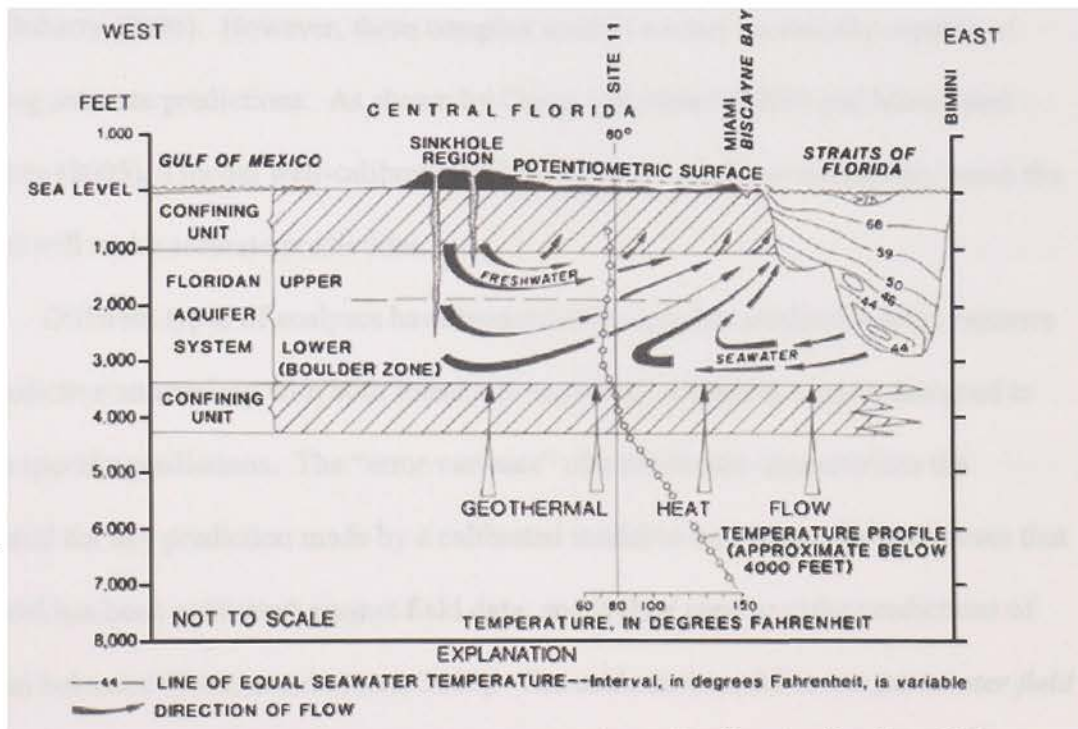


Figure 24: Kohout's conceptualization of convective flow in the Floridan Aquifer (from Kohout, 1965).

groundwater flow in coastal aquifers, as well as make predictions such as movement of the saltwater interface (Shoemaker and Edwards, 2003). It is hypothesized that certain types of data, for example temperature or salinity, could improve a numerical model's ability to make a prediction. Could temperature data be used as a tracer for the origin of the water (Anderson, 2005) or aid in predicting movement of the saltwater-freshwater interface in a model developed for a system (such as the Floridan Plateau)?

Models that simulate density-dependent flow resulting from differences in temperature and solute concentrations are often complicated, and therefore costly to develop. Highly complex models with a large number of parameters enable simulation of complicated environmental processes as shown by Hunt and others (2007) and Moore and Doherty (2006). However, these complex models are not necessarily capable of making accurate predictions. As shown by Carter and others (2006) and Moore and Doherty (2005), a model well-calibrated to historical data does not necessarily mean the model will make accurate predictions.

Different types of analyses have been used to calculate predictive error variance or predictive uncertainty with both linear and nonlinear numerical models designed to make specific predictions. The "error variance" of a prediction characterizes the potential for any prediction made by a calibrated model to be wrong. This supposes that a model has been calibrated against field data, and is then used to make predictions of system behavior (Tonkin and others, 2007). The calibrated model is *one parameter field* that represents the system. This is a similar, but slightly different concept to that of "predictive uncertainty". Predictive uncertainty attempts to characterize the potential variability of a prediction, based on the uncertainty associated with *multiple parameter*

fields employed by a model (Tonkin and others, 2007). The model is constrained because the parameter fields must correctly simulate historical system behavior; however, there is not a single calibrated model, but multiple models. When discussing linear or nonlinear models, the term “linear” refers to the relationship between parameters employed by the model and outputs calculated by the model. These relationships are assumed to be representable by a simple matrix, whose coefficients have no dependence on parameter values (essentially, an input parameter change results in a linear response in model output). A model is considered “nonlinear” when an input parameter change does not result in a linear response in model output. Therefore, the coefficients in a matrix, which represents the sensitivity of a model output to parameter input, are dependent on the parameter value (Aster and others, 2005).

Simple models, with a small number of parameters, have been used to calculate predictive error variance using linear analysis by Draper and Smith (1981) and nonlinear analysis by Vecchia and Cooley (1987) and Christensen and Cooley (1999). Moore and Doherty (2005) also derive a linear equation through which post-calibration predictive error variance can be calculated for a model. However, these models are calibrated with a small number of parameters and the subjective judgment of the model developer plays a large part in the simplification process. Therefore, the parameter simplification can hinder the model’s ability to make an accurate prediction. Several nonlinear methods have also been developed to quantify predictive error of highly parameterized models using regularized inversion including Tonkin and Doherty (2005), Tonkin and others (2007), and Tonkin and Doherty (2008).

When addressing predictive uncertainty, the uncertainty related to a model prediction, there is not an assumption of a single “calibrated” model. The concept of uncertainty is based on the fact that because model parameters and inputs are uncertain, then so too are model outputs. “Predictive uncertainty analysis abandons the idea of parameter uniqueness by acknowledging that many different parameter sets enable the model to reproduce the available observations” (Tonkin and others, 2007); therefore, models that are parameterized in many different ways can be considered to be “correct” (at various levels of confidence) and used to make a prediction. This notion of uncertainty is encapsulated in Bayes Theorem (1763), where parameter and predictive probability/uncertainty can be calculated based on the available observation data and multiple parameter sets of “maximum likelihood”. Parameter and predictive uncertainty analysis can be implemented using a constrained Monte Carlo approach (Zimmerman, 1998; Carrera and others 2005) or other methods such as the Generalized Likelihood Uncertainty Estimation (GLUE) of Beven and Binlay (1992). A new nonlinear method, referred to as null-space Monte Carlo, described by Tonkin and Doherty (2008) can be readily used in the highly parameterized setting.

Previous studies have gone to great lengths to determine predictive uncertainty and predictive error variance, using either a calibrated or uncalibrated model. However, few modeling studies have been specifically designed to guide the collection of field data to improve a model’s ability to make predictions. The data collection strategy is often designed to fill in “gaps” in the model domain. It is hypothesized that there are times when the data collected will not improve the prediction for which the model was developed. Therefore, the data are not worth collecting in order to increase the model’s

predictive capability. It is also hypothesized that the quantification of the worth of data can be calculated prior to data acquisition. When predictive uncertainty can be quantified, so too can the reduction in predictive uncertainty accrued through collection of different types of data; therefore, optimization of data acquisition can be undertaken.

Two methods currently exist in groundwater modeling that address quantification of the worth of data when analyzing predictive error variance or predictive uncertainty in a numerical model. Hill and Tiedeman (2007) and Tonkin and others (2007) present a method that uses the OPR-PPR (Observation-Prediction and Parameter-Prediction) statistic to quantify the worth of data in reducing predictive error variance. The OPR-PPR statistic can only be used in an overdetermined modeling context (“overdetermined” is defined as having more observations than parameters; therefore, the parameters employed by the model are few enough to be estimated uniquely on the current calibration dataset) and the model must be calibrated before the statistic for data worth can be calculated. In contrast, Christensen and Doherty (2008) present a methodology to address data worth in reducing predictive uncertainty that does not rely on the need for formulation of an overdetermined inverse problem. While the method takes into account the existence of a historical dataset, it does not assume the existence of a calibrated model. Therefore, its formulation of data worth is based on the reduction in predictive uncertainty accrued through acquisition of new data, and not the reduction in predictive error variance of a model that has notionally been calibrated against a historical dataset.

The predictive uncertainty method presented by Christensen and Doherty (2008) is linear, which is both its strength and its weakness. The assumption of a linear relationship between model parameters and model outputs allows for rapid computation

of parameter/predictive uncertainty with/without inclusion of past and/or future data. This linear relationship can be described by a matrix with coefficients that are parameter-independent, where an input in parameter change results in a linear response in model output. These coefficients are sometimes referred to as “sensitivities” of model outputs with respect to parameters. Using the linear method, only sensitivities of model outputs with respect to parameters are required for computation of uncertainty (and uncertainty reduction); therefore, the actual values of parameters and observations comprising the historical dataset do not need to be known. Only coefficients in the matrix that relates parameters to model outputs are necessary (the sensitivity matrix). A disadvantage of the linear method is that often model outputs are not linear with respect to the parameters that they employ (the outputs are dependent on the current value of the parameter). When applying a linear method to a nonlinear model, the results from the linear analysis may not be reliable.

The linear method presented in Christensen and Doherty (2008) is used herein to quantify the value of collecting temperature and solute concentration data in a variable-density flow, heat and solute transport model. The intent is to reduce the uncertainty associated with predicted interface movement; therefore, only data that improve such predictions are considered necessary. According to Kohout’s conceptualization (1965), geothermal heating could potentially affect the flow in a carbonate platform; therefore the interface position could be altered as well. The model used is the well-documented numerical box problem, referred to as the Henry-Hilleke problem, which was developed based on Kohout’s conceptualization of the Floridan Plateau (Henry and Hilleke, 1972). Attention is also devoted to the issue of where measurements of either type are most

effectively made. The extent to which application of the methodology is compromised by its linear roots is explored through repeating the analysis using a number of different realizations of model hydraulic property fields. The Henry-Hilleke model is considered a nonlinear model because the coefficients of a calculated sensitivity matrix (which relates the sensitivity of model output to parameters) are parameter-dependent.

The objective here is to show that the linear method from Christensen and Doherty (2008) can be (1) applied to a nonlinear variable-density flow and transport model to quantify the worth of temperature and concentration data, (2) shown to take into account the actual known heterogeneity determined by aquifer testing and geostatistical analysis, (3) used in a model prior to calibration, and (4) used in an underdetermined model (where there are more parameters than observations).

This chapter is organized as follows. The theory of the method employed for assessment of data worth is first presented. Then, the numerical model used in the current study is described. The linear method is then applied to the numerical model in order to assess the relative merits of acquisition of temperature and concentration data, and to assess locations within the model domain at which acquisition of such data would be most effective. The linear method is then tested against a series of numerical model simulations with spatially varying parameter fields to test the linear method on a nonlinear numerical model. The paper concludes with a discussion of results and conclusions from the chapter. The conclusions include the limitations of the method with recommendations for future research.

3.2 Theory

From a Bayesian viewpoint, past measurements of system state that comprise a model's calibration dataset serve to constrain the values of parameters that can be used by that model such that only parameters which allow the model to replicate historical system behavior are admissible. Where model parameters, as well as the noise associated with historical measurements of system state display Gaussian variability, formulation of a linear equation which describe the constraining effect of these measurements can be derived.

Let \mathbf{x} be a vector of Gaussian random variables with covariance matrix $C(\mathbf{x})$. Let it be partitioned into two sub-vectors \mathbf{x}_1 and \mathbf{x}_2 such that

$$\mathbf{x} = \begin{bmatrix} \mathbf{x}_1 \\ \mathbf{x}_2 \end{bmatrix} \quad (32)$$

On the basis of this same partitioning, let

$$C(\mathbf{x}) = \begin{bmatrix} C_{11} & C_{12} \\ C_{21} & C_{22} \end{bmatrix} \quad (33)$$

Now let it be supposed that the elements of \mathbf{x}_2 become known. Then C'_{11} , the covariance matrix of \mathbf{x}_1 conditional on knowing \mathbf{x}_2 , is readily computed as (see, for example, Koch, 1987)

$$C'_{11} = C_{11} - C_{12} C_{22}^{-1} C_{21} \quad (34)$$

Before applying this concept in the environmental modeling context, vectors and matrices of relevance to this context must be defined.

Let \mathbf{p} denote the set of parameters employed by a model, these presumably representing hydraulic properties distributed throughout a model domain. It is assumed that the parameters, \mathbf{p} , are represented at a level of detail that is commensurate with the sensitivity of predictions of interest to these parameters. Let the vector \mathbf{h} represent measurements of system state (a potential “calibration” dataset from the field), and the vector $\boldsymbol{\varepsilon}$ represent the noise associated with these measurements. \mathbf{X} is the sensitivity of each model output, corresponding to an observation, to each parameter in the model—the coefficients discussed previously in the introduction to the chapter. Use of the \mathbf{X} matrix thus comprises an assumption of linear model behavior.

\mathbf{h} has a relation to the parameters, \mathbf{p} , described by

$$\mathbf{h} = \mathbf{X}\mathbf{p} + \boldsymbol{\varepsilon} \quad (35)$$

Let the scalar s represent a model prediction of interest, and let the vector \mathbf{y} represent the sensitivity of that prediction to model parameters, where

$$s = \mathbf{y}^t \mathbf{p}. \quad (36)$$

The precalibration uncertainty of the prediction, s , can then be defined by the variance

$$\sigma_s^2 = \mathbf{y}^t \mathbf{C}(\mathbf{p}) \mathbf{y}, \quad (37)$$

Equation (37) calculates the uncertainty as a function of parameter variability and the dependence of a prediction on model parameters. It does not consider the reduction in uncertainty if additional data (\mathbf{h}) are collected and added to the model.

Combining (35) with (36) leads to

$$\begin{bmatrix} s \\ \mathbf{h} \end{bmatrix} = \begin{bmatrix} \mathbf{y}^t & \mathbf{0} \\ \mathbf{X} & \mathbf{I} \end{bmatrix} \begin{bmatrix} \mathbf{p} \\ \boldsymbol{\varepsilon} \end{bmatrix}. \quad (38)$$

Then, using standard matrix relationships for propagation of covariance, the joint covariance matrix of s and \mathbf{h} is calculated as

$$\begin{aligned} C\left(\begin{bmatrix} s \\ \mathbf{h} \end{bmatrix}\right) &= \begin{bmatrix} \mathbf{y}^t & 0 \\ \mathbf{X} & \mathbf{I} \end{bmatrix} \begin{bmatrix} C(\mathbf{p}) & 0 \\ 0 & C(\boldsymbol{\varepsilon}) \end{bmatrix} \begin{bmatrix} \mathbf{y} & \mathbf{X}^t \\ 0 & \mathbf{I} \end{bmatrix} \\ &= \begin{bmatrix} \mathbf{y}^t C(\mathbf{p}) \mathbf{y} & \mathbf{y}^t C(\mathbf{p}) \mathbf{X}^t \\ \mathbf{X} C(\mathbf{p}) \mathbf{y} & \mathbf{X} C(\mathbf{p}) \mathbf{X}^t + C(\boldsymbol{\varepsilon}) \end{bmatrix} \end{aligned} \quad (39)$$

In equation (39), $C(\mathbf{p})$ is the covariance matrix of innate parameter variability (parameter variability that would be expected to exist in the real world), this expressing the pre-calibration uncertainty of hydraulic properties within the model domain. The diagonal elements of the $C(\mathbf{p})$ matrix express the extent to which the hydraulic property is unknown at any one point within the model domain. The off-diagonal elements of the covariance matrix express the extent to which a single hydraulic property is likely to show spatial continuity, or is likely to be correlated with properties of other types. In practice, the information for the $C(\mathbf{p})$ matrix for the aquifer system would be obtained from aquifer tests and geostatistical analysis. The $C(\mathbf{p})$ matrix could also be considered to be an encapsulation of our present state of ignorance – an acknowledgement of the fact that the exact values of hydraulic conductivity everywhere within the model domain are unknown, but that realistic bounds can be placed on the variability of the system. $C(\boldsymbol{\varepsilon})$ is the covariance matrix of measurement noise.

To condition a covariance matrix based on acquired information, the error variance (or variance of the predictive uncertainty in this method) of a prediction s , if data \mathbf{h} are acquired, is as follows (application of (34) to equation (39))

$$\sigma_s^2 = \mathbf{y}^t \mathbf{C}(\mathbf{p}) \mathbf{y} - \mathbf{y}^t \mathbf{C}(\mathbf{p}) \mathbf{X}^t [\mathbf{X} \mathbf{C}(\mathbf{p}) \mathbf{X}^t + \mathbf{C}(\boldsymbol{\varepsilon})]^{-1} \mathbf{X} \mathbf{C}(\mathbf{p}) \mathbf{y} . \quad (40)$$

Equation (40) (Doherty, 2007a; Christensen and Doherty, 2008) expresses the uncertainty variance (square of standard deviation) of the prediction s . The first term on the right side of equation (40) is the pre-calibration uncertainty of the prediction (equation (37)). The second term expresses the amount by which this pre-calibration uncertainty is reduced through the acquisition of additional data.

An important characteristic of equation (40) is that it contains neither parameter values, nor the values of model outputs; it only features the sensitivities of model outputs to parameters, these being encapsulated in the matrix \mathbf{X} and vector \mathbf{y} . Because only sensitivities are necessary, actual calibration does not have to be undertaken and actual data does not have to be collected (\mathbf{h} represents potential observations to be collected). Therefore, it can be used to optimize data acquisition for reducing the predictive uncertainty by quantifying the contribution of data that have not yet been collected. The equation can also be applied to an underdetermined model, with more parameters than observations, because calibration is not required. Using this method, it is also possible to upgrade an existing dataset (the dataset being the potential observations, \mathbf{h}) with new information by simply adding rows to the \mathbf{X} matrix, which comprises the sensitivities of corresponding model outputs to parameters employed by the model. The reduction in σ_s^2 thereby accrued can be considered a measure of the worth of such additions to a dataset.

The linear method is Bayesian as long as the observation and parameter values are normally distributed, requiring only observational and predictive sensitivities to individual parameters to be calculated by the model; actual field values are not required.

A Bayesian method is based on the probability theory presented by Bayes (1763). Using a Bayesian method, we are calculating probabilities to get “maximum likely” answers, as opposed to a single correct answer. In applying a Bayesian approach to groundwater modeling, we examine the uncertainty associated with a prediction of interest both before and after conditioning of parameters employed by the model from potential observations of system state. Model “calibration” from a Bayesian point of view does not lead to a single set of parameters that can be used to make a prediction. Rather it leads to a reduction in the uncertainty range of parameters employed by the model and on predictions that depend on those parameters. The aim of the present study is to determine what observations are most effective in reducing this predictive uncertainty by applying the linear equation (40) to a specific nonlinear numerical model, discussed next.

3.3 Model Development

The model used for this analysis is the Henry-Hilleke problem (Figure 25; Table 6; Table 7; Henry and Hilleke, 1972). Henry and Hilleke (1972) described a laboratory experiment and numerical modeling effort designed to represent a cross section through half of Florida’s carbonate platform where groundwater flow is affected by salinity and temperature variations. SEAWAT (Thorne and others, 2006; Langevin and others, 2008) was used to simulate this benchmark problem (results are presented in Chapter 2), in which variable-density flow results from differences in temperature and solute concentrations.

Table 7: Input parameters for the Henry-Hilleke problem.

Input Parameter	Value	Units	Comments
Columns/Layers	41	-	Assigned
$\Delta x(\text{DELR})/\Delta z(\text{DELZ})$	0.025	m	Assigned
K	864	m/d	Hydraulic conductivity
θ	0.35	-	Porosity
D_m	2.0571	m ² /d	Molecular diffusivity
D_t	20.571	m ² /d	Bulk thermal diffusivity
s	0.01	-	Storage
ρ_{solid}	2710	kg/m ³	Density (calcite aquifer)
K_d	2E-04	m ³ /kg	Retardation (temperature)
α	0	m	Dispersivity
ρ_f	1000	kg/m ³	Density of freshwater
ρ_s	1025	kg/m ³	Density of seawater
$\frac{\partial \rho}{\partial C}$	0.7	-	Density change with concentration
$\frac{\partial \rho}{\partial T}$	-0.375	kg/(m ³ °C)	Density change with temperature
Q_m	7.2	m ³ /d	Total flow in along the left-hand boundary, split into 41 nodes.

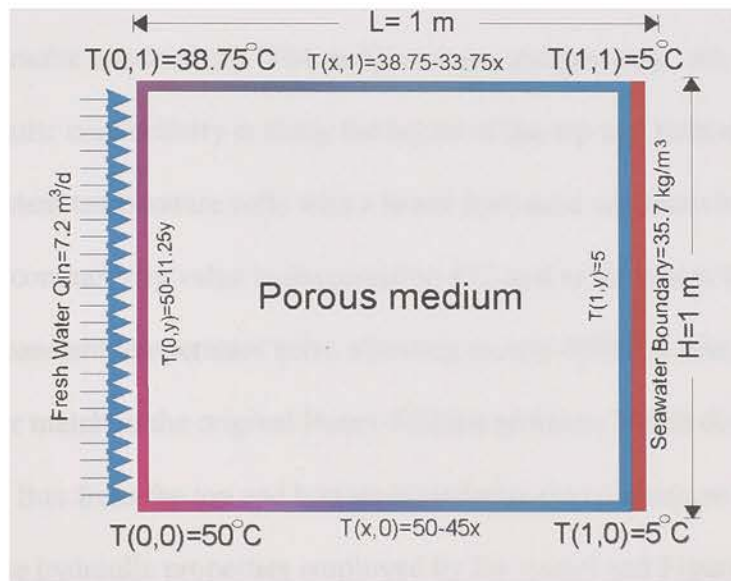


Figure 25: Set up of the Henry-Hilleke problem showing boundary conditions that include: (1) freshwater input, (2) seawater boundary, and (3) temperature boundaries.

The design of the Henry and Hilleke problem is shown in Figure 25. Model parameters, grid dimensions, and solution schemes are given in Table 6 and Table 7. The cross section is 1.025 m by 1.025 m in the x-z vertical plane. However, the rectangular

area defined by the centers of the four corner cells is 1 m by 1 m. The right boundary has seawater concentrations of 35.7 kg/m^3 with a constant-head flow boundary and the left boundary has a constant influx of freshwater. The model has constant temperature cells surrounding the domain (Figure 25). The right boundary has a constant temperature of 5°C , the lower left corner has a constant temperature of 50°C , and the upper left corner has a constant temperature of 38.75°C . Temperatures vary linearly along the boundary. Equations used to calculate the constant temperature at each cell along the boundary are shown in Figure 25.

3.3.1 Model Parameterization

The original model is homogeneous; with constant values for vertical and horizontal hydraulic conductivity (864 m/d), storage, and porosity. An exception to the constant hydraulic conductivity is along the layers of the top and bottom boundaries, which are constant temperature cells with a lower hydraulic conductivity of 432 m/d . The hydraulic conductivity value is decreased to 432 m/d to minimize the advective heat flux from the constant temperature cells, allowing mostly diffusive heat flux. This enables a better match to the original Henry-Hilleke problem, which does not simulate advective heat flux from the top and bottom boundaries (see discussion in Chapter 2). Table 7 lists the hydraulic properties employed by the model and Figure 26 shows the concentration and temperature fields computed using the model.

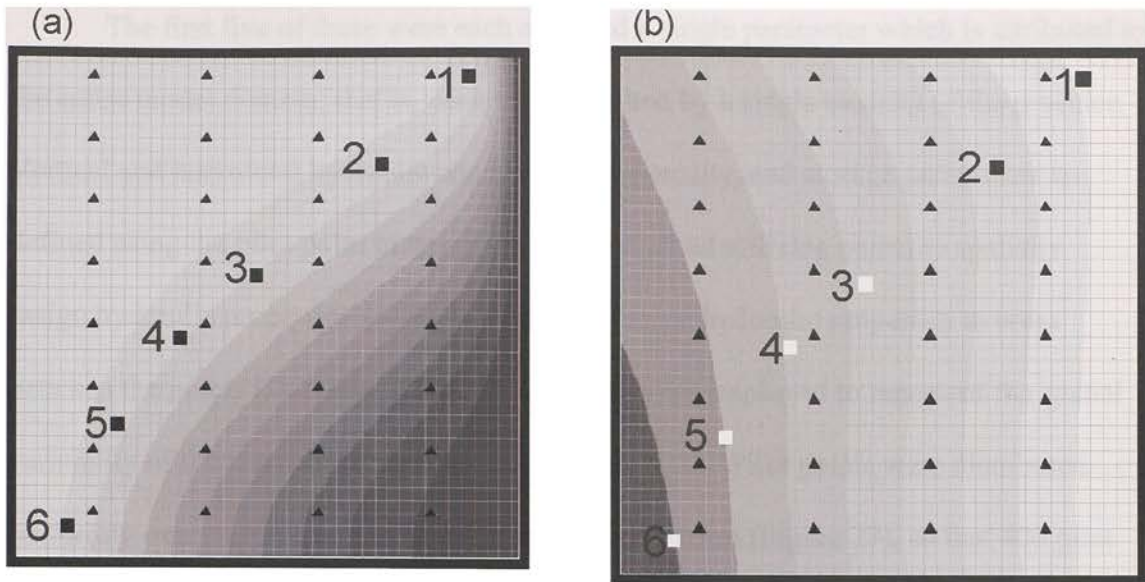


Figure 26: Henry-Hilleke problem (a) salinity contour results, 0 kg/m³ in light gray to 35.7 kg/m³ in dark gray. Simulated observations: black triangles. Predictions: black squares (labeled 1-6). (b) Temperature contour results from 5 °C in light gray to 50 °C in dark gray. Predictions: white/black squares.

The following parameter types are assumed to be approximately known in the Henry-Hilleke model, and therefore will be used in equation (40):

- dispersivity;
- molecular and thermal diffusion;
- retardation of heat;
- density of solid;
- salinity value along right boundary;
- temperature values along all boundaries;
- porosity;
- storage coefficient;
- vertical and horizontal hydraulic conductivities.

The first five of these were each assigned a single parameter which is attributed to the entire model domain; that is, each was described by a single element of the \mathbf{p} vector. Vertical and horizontal hydraulic conductivities, porosity, and storage parameters are defined using the pilot point method, which is a method utilizing points to spatially assign hydraulic properties and interpolation to assign hydraulic properties to areas between the points (Doherty, 2004). Pilot points were employed to represent the spatial variability of the last four of the above parameter types. Pilot points were distributed uniformly over 41×41 grid at a spatial interval of 0.05 m (Figure 27), so that 400 pilot points were assigned to each of these parameter types (with the exception of temperature). Pilot points were also employed along respective model boundaries for representation of spatial variability of temperature boundary values; these were uniformly replaced with a spacing of 0.025 m. A total of 1808 parameters thus comprise the model parameterization scheme encapsulated in the vector \mathbf{p} ; that is, the vector \mathbf{p} possesses 1808 elements.

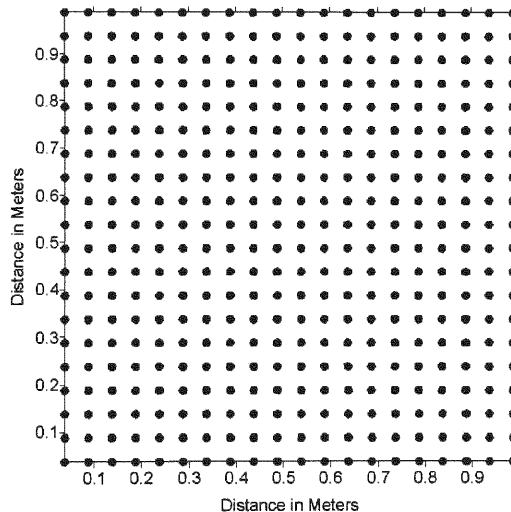


Figure 27: Figure showing model domain with pilot points that represent spatially varying parameters.

Even though the base model contains constant values for each pilot point assigned to a property (for example, 400 horizontal hydraulic conductivity pilot points are all assigned a value of 864 m/d), pilot points allow *observation* and *prediction sensitivities* (the coefficients of the sensitivity matrix, \mathbf{X}) to be calculated based on the possibility that the parameters vary spatially. The number of pilot points was chosen to allow the potential for a significant amount of parameter heterogeneity, while also limiting the number of parameters to a reasonable amount for the calculation of predictive uncertainty (for example, pilot points are not placed in every cell of the model, but in every other cell).

3.3.2 *Observations and Predictions*

Thirty-two temperature and 32 concentration observations were added to the model; these are simulated observations that do not actually exist in the field (these observations would be represented by \mathbf{h} from equation (35) and are seen in Figure 26). The potential for these 32 concentration and 32 temperature measurements to reduce the uncertainty of a defined prediction(s) can then be tested. With 64 observations, the \mathbf{X} matrix of equation (40) thus contains 64 rows (representing observations) and 1808 columns (representing parameters). More observations were not added to the model because the \mathbf{X} matrix could potentially become so large that inversion (necessary to calculate predictive uncertainty) of the matrix would be numerically difficult.

Movement of the interface for a prediction scenario was simulated by reducing the freshwater input along the left-hand side of the model by 25%. The change in salinity at six prediction sites was calculated with the intent of predicting interface movement

inland by a reduction of freshwater recharge (Figure 26). Sensitivities of each of these concentrations (in the prediction scenario) to the 1808 parameters employed by the model thus comprise the elements of the \mathbf{y} vector used in equation (40). More than six predictions could be analyzed; however, for the current purpose of predicting interface movement, six spatially varying observations along the interface are assumed to be sufficient.

3.3.3 Covariance Matrices

The covariance of model parameters is expressed through the $C(\mathbf{p})$ matrix of innate parameter variability discussed above and used in equation (40). The covariance matrices created for spatially-varying model parameters are based on log-transformed exponential variograms, with ranges of approximately 0.45 m and sills calculated from values in Table 8 (the sill is the variance, which is the square of the standard deviations presented in Table 8). The range was chosen based on the fact that the simulated problem is only 1 m by 1 m. The low to high values for each parameter in Table 8 were chosen with the assumption that a carbonate aquifer can have a high range of hydraulic conductivities, porosities, etc... A $C(\mathbf{p})$ matrix for the temperature boundary was also created, but this was not log transformed. The $C(\mathbf{p})$ matrix describing temperature variability perturbations (from a uniform gradient) along the boundary was based on a variogram with a sill of 0.25°C^2 (standard deviation of $\pm 0.5^{\circ}\text{C}$) and range of 0.3 m.

Measurement error values used to create the $C(\boldsymbol{\varepsilon})$, the covariance of the measurement error, were obtained assuming a normal distribution and utilizing margins of error from actual field instrumentation used to collect temperature and salinity data,

where temperature is +/- 0.01°C and salinity is +/- 0.3% of the measured value. The $C(\epsilon)$ matrices are used with the calculated $C(p)$ matrices employed in equation (40).

Table 8: Values used to calculate the standard deviation for the parameters used in the predictive uncertainty exercise. The * denotes model parameters that vary spatially.

Parameter	Low Value	Log (Low)	High Value	Log (High)	StDev= ((logH-logL)/4)
Horizontal K * [m/d]	100	2	1200	3.079	0.269795
Vertical K * [m/d]	100	2	1200	3.079	0.269795
θ *	0.1	-1	0.5	-0.301	0.174743
s *	1E-05	-5	0.1	-1	0.269795
ρ_{solid} [kg/m ³]	1000	3	3000	3.477121	0.119280314
K_d [m ³ /kg]	1E-07	-7	0.001	-3	1
D_l [m ² /d]	10	1	30	1.477121	0.119280314
D_m [m ² /d]	1	0	3	0.477121	0.119280314
α [m]	0.02	-1.699	0.2	-0.69897	0.25
Concentration Boundary [kg/m ³]	30	1.4771	40	1.60206	0.031234684

3.4 Application

The following method was employed to assess the importance of individual observations in the reduction of predictive uncertainty in the numerical model. The sensitivity matrix (X) was computed for the Henry-Hilleke problem, the predictive scenario was then run (by decreasing freshwater recharge 25%) to obtain the prediction sensitivities encapsulated in the vector, y . The variance for the predictive uncertainty for a specific prediction is calculated using equation (40). The variance calculation includes the effect of the 32 temperature and 32 salinity observations and the parameter $C(p)$ matrices described previously. One observation is then removed from the model, and the variance is calculated again for a prediction. The difference between the variance calculated before and after the removal of a specific observation is the increase in uncertainty for the prediction pursuant to removal of the observation. For example, if

removal of an observation has no effect on the uncertainty of the prediction, then that observation is not worth collecting. However, if the uncertainty is increased for the prediction when an observation is removed from the data set, then that specific observation improves the accuracy with which the prediction can be made. This exercise was completed for all six predictions.

3.4.1 *Testing the Effects of Nonlinearity*

As previously stated, the matrix \mathbf{X} represents the sensitivities of model outputs (\mathbf{h}) to parameters employed by the model; use of this matrix (in equation (40)) thus comprises an assumption of linear model behavior (equation (40) assumes the parameter inputs and model outputs are linearly related). It is important distinguish between the values of parameters employed by the model for the purpose of computation of the \mathbf{X} matrix and \mathbf{y} vector of equation (40), and the type of parameter variability assumed for the purpose of filling the $\mathbf{C}(\mathbf{p})$ matrix used in this same equation. *Uniform* parameters were employed by the original Henry-Hilleke model for computation of sensitivities in the \mathbf{X} matrix. The $\mathbf{C}(\mathbf{p})$ matrices for equation (40) are developed based on the natural parameter variability one would expect to calculate from field tests or geostatistical analyses.

This research is a first attempt to investigate the extent to which nonlinear model behavior invalidates (or not) the use of equation (40) for assessment of observation worth. This is done by generating *non-uniform* parameters to compute sensitivities used in the \mathbf{X} matrix (as opposed to the uniform parameter field used in the original Henry-

Hilleke simulation). Then, calculations of observation worth can be repeated using an X matrix and y vector computed on the basis of these non-uniform parameters.

The non-uniform parameters were created by generating a series of stochastic realizations for the temperature boundary conditions, vertical and horizontal hydraulic conductivity, storage, and porosity. The stochastic fields were created based on the same $C(\mathbf{p})$ matrices discussed in the “Covariance Matrices” section (and used previously in equation (40)) to describe the spatial variability of each property. Separate random numbers were also generated for each of the parameters in Table 8 that do not vary spatially. These new parameters were generated from a normal distribution with standard deviations calculated from Table 8. The objective here is to test a linear method on a nonlinear model by generating parameters fields and variables that are considered relatively extreme in values from low to high (the parameter ranges, used to define the sills for the variograms utilized to create the $C(\mathbf{p})$ matrices, are purposely high; Table 8). Therefore, parameter fields are quite different; however, each of these parameter sets could theoretically represent a carbonate aquifer (such as the Floridan Plateau).

The different stochastic realizations and generated parameters were combined, creating additional Henry-Hilleke simulations (necessary to compute the additional X matrices). After creating multiple simulations, it was found that run times and predictive uncertainty calculations were relatively long (numerous days to complete each analysis). Therefore, only five new simulations were chosen to complete this analysis with the assumption that a total of six simulations (the base Henry-Hilleke plus the additional five) would suffice in testing the linear method on a series of nonlinear simulations.

The resulting sensitivity matrices (\mathbf{X}) for all six Henry-Hilleke simulations (the base simulation plus the five additional parameter sets) are different, revealing the nonlinearity of the model. If the Henry-Hilleke model was linear, the sensitivity matrices (i.e., coefficients) for each simulation would be identical regardless of the parameter values. (However, it is important to note that the degree of model nonlinearity is not known at this time and is not included in this research.) The process of computing predictive uncertainty reductions from equation (40) related to the removal of observations was then repeated for each of the five additional simulations. Comparing the results from each linear analysis applied to the six different simulations is a first step in determining the applicability of the linear method to this nonlinear model.

3.5 Results and Discussion

Reduction in uncertainty variance calculated using equation (40) is plotted at the site of each observation. Figure 28 is an example of the results, where the changes in variance for predictions 2 and 3 are contoured for salinity and temperature observations. The concentrated areas with the densest contour lines reveal the observation(s) of greatest worth. In the analysis of the original Henry-Hilleke simulation, the location of a prediction relative to the location of the interface is most important when analyzing the value of salinity data. (The salinity observation closest to the prediction in the direction of interface movement reduces the predictive uncertainty the most.) When analyzing predictive uncertainty for temperature for predictions 2 and 3, the bottom left-hand corner, where the change in temperature with distance is the greatest, appears to be one of the better locations to collect temperature data. This applies in the majority of the

predictions (1-6) (Figure 28). Salinity data also contribute more to reducing predictive uncertainty than temperature data *in this particular problem for these six predictions*. The contribution from salinity data to reducing predictive uncertainty is an order of magnitude higher than the contribution from temperature data.

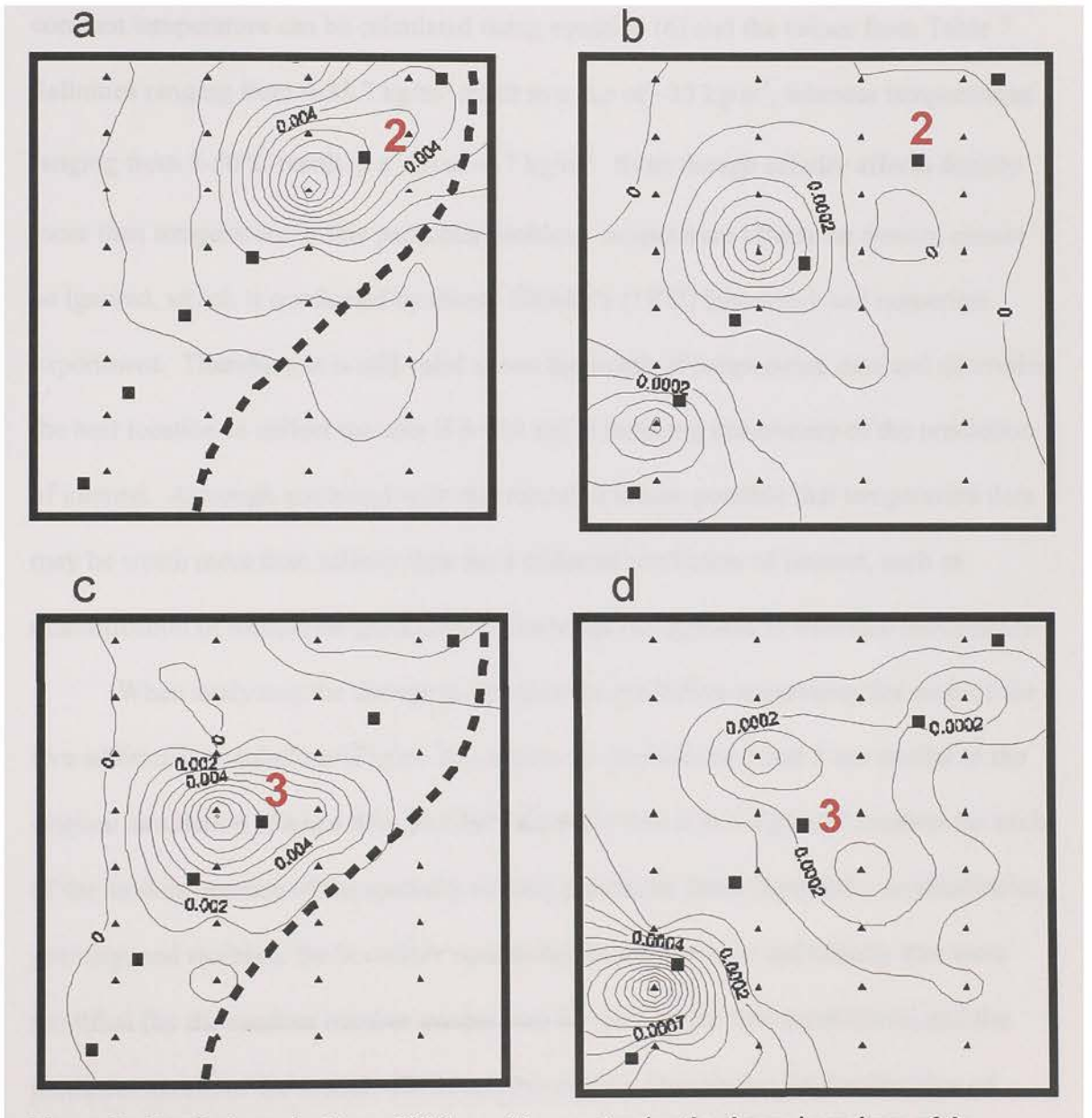


Figure 28: Results from the Henry-Hilleke problem contouring the change in variance of the predictive uncertainty for (a) prediction 2 for the concentration observations (the dashed dark line is 50% seawater), (b) prediction 2 for the temperature observations, (c) prediction 3 for the concentration observations, and (d) prediction 3 for the temperature observations.

Given the salinity range in the model $\Delta C = 35.7 \text{ kg/m}^3$, and the temperature range in the model $\Delta T = 45^\circ\text{C}$ (5-50°C), it is not surprising that salinity data might have more worth than temperature data for this specific prediction. The change in density with temperature at a constant concentration, and change in density with concentration at a constant temperature can be calculated using equation (6) and the values from Table 7. Salinities ranging from 0-35.7 kg/m³ result in a $\Delta\rho$ of $\sim 25 \text{ kg/m}^3$, whereas temperatures ranging from 5-50°C result in a $\Delta\rho$ of $\sim 17 \text{ kg/m}^3$. Even though salinity affects density more than temperature in this particular problem, temperature effects on density cannot be ignored, which is confirmed by Henry-Hilleke's (1972) laboratory and numerical experiment. Therefore, it is still valid to test the worth of temperature data and determine the best location to collect the data if it will aid in reducing uncertainty of the prediction of interest. Although not tested with this model, it is also possible that temperature data may be worth more than salinity data for a different prediction of interest, such as quantification of submarine groundwater discharge (as opposed to interface movement).

When analyzing the change in variance for predictive uncertainty for each of the five additional simulations (Figure 29), results for predictions 2 and 3 are similar to the original simulation (Figure 28). The 50% seawater line *is in a different* location for each of the models because of the spatially varying parameter fields (hydraulic conductivities, porosity, and storage), the boundary conditions for temperature and salinity that were modified (by the random number generation) for each of the five simulations, and the nonlinear nature of the model. However, the salinity observation, in the direction of interface movement, is most important for a specific prediction relative to interface location regardless of the new parameter field. This is confirmed by the relative rank of

each observation in reducing predictive uncertainty for Predictions 2 and 3 (Figure 30). The same two observations have the highest rank (which means they reduce the predictive uncertainty the most) for each of the predictions shown (2 and 3). Although results are not shown for all six predictions, the results for the other four predictions are similar to predictions 2 and 3.

The change in variance for the temperature observations (Figure 29) reveals that for each stochastic realization, a number of different observations contribute to reducing the predictive uncertainty in each simulation. However, the observation in the bottom left corner contributes most to reducing the uncertainty in both predictions 2 and 3 for all the simulations regardless of the location of the prediction. Results from the relative rank of the observations to reducing the predictive uncertainty (Figure 30) confirm the results from Figure 29, revealing that the observation in the bottom left corner is of greatest worth to reducing predictive uncertainty in all of the simulations.

The results, indicating that the best location to collect temperature data at the bottom left corner, were not expected prior to this analysis. It was originally hypothesized that the salinity and temperature data would both reduce predictive uncertainty; however, it was thought that the same observation location for both salinity and temperature would reduce the predictive uncertainty for a specific prediction. However, upon further investigation, the bottom left corner is where the change in temperature with distance is the greatest and is the warmest area in each simulation (Figure 25 and Figure 26). This warm area is where the water is heated and the less-dense warmed water begins to rise, causing circulatory flow to occur according to Kohout's conceptualization (Figure 24; 1965) and laboratory results from Henry and

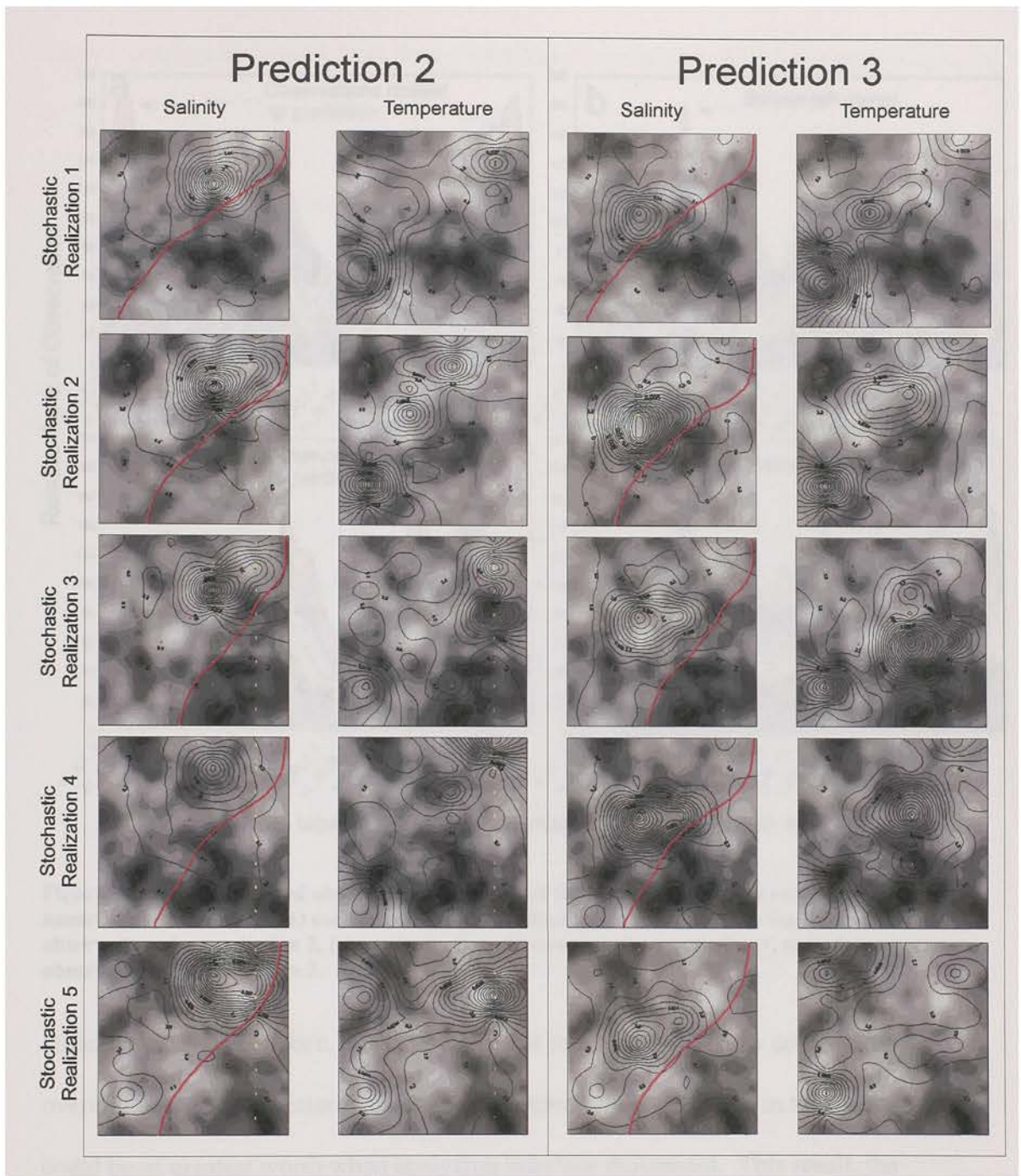


Figure 29: Contours of change in variance (calculated from equation (40)) of the predictive uncertainty for predictions 2 and 3 in the black contour lines for both salinity and temperature for each of the 5 additional Henry-Hilleke simulations. The stochastic realizations are shown as filled contours in gray to black and correspond to the log of the horizontal hydraulic conductivity. The dark red line shows the 50% seawater line. *NOTE: The actual values of the black contour lines representing the change in variance/predictive uncertainty are not pertinent in this figure, only what the contour lines represent. The densest areas of contour lines reveal the location(s) of the most important observation(s) in reducing the uncertainty of the prediction of interest.*

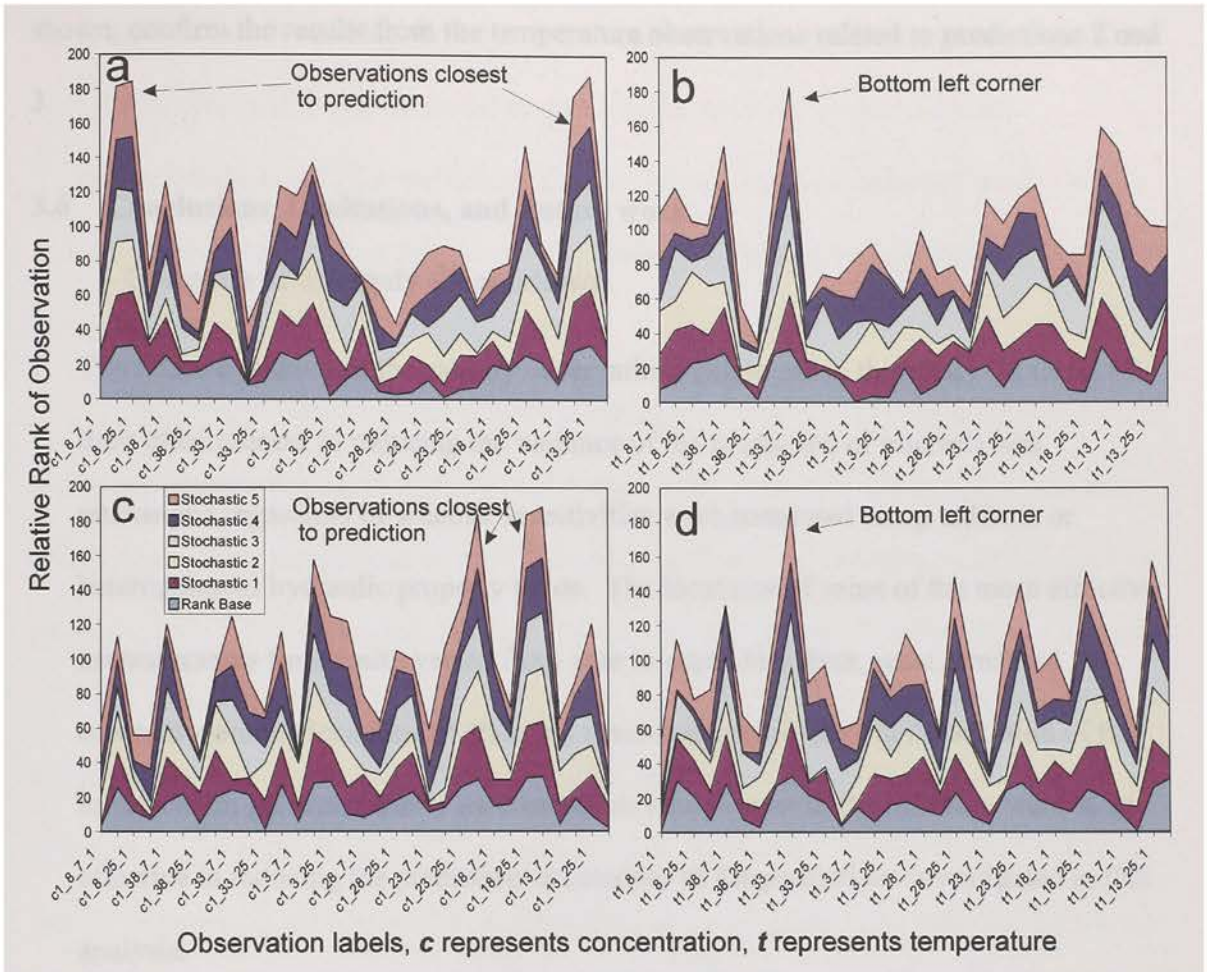


Figure 30: Relative rank of observations (for each of the 6 simulations) that reduce the predictive uncertainty the most for (a) concentration observations for prediction 2, (b) temperature observations for prediction 2, (c) concentration observations for prediction 3, and (d) temperature observations for prediction 3.

Hilleke (1972). Therefore, it is concluded that this circulatory flow could affect the overall location of the interface and that a temperature observation in this warm area could be of greatest worth when analyzing interface movement. This result, the temperature observation of greatest worth in the bottom left corner, applies even when the prediction related to movement of the interface is relatively far away, such as predictions 2 and 3 (Figure 28). The results for the other predictions, although not

shown, confirm the results from the temperature observations related to predictions 2 and 3.

3.6 Conclusions, Limitations, and Future work

Outcomes of this study are as follows:

1. The relative ranking of the salinity observations employed in this study (in terms of their effectiveness in reducing the variance of the prediction of interest) was unchanged regardless of whether sensitivities were computed using uniform or heterogeneous hydraulic property fields. The locations of some of the more effective measurements for salinity varied from case to case. However, what remained constant were the locations of effective measurements relative to the location of the interface. In general, salinity measurements taken closer to the interface were most effective in reducing the predictive uncertainty of the predictions investigated in this analysis.
2. If temperature data is being collected to predict interface movement in problems that are analogous to the Henry-Hilleke problem investigated here, the most worthy observation is in an area where the change in temperature with distance is relatively sharp, in the warmest area beneath the surface.
3. Overall, salinity data contributes more worth to reducing predictive uncertainty in interface movement than temperature data (Figure 28), with salinity data reducing uncertainty an order of magnitude more than temperature in most cases for this particular problem.

4. It appears that the linear method presented can be applied to this nonlinear variable-density flow and transport model to quantify the worth of temperature and concentration data. The method can be applied to an underdetermined model before calibration, while taking into account the actual heterogeneity determined through geostatistical analysis of collected data.

The Henry-Hilleke model has been employed to demonstrate the application of an easily-implemented methodology through which future data acquisition of maximum worth can be targeted, and hence furnish maximum returns on the investment devoted to its acquisition. The theoretical underpinnings of the methodology rest on an assumption of linear model behavior. This is both its strength and its weakness. The strength of the methodology is that it can be implemented at a relatively light numerical cost even in complex model settings, and in highly parameterized contexts. Furthermore, the actual values of parameters, observations, and predictions do not need to be known – for only their dependence on parameter values employed by the model are employed in the equations on which the methodology is based. Therefore, the methodology does not require model calibration. However, the assumption of linear model behavior is also a limitation and weakness of the method because outcomes of calculations which rest on this assumption are approximate, with the level of approximation increasing with the level of model nonlinearity.

The mathematics of a linear analysis are such that, when applied to a series of linear models, would give identical results. Therefore, if the model used in this study was linear, the results from the linear method would result in identical sensitivities and predictive uncertainties regardless of the parameters employed in the model. The

sensitivities of model-calculated concentrations and temperatures, especially those in the vicinity of an interface, with respect to parameters employed by the model are dependent on the current position of the interface, which is in turn dependent on parameters employed by the model. This dependence is illustrated in Figure 29, where the use of 5 different sets of parameters results in different interface locations. Here, the results from the linear method are not identical, only alike in a relative sense in that the ranking of observations of greatest worth are similar; consequently the Henry-Hilleke model is nonlinear. However, the linear method still appears to work in this nonlinear model because each simulation points towards using the same observations to reduce predictive uncertainty regardless of parameter field.

Part of the purpose of the present study was to investigate the extent to which use of a methodology based on an assumption of linear model behavior is invalidated by such parameter dependence of model outcomes. This particular analysis appears to have demonstrated that the methodology can potentially provide useful qualitative insights and information that can guide acquisition of future data, such that the data collected is as information-rich as possible in relation to predictions of future behavior required of a model. However, in interpreting this information, it is incumbent on the modeler to be cautious in the application of the method by making allowances for the nonlinear nature of the model which he/she is potentially employing. Thus while it may not be feasible to expect that an analysis based on equation (40) can yield the exact locations at which information can be gathered at a specific study site (especially one at which a high level of hydraulic property heterogeneity is expected to prevail), it may yield some important principles on which selection of these localities can be based.

What is presented here is a first step towards testing use of this linear method on a nonlinear model. The degree or source of nonlinearity in the Henry-Hilleke model is not known or studied as part of this research; therefore, there is not a clear quantification of when the linear method can be employed with confidence to another nonlinear model. The applicability of the linear method would depend on the degree of model nonlinearity. More research needs to be done to develop specific guidelines for applicability of this linear method to other nonlinear models.

The applicability of this linear method to varying degrees of nonlinear models could potentially be accomplished with the following protocol. First, perform a nonlinear analysis for reduction of predictive error variance on a series of nonlinear numerical problems with different degrees of linearity. Then, compare results between the application of the linear method presented in this paper and the results from the nonlinear method. The nonlinear analysis for predictive error variance and/or uncertainty could be achieved with the following steps:

- 1) An extensive Monte Carlo analysis with many parameter fields where each model is required to be calibrated.
- 2) A prediction is then made on the basis of each model parameterization.
- 3) Correlation between observation worth and the predictions of interest indicate data of greatest worth.

A nonlinear analysis, such as this, would necessitate that approximately 1000 system realizations be created; then each system (or model) requires calibration to available data. Even using a new, relatively fast, method available, called null-space Monte Carlo (Tonkin and Doherty, 2008), would require an order of 5 to 10 runs per parameter field.

However, this is very time consuming and a simpler numerical model with shorter run times than Henry-Hilleke would be preferable if performing this nonlinear analysis.

A linear analysis is appealing because it only requires calculation of observation and prediction sensitivities to individual parameters based on the model; therefore, the model does not need to be calibrated and actual field data are not necessary. A linear analysis is also attractive because the computationally intensive model runs necessary for a nonlinear analysis are not required. The question addressed in this study is: can the pleasing aspects of a linear analysis potentially be applied to assessing data worth in a nonlinear model? The present study has shown, for this analysis in which a number of parameter fields were used in a nonlinear model, that the mathematics from a linear assumption can potentially be applied in quantifying the worth of data. The analysis is also unique in that it can be done using information on the aquifer system obtained from measurements and geostatistical analysis (through the $C(\mathbf{p})$ matrix); therefore, the model parameters vary based on scientific information.

A simple precalibration linear analysis, such as presented in this chapter, can be done to help guide a data collection effort if additional data need to be acquired to aid in reducing the uncertainty of model predictions. The analysis can potentially save time and money, both in the calibration process and the data collection strategy, whereas a nonlinear analysis may not be financially feasible. The results presented here are for a benchmark problem used in the testing of numerical modeling codes; it is possible that this conclusion is transferable to other nonlinear modeling contexts with additional research. However, caution must be taken in applying this method because reliable results of predictive uncertainty would depend on the degree of model nonlinearity.

4 SIMULATION OF SUBMARINE GROUNDWATER DISCHARGE SALINITY AND TEMPERATURE VARIATIONS: IMPLICATIONS FOR DATA COLLECTION

4.1 Introduction

Groundwater being discharged into the sea has been noted throughout history; in the first century, fresh groundwater discharging to the ocean was used for water supply in the coastal area of Syria (Kohout, 1966). The study of submarine groundwater discharge (SGD) progressed rapidly in the mid 1990's with publications from Moore (1996), Moore and Church (1996) and Younger (1996); however, the term SGD or SGWD (submarine groundwater discharge) emerged in the literature in the early 1970's (Zektser and others, 1973). Often referred to as submarine springs or submarine groundwater discharge, this water varies in concentrations from fresh to brine, and has varying temperatures depending on the source. More recently, Price and others (2006) coined the term coastal groundwater discharge (CGD), which more specifically refers to the brackish to saline portion of the SGD. It is difficult to quantify SGD; however, because spatial variations in recharge, aquifer hydraulic properties, tides, and other complicating factors can substantially affect patterns and rates of groundwater flow to the ocean. The presence of geological heterogeneity, for example, can obscure the measurement of SGD (Bokuniewicz and others, 2003).

In recent years, SGD in coastal areas is a topic of increasing concern to marine scientists, primarily because terrestrially-derived groundwater could release nutrients and other potentially harmful contaminants into ecologically sensitive marine environments

(Moore, 1999; Taniguchi and others, 2002; Finkl and Krupa, 2003). The source of nutrients to the groundwater system is typically from agriculture (fertilizers) and animals or humans (waste). The nutrients can leach into the shallow fresh groundwater of a coastal aquifer which, in turn, could discharge into the ocean as part of the SGD (Figure 31), potentially disrupting a fragile ecosystem. If the water remains in the ground for long periods of time before being discharged, more nutrients could be leached from the aquifer and discharged to the coast. Even the recirculated seawater portion of the SGD could leach additional nutrients from the aquifer (Shellenbarger and others, 2006). Studies have shown that increased nutrients in SGD could potentially cause toxic algal blooms (Laroch and others, 1997; Breier, 2006). Research has also shown the tides can significantly affect SGD and the contribution of land-derived chemical input (Barry and others, 1999), as well as cause biogeochemical reactions in the tidal zone between an estuary and the aquifer groundwater (Robinson and others, 2006a; Robinson and others, 2006b). These underground mixing zones of saltwater and freshwater in coastal aquifers where geochemical reactions are often occurring are referred to as subterranean estuaries (Moore, 1999).

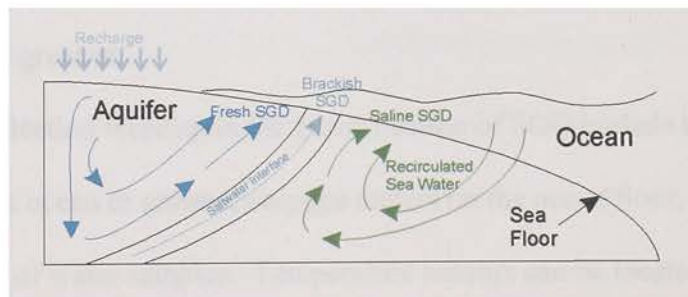


Figure 31: Diagram showing groundwater flow lines in a coastal area with a saltwater-freshwater interface. SGD is fresh, brackish, or saline, depending upon the location and source of water. The SGD can carry nutrients or other contaminant from the aquifer to the ocean.

Groundwater that is discharged to the ocean in coastal areas is often (1) fresher, depending upon the environment, (2) a different temperature than the surrounding ocean water, depending on the time of year and source of groundwater, (3) a different age than the surrounding ocean water, and (4) could contain additional nutrients or chemical concentrations than the ocean water. Therefore, multiple data collection techniques including aerial imagery, electromagnetic resistivity, temperature sensors, seepage meters, and geochemistry enable different means of identifying not only the location of SGD, but also the amount, concentration, temperature, age, and source. Combining these different data techniques can enable a reasonable quantification of SGD.

Aerial survey techniques that utilize electromagnetic (EM) and thermal imagery provide a direct means to map zones of increased SGD (Weiss and others, 2005). EM methods can be used to detect subsurface salinity differences, whereas thermal imagery can detect small water temperature variations at the sea surface (as small as 0.08°C in calm seas). Therefore, it is possible to detect SGD with an aerial survey if the salinity or temperature difference between SGD and the ocean is relatively large. The best time to conduct an aerial survey is when salinity and temperature differences between SGD and surface waters are the greatest.

Other data collection techniques for quantification of SGD include temperature and EM sensors in the ocean or ground, seepage meters on the ocean floor, and geochemical analysis of water samples. Temperature sensors can be located in the coastal area to measure not only temperature of surface waters, but also the temperature of groundwater by deploying waterproof sensors in wells (Stonestrom and Blasch, 2003). These temperature measurements can be utilized in conjunction with thermal imagery

data in SGD mapping. Temperature measurements and temperature profiles can also be used to trace source waters (Anderson, 2005) as well as estimate fresh SGD (Taniguchi and others, 2002). Streaming resistivity profiling and EM resistivity instrumentation can be used to measure salinity changes in surface and subsurface waters to give an indication of fresh SGD (Swarzenski and others, 2004a; Swarzenski and others, 2007). Seepage meters, which are deployed on the ocean floor, measure flux out of the aquifer into the ocean over a specific area of the sea floor (Finkl and Krupa, 2003). Geochemical sampling can determine the input of nutrients such as nitrates and ammonium in SGD (Swarzenski and others, 2004a). Helium-tritium isotope techniques can be utilized to determine the apparent age of groundwater (Price and others, 2003; Swarzenski and others, 2004a); while radium, radon, and methane (Breier, 2006; Moore and others, 2006) can be used to quantify SGD because groundwaters have higher concentrations of these constituents compared to surface waters.

Variable-density numerical models are often used for management purposes to simulate groundwater flow in coastal aquifers, including saltwater intrusion (Dausman and Langevin, 2005) and SGD. A deep (~3 km) model of North Carolina was developed to investigate fresh and saline SGD, as well as geothermal convection in a coastal setting (Wilson, 2005). Langevin (2001) used a variable-density flow and transport model to quantify rates of fresh SGD into Biscayne Bay in southeastern Florida. Smith and Zawadski (2003) calibrated a two-dimensional cross-sectional model to seepage measurements in the northeastern Gulf of Mexico. Previous research with data collection and modeling has also shown that seasonality can affect the amount of SGD resulting from water-table changes (Michael and others, 2005). However, few numerical modeling

studies in coastal areas, if any, have been designed to guide data collection efforts or had the capability of simulating apparent age. Age simulations could give insight to groundwater residence times before discharge; therefore, predictions could potentially be made to determine the addition of nutrients leached into the SGD (Lerner and Ockelford, 2006). Age data, if collected, could additionally be used to calibrate a numerical model.

The purpose of this chapter is to reveal an innovative use of SEAWAT and answer challenging questions about the detection of SGD. This chapter shows how a numerical model developed using SEAWAT can (1) simulate estimates of SGD flux, temperature, salinity and age, (2) be used to understand complicated coastal systems by simulating multiple species (temperature, salinity, and age) with different types of geology, and (3) be used to guide and give insight to some data collection efforts in studies of SGD. A 3-dimensional (3-D) variable-density numerical model was developed using generalized hydrological conditions for southeastern Florida. The model was calibrated using existing data. This 3-D model was then used to create a 2-dimensional (2-D) model, which had shorter run times and could simulate multiple species. The 2-D model was verified using additional data. The 2-D model was then used to determine when and where SGD rates are the greatest and to quantify expected temperature, salinity, and age differences between groundwater and ocean water. The model is unique in that it represents SGD characteristics, including salinity, temperature, and age, at short-term (tidal) and longer-term (seasonal) time scales.

4.2 Methods

A 3-D model was developed using idealized hydrogeological conditions and hydraulic parameters common to the Biscayne aquifer in southeastern Florida. The 3-D model was calibrated with water-level and salinity data collected by the USGS in Broward County from 2001-2002 (Dausman & Langevin, 2005) (Figure 32). Parameters from the 3-D model were then used to create a 2-D model to evaluate transient variations in the salinity, temperature, and age of SGD (using 3 species: salinity, heat, and age). The 2-D model has much faster run times than the 3-D model; therefore, more species can be simulated as well as a longer time period.

The 2-D numerical model is intended to represent generalized flow conditions in the Biscayne aquifer in southeastern Florida rather than one specific location. Results from the 2-D model are compared to different types of data (temperature and discharge) collected from various sources (NOAA, FIU, and USGS). The comparison of the model to different types of data is undergone to verify the 2-D model. After the 2-D model is verified, it is then shown how the model can be used to guide data collection and give insight into the groundwater system and properties affecting SGD.

4.2.1 *Continuous Water-Level and Salinity Data Collection*

The 3-D model was calibrated with water-level and salinity data collected as part of this research (an H-310-15 pressure transducer and a YSI-600R probe were used to collect water levels and specific conductance). The borehole equipment collected water levels and fluid conductivity in five fully cased monitoring wells in Broward County with open holes or screened intervals open in the freshwater-saltwater interface in the

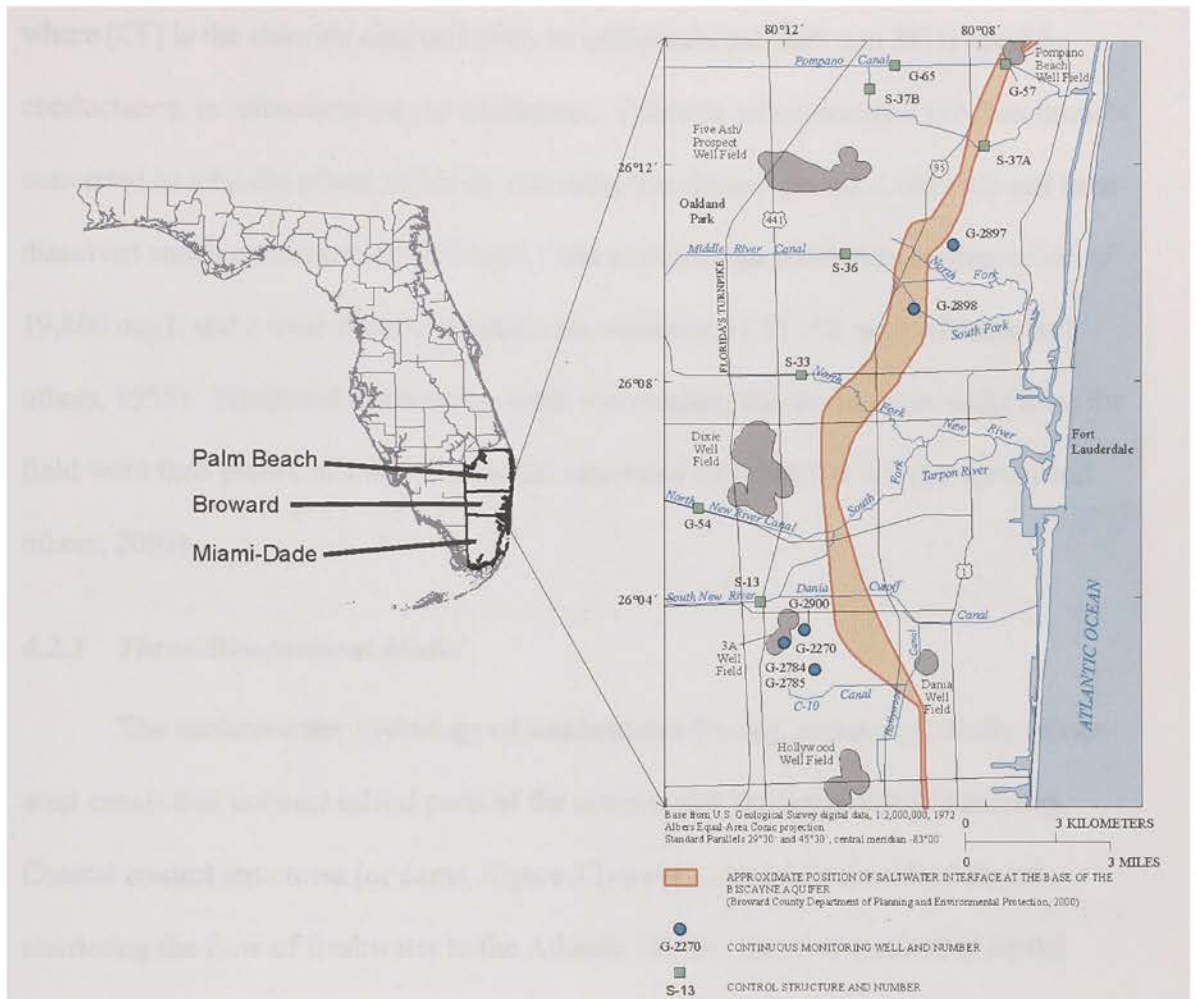


Figure 32: Map of Florida with the 3 counties underlain by the Biscayne aquifer. Broward County is enlarged showing the location of monitoring wells collecting continuous water-level and salinity data.

Biscayne aquifer. Additionally, water levels were recorded in a shallow freshwater well near one of these wells. The transducers collected water levels and specific conductance every 15 minutes for 14 months. The intention of the deployment of the transducers was to capture movement of the saltwater interface (Figure 32) resulting from tidal fluctuations. The specific conductance was converted to total-dissolved solids using the following equation (Langevin, 2001)

$$[Cl^-] = 1.10^{-6}(SC)^2 + 0.3224(SC) 177.7, \quad (41)$$

where $[Cl^-]$ is the chloride concentration, in milligrams per liter; and SC is specific conductance, in microsiemens per centimeter. Chloride concentrations are then linearly converted to total-dissolved solids by assuming that freshwater has a chloride and total-dissolved solids concentration of 0 mg/L; and seawater has a chloride concentration of 19,800 mg/L and a total-dissolved solids concentration of 35,000 mg/L (Parker and others, 1955). Simulated observation wells representing the observation wells from the field were then placed in a 3-D model simulated using SEAWAT (Langevin and others, 2003).

4.2.2 Three-Dimensional Model

The surface-water hydrology of southeastern Florida consists primarily of east-west canals that connect inland parts of the county with the Intracoastal Waterway. Coastal control structures (or dams, Figure 32) within the canals are often closed, restricting the flow of freshwater to the Atlantic Ocean. The 3-D numerical model developed was designed to utilize this commonly occurring hydrologic pattern (Figure 33). The three-dimensional finite-difference grid used for the model consists of 15 layers; the top layer is 10.5 m thick, and each underlying layer is 7.5 m thick. Each model cell is 150 m by 150 m and the model contains 23 rows and 152 columns (a more specific description of this model can be found in Dausman and Langevin, 2005). Rather than developing a numerical model for all of southeastern Florida, this representative model was developed to capture the generalized coastal flow patterns that occur in a typical area with the Biscayne aquifer and the surficial aquifer system.

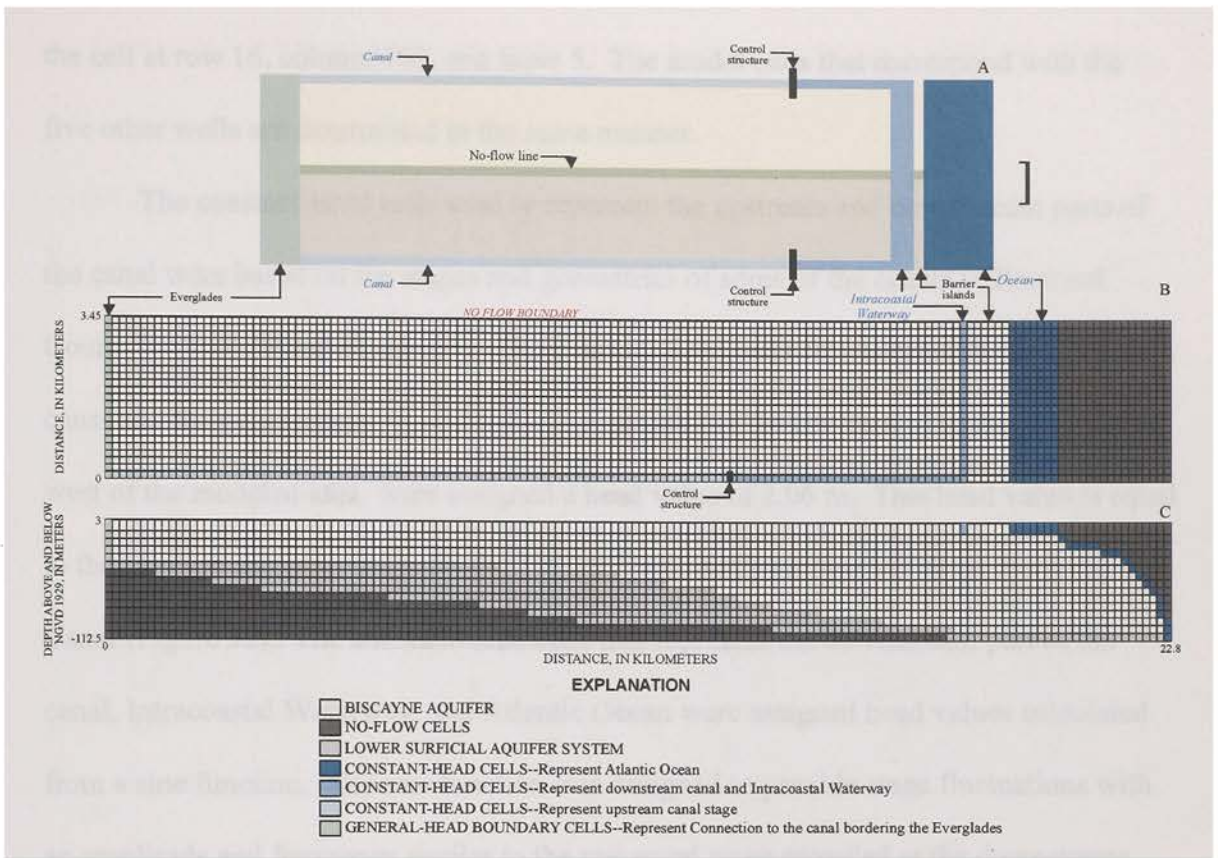


Figure 33: 3-Dimensional model representative of the surficial aquifer system in southeastern Florida. (A) Schematic showing conceptual view of an area where the northern part is symmetrical to the southern part, and (B) map view, and (C) cross-sectional view of model grid showing the boundary conditions and aquifer parameters.

Although the monitoring wells are located in different parts of Broward County (Figure 32), data from all these wells were used to determine the representative aquifer parameters. Consequently, the estimated values for the aquifer parameters are more representative for all of the Biscayne aquifer than for one specific area. Simulated observation wells are located in the model not by geographic location but instead by distance and direction from a control structure and by the depth of the open hole. For example, well G-2900 is about 1 km from the nearest canal, almost 2 km east of structure S-13, and is about 35 m deep. In the model, these distances and depth correspond with

the cell at row 16, column 103, and layer 5. The model cells that correspond with the five other wells are determined in the same manner.

The constant-head cells used to represent the upstream and downstream parts of the canal were based on the stages and geometries of some of the canals in Broward County (Figure 32 and Figure 33). The constant-head cells representing the upstream canal and the general-head boundary cells representing the connection to the Everglades, west of the modeled area, were assigned a head value of 2.06 m. This head value is equal to the average upstream stage for the 1990-99 period at structure S-37B on the Pompano Canal (Figure 32). The constant-head cells that represent the downstream part of the canal, Intracoastal Waterway, and Atlantic Ocean were assigned head values calculated from a sine function. The sine function was designed to provide stage fluctuations with an amplitude and frequency similar to the measured stage recorded at the downstream side of structure S-36 (Figure 34).

A total of 14.02 cm of precipitation (or rainfall) is applied to the 1-month model, which represents the average rainfall from 1990-99 in a series of stations located in Broward County (rainfall data came from the South Florida Water Management District, SFWMD). Evapotranspiration is calculated by the model based on depth to the water table, an extinction depth of about 1.5 m (~5 ft) (Langevin, 2001), and an average maximum evapotranspiration rate based on the values presented by Merritt (1996). An average land surface value of 3 m was used to calculate depth to water for the entire model.

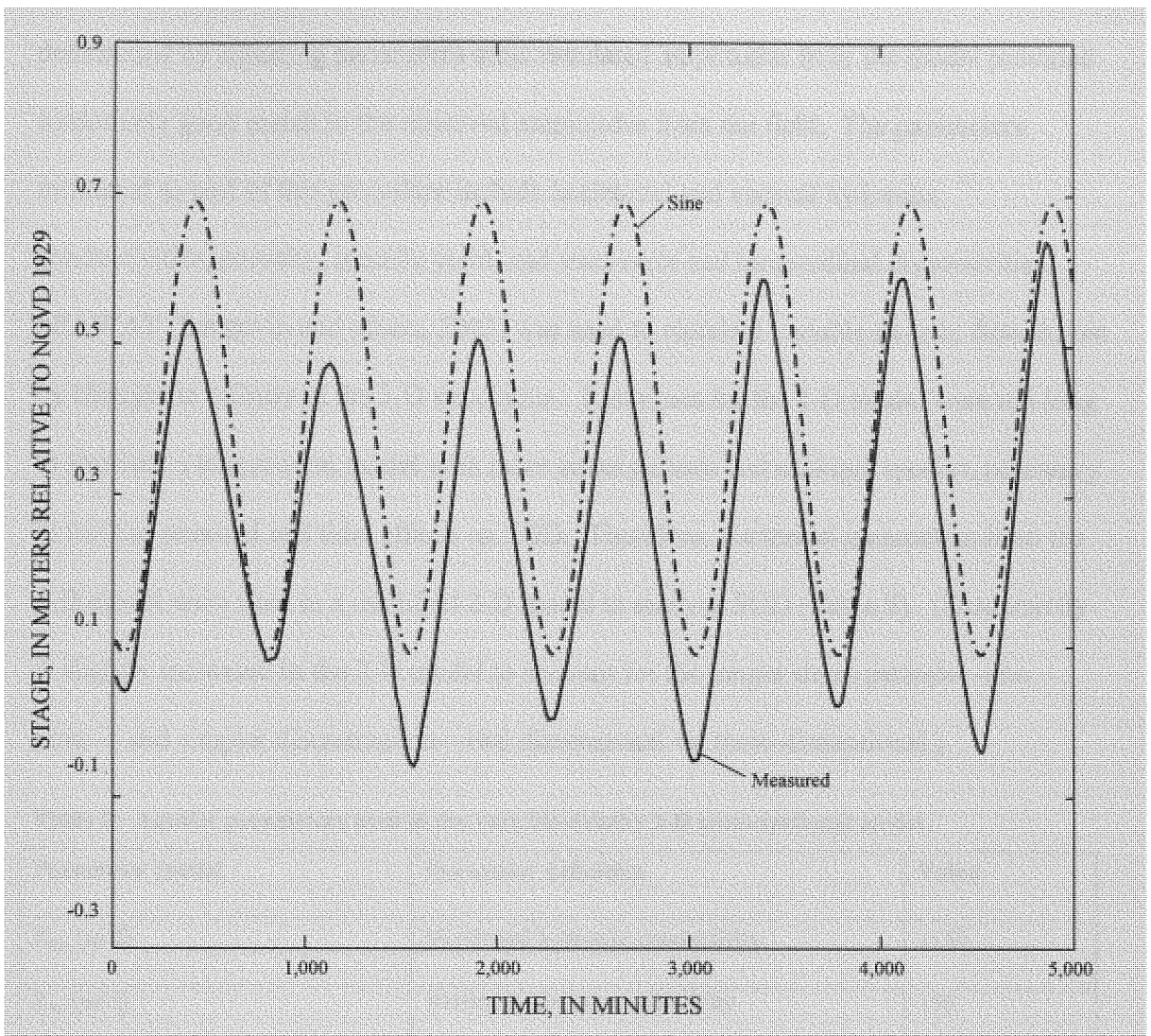


Figure 34: Stage measured downstream at structure S-36 (Figure 31) compared to the sine wave used as the ocean stage for the 3-D model.

A 1-month simulation with 15-minute stress periods and the tidally varying ocean boundary (using the sine wave, Figure 34) was performed to determine representative model values for selected aquifer parameters (all other boundary conditions were held constant). The underlying concept behind this approach is that the diurnal fluctuations in water level and specific conductance, as measured in five of the six continuous monitoring wells (Figure 32), are caused by ocean tides. Representative values were

determined by adjusting parameters until simulated amplitudes from the model provided a relatively good match to the observed amplitudes from the field. The parameters estimated as part of this procedure include horizontal and vertical hydraulic conductivities, porosity, specific yield, and transverse and longitudinal dispersivities. SEAWAT (Langevin and others, 2003) was used to simulate variable-density flow driven by changes in salinity in the 3-D simulation. Run times for the 3-D model were too long to simulate a longer-term model with more stress periods and multiple species, necessary to test the seasonal and tidal effects on SGD. Therefore, the model parameters from the 3-D model were used in a modified 2-D model to analyze SGD (Table 9). (Dispersivity is slightly increased in the 2-D model to account for the longer stress periods—one hour— and simpler discretization—two dimensional vs. three dimensional.)

Table 9: Aquifer parameters used in the variable-density 2-D cross-sectional model.

Parameter [units]	Parameter definition	Value
K_H , [m/d]	Horizontal hydraulic conductivity	1150
K_v , [m/d]	Vertical hydraulic conductivity	150
α_L , [m]	Longitudinal dispersivity	3.0
α_T , [m]	Transverse dispersivity	0.3
S_y [dimensionless]	Specific yield	0.1
S [dimensionless]	Storage	10^{-5}
θ [dimensionless]	Porosity	0.1
D^* , [m^2/d]	Bulk thermal diffusivity	0.67996
μ , [kg/(m d)]	Equivalent freshwater viscosity	86.4
ρ_f , [kg/m^3]	Density of freshwater	1000

ρ_s , [kg/m ³]	Density of seawater	1025
$\frac{\partial \rho}{\partial C}$ [dimensionless]	Density change with concentration	0.7

4.2.3 Two-Dimensional Model

SEAWAT was used in the 2-D model to simulate density-dependent flow caused by changes in salinity, as well as to simulate changes in temperature and age (Thorne and others, 2006; Langevin and others, 2008). Apparent age is simulated using a zeroth-order reaction (see Chapter 1; Goode, 1996; Zheng, 2006). The 2-D model simulated three species: (1) salinity, (2) heat, and (3) age. The data used in the boundary conditions for the 2-D model were obtained from various places in southeastern Florida including Miami-Dade, Palm Beach, and Broward Counties (Figure 32). The 2-D vertical cross-sectional model was aligned along a west-to-east groundwater-flow line perpendicular to the coastline. The model represents a 1-year period from 1 January 1998, to 31 December 1998, using hourly stress periods (to capture tidal to seasonal variations in the system). Consecutive simulations were run using water levels, salinities, and temperatures from the previous model run until salinities and temperatures achieved dynamic equilibrium.

After the salinities and temperatures reached equilibrium, the third species, age, was added. The age of all the water in the model starts at zero. The three cases were first run for 10 years (repeating the one-year simulation 10 times with age from the previous model run). All new water input into the system (via recharge or the ocean) from boundaries comes in at an age of zero. The apparent age of SGD can then be determined by analyzing the age of the water at the areas of discharge. Also, areas of prominent recharge can be observed by their resulting age values being close to zero after a 10-year

simulation. Then, the three separate cases were run for 100 years to assure ages of the main areas of SGD reached equilibrium; when the age of the main points of discharge from the three cases is no longer changing.

The 2-D model grid contains 152 columns and 14 layers; each cell is 150 by 7.5 m, with the top layer 10.5 m (Figure 35). The model is essentially the same as a cross section through the 3-D model (Figure 33C), without the lower part of the surficial aquifer system and the Intracoastal Waterway. The active cells represent the Biscayne aquifer (Table 9), which is underlain by the low-permeability unit of the lower surficial aquifer system (represented with no-flow cells in the 2-D model). The specified-head cells along the sea floor represent the ocean. The ocean water levels and temperature values vary hourly according to measured data collected by National Oceanographic and Atmospheric Administration (NOAA) at the Virginia Key station in 1998 (off the coast of Miami-Dade County, Figure 32 and Figure 36). The salinity value is specified at 35 g/L of total-dissolved solids (TDS). General-head boundary (GHB) cells on the western model boundary were used to represent hydraulic connection with the Florida Everglades and were held constant at 1.48 m with a conductance of 8635 m²/day and a concentration of zero. Temperature of the GHB cells and recharge changed hourly according to measured data from 1998 at the NOAA Lake Worth station on the coast of southeastern Florida in Palm Beach County (Figure 32 and Figure 36). Net recharge, approximated as 15% of rainfall, is applied to the model and changes daily according to data collected by the SFWMD at multiple rainfall stations in Broward County (Figure 36).

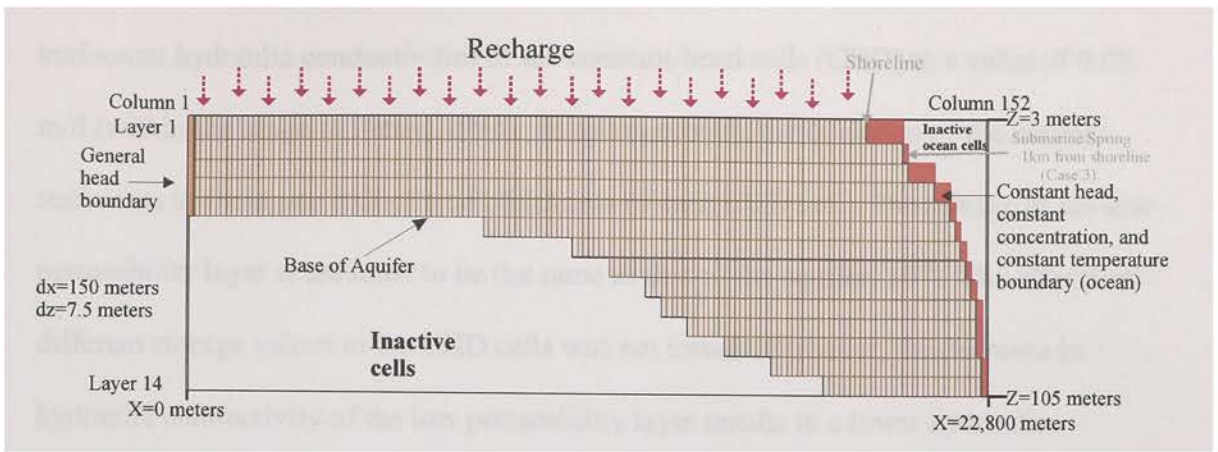


Figure 35: Boundary conditions and finite difference model grid for 2-D model.

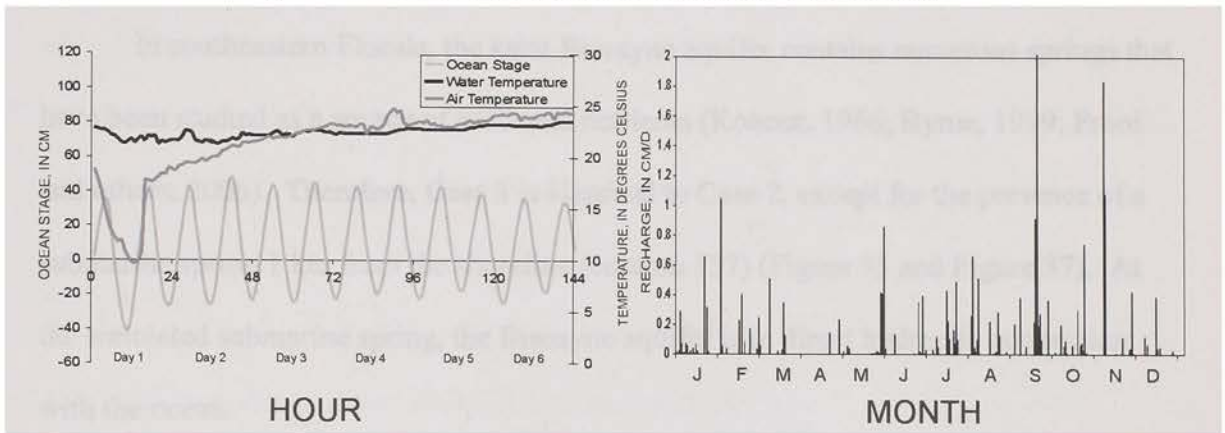


Figure 36: (a) The first 6 days of the stage in the ocean boundary, temperature of the ocean boundary, and air temperature used in the recharge and general-head boundary cells in the 2-D model. (b) Recharge applied to the 2-D model.

Three scenarios were simulated to quantify different types of hydraulic connection with the ocean and to observe the hydrogeologic effects on salinity, temperature, and age of SGD. In the first case, the Biscayne aquifer is in direct hydraulic connection with the ocean (Figure 37). In Case 2, a low hydraulic conductivity layer is assigned along the sea floor (representing low-permeability marine sediments) to reduce the hydraulic connection with the ocean (Figure 37). Fetter (1994) documents a low-permeability layer of sediments on the ocean floor with a range between 0.00864-0.864 m/d. This low-permeability layer is included in the model by setting the vertical and

horizontal hydraulic conductivities of the constant-head cells (CHD) to a value of 0.05 m/d (within the range of Fetter, 1994). In this approach, the thickness of the marine sediments is about one half of a cell thickness of each CHD cell. The storage of the low permeability layer is assumed to be the same as that of the aquifer, 10^{-5} . The affects of different storage values in the CHD cells was not tested. However, the decrease in hydraulic conductivity of the low permeability layer results in a lower hydraulic diffusivity, resulting in a damping of the ocean tides.

In southeastern Florida, the karst Biscayne aquifer contains numerous springs that have been studied as a source of SGD and nutrients (Kohout, 1966; Byrne, 1999; Proni and others, 2006). Therefore, Case 3 is identical to Case 2, except for the presence of a submarine spring 1 km from the shoreline (column 137) (Figure 35 and Figure 37). At the simulated submarine spring, the Biscayne aquifer is in direct hydraulic connection with the ocean.

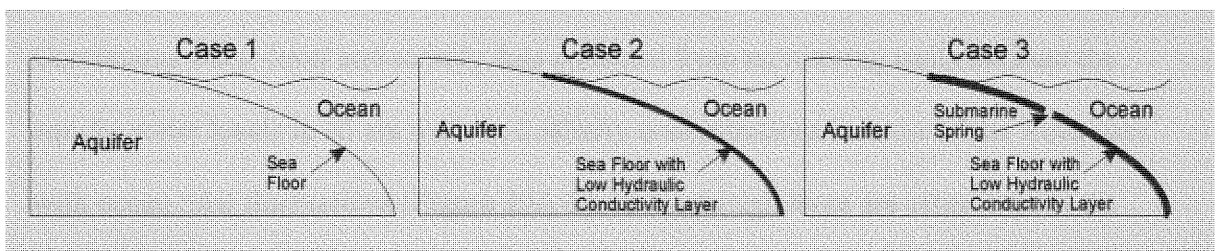


Figure 37: Conceptual models of hydraulic connection between the aquifer and the ocean.

4.2.4 Data Collection of Submarine Groundwater Discharge Used to Test Two-Dimensional Model

Ample data related to SGD have been collected in the coastal areas of southeastern Florida, particularly in Miami-Dade County (Figure 32 and Figure 38), where the coastal waters include Biscayne Bay. This bay is a part of a nationally

protected park (Biscayne National Park—BNP), which contains a fragile ecosystem that is sensitive to environmental changes such as nutrient input from SGD. Even though there have been many types of data collected over the last 10 years, the data collected that were used to verify the 2-D model include: (1) seepage meter data collected in Biscayne Bay by Peter Swarzenski (2004a, 2004b, 2007) and Mike Byrne (1999) from the USGS, (2) surface water and groundwater temperature collected by René Price and Jeremy Stalker (Florida International University—FIU) in Miami-Dade County near the coast, (3) surface water and groundwater temperature data in Biscayne Bay collected by Chris Reich from the USGS, and (4) temperature data from Biscayne Bay and at a spring in the bay, which John Proni and others (2006) from NOAA had collected.

4.3 Results

4.3.1 Data Collection and Three-Dimensional Model

Continuous water-level and salinity data collected from monitoring wells indicate the aquifer water levels in all six wells and salinity concentrations in some of the wells vary with ocean tidal fluctuations (Figure 39A-F). Even though there are other impacts on water-level and salinity fluctuations (such as rainfall and canal stage openings, Figure 39F), the goal with this data is to use the tidal fluctuations to get representative parameters for the 3-D model. Therefore, the tidal amplitudes from the field data were used for comparison to the model.

Numerous 1-month simulations were done to estimate values for horizontal and vertical hydraulic conductivities, porosity, specific yield, and dispersivity until the closest agreement was obtained between field and simulated data. Horizontal and vertical

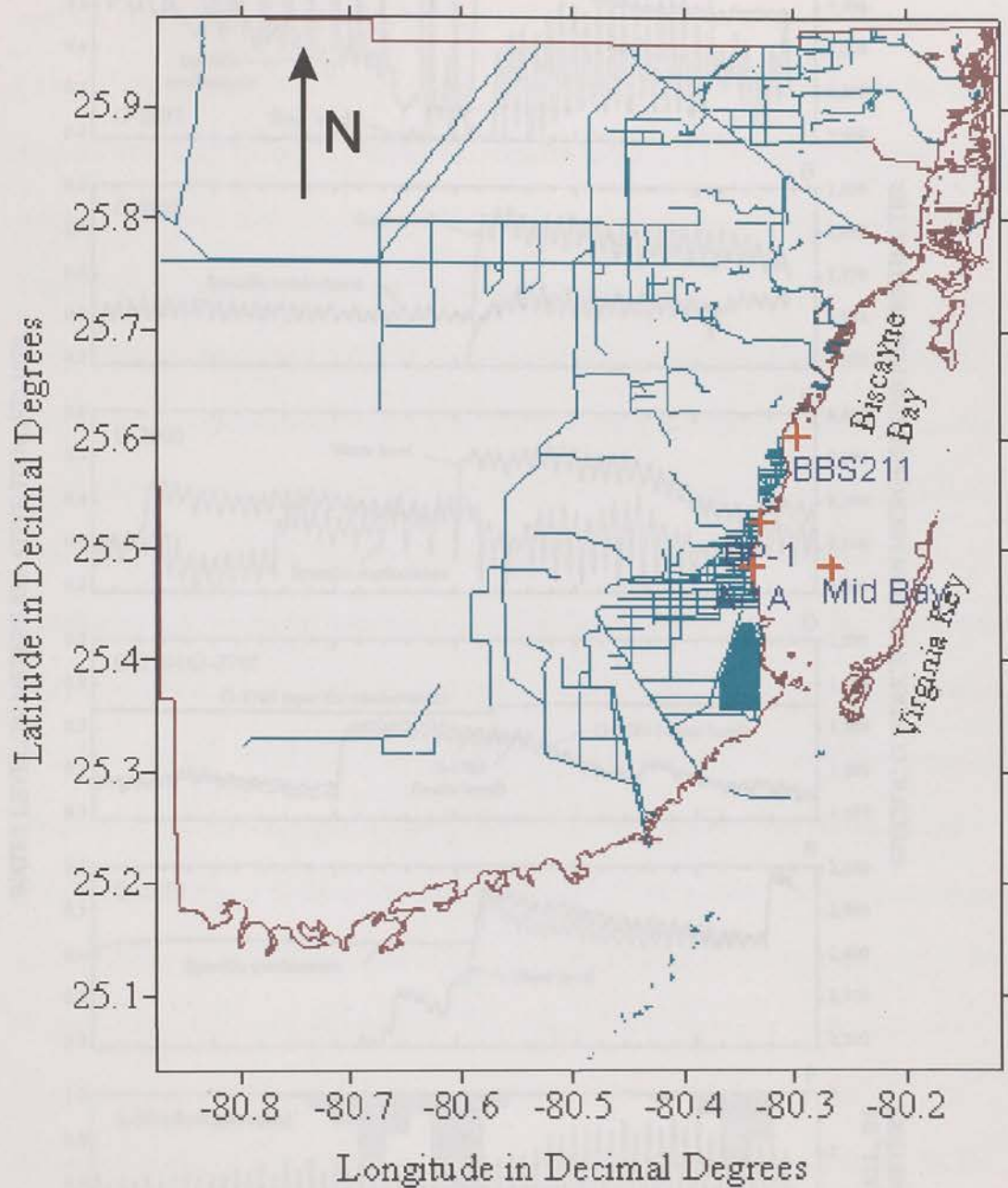


Figure 38: Map showing locations where data were collected off the coast of Miami-Dade County in Biscayne Bay used to verify the 2-D model.

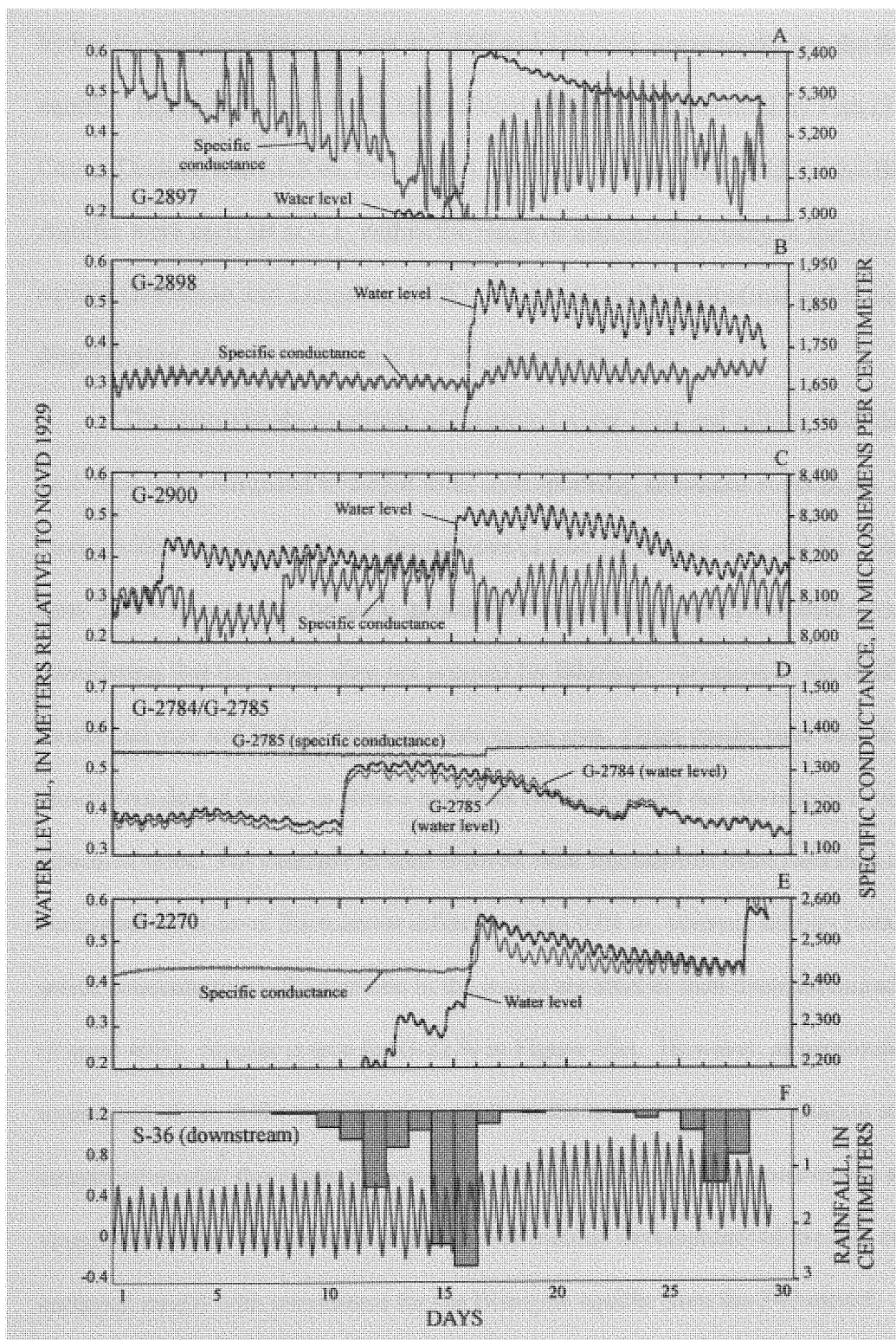


Figure 39: (A-E) Continuous 15-minute record of water-level and specific conductance data for selected monitoring wells (Figure 32), and (F) downstream canal stage and rainfall at structure S-36. The continuous 15-minute stage data for S-36 is shown to illustrate tidal effects.

hydraulic conductivities were set at 1,150 and 150 m/d, respectively, for the Biscayne aquifer. Hydraulic conductivity values were within ranges reported by Fish (1988) and Camp, Dresser, and McKee, Inc. (1980). Porosity and specific yield for the Biscayne Aquifer were each set at 0.1, within the range of estimated porosity in the Biscayne aquifer (Dausman and Langevin, 2005). Model-derived longitudinal and transverse dispersivities were set at 2 m and 0.2 m, respectively.

The approximate amplitude of measured water-level and salinity fluctuations in each well were compared to output from corresponding simulated wells in the 1-month model with constant amplitude fluctuations (Table 10, Figure 40A and B). The values from Table 10 appear to be good matches between the simulated and field data, considering that the model does not account for lithologic variations in the field because of model cell size and lack of lithologic data in the area. Other model runs with different parameters do not reveal as close a match as the final model run developed to simulate the effects of tides. For example in well G-2900, tidal fluctuations from field data and simulated water-level fluctuations differ by about 0.01 m, whereas salinity (total-dissolved solids concentrations) fluctuations in the model are smaller than those measured in the field (Figure 40B). Similar is true for G-2270 in Figure 40A. However, as previously mentioned, these differences likely result from the lack of lithologic variation in the simplified model; therefore, the results are considered a relatively good match for the simplified model. Completion of this model enabled development of the 2-D cross sectional model with parameters for the Biscayne aquifer from the 3-D model.

Table 10: Approximate amplitude of the tidal fluctuations observed in measured and simulated salinity and water-level data from selected continuous monitoring wells.

Well Numbers	Salinity amplitude based on total-dissolved solids concentrations (milligrams per liter)		Water-level amplitude (meters)	
	Measured field data (estimated)	Simulated representation in model	Measured field data (estimated)	Simulated representation in model
G-2270	2.0	0.68	0.02	0.011
G-2784	None (fresh)	None (fresh)	0.03	0.05
G-2785	1.0	1.0	0.03	0.05
G-2897	40.0	6.0	0.02	0.043
G-2898	30.0	58.0	0.08	0.032
G-2900	30.0	7.0	0.04	0.031

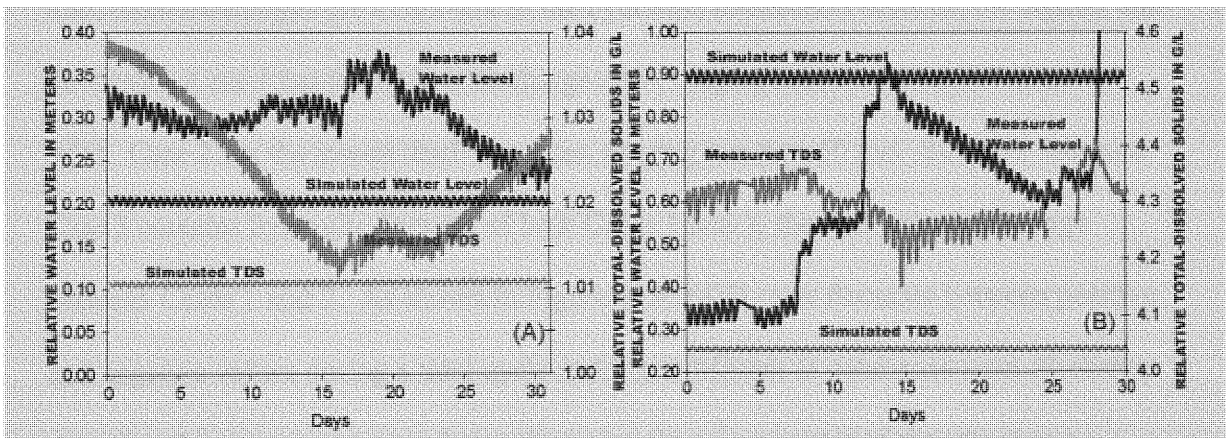


Figure 40: 30-day graph of continuous 15-minute record of water levels and specific conductance (converted to TDS) in 2 of the observation wells [(A) G-2270 and (B) G-2900] compared to simulated observation wells in model. (NOTE: The *amplitude* of the fluctuations between measured and simulated values are intended to be compared, not the actual values of water level and specific conductance.)

4.3.2 Two-Dimensional Model

Simulation results include groundwater discharge rates (and salinities, temperatures, and age) for each hourly stress period and for each model cell. The

discharge rates were combined or averaged in different ways to highlight the differences between the three cases. Flow rates to individual model cells are expressed in units of m/d. When discharge rates are combined, they are expressed in units of m³/d per meter of shoreline (expressed as m²/d), or in the case of a cumulative discharge, as m³ per meter of shoreline.

4.3.2.1 Discharge

Figure 41A shows the total SGD (calculated by summing the discharge for the ocean cells) as a function of time for the first 7 days of the simulation. The highest discharge rates (positive indicating flow from the aquifer into the ocean) occur during low tide; the lowest rates occur during high tide. As expected, the minimum and maximum discharges are a function of the hydraulic connection between the aquifer and the ocean. Case 1 has the highest discharge rates, ranging between about 150 and -150 m²/d. Case 2 has the lowest discharge rates, ranging between 50 and -50 m²/d. Because Case 3 contains hydraulic features of both Cases 1 and 2, the discharge rates range between Cases 1 and 2. As shown in Figure 41A, SGD rates fluctuate between positive and negative values during a tidal cycle making it difficult to determine a net discharge rate. For this reason, the cumulative discharge (in m³ per meter of shoreline) as a function of time was calculated for all the model cells representing the ocean for Cases 1-3 (Figure 41B). The final value of about 3,000 m³/m of shoreline over the course of 1 year is equivalent to an average SGD rate of about 5.5 cm/d (calculated from the 150-m cell width). This is approximately equivalent to the freshwater discharged in all 3 models (Figure 41C), with Case 1 discharging slightly more than Cases 2 and 3. The combined

averaged discharge for all three simulations shown in Figure 41C reveals that the largest total discharge occurs in Case 1, followed by Cases 3 and 2, respectively.

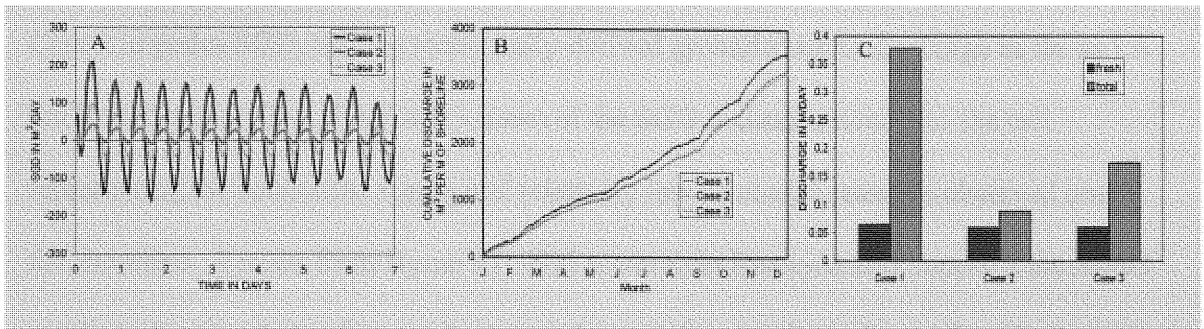


Figure 41: (A) The SGD (calculated by summing discharge/recharge to/from all constant-head cells representing the ocean) for each case over time. The first 7 days of the model run are shown. (B) Cumulative discharge to all cells representing the ocean with time (calculated using water into and out of the constant-head cells representing the ocean). (C) Fresh discharge in the model compared to the total discharge to the ocean (these values are not calculated using water entering the model from the ocean, only water being discharged to the ocean).

Figure 41C suggests that approximately the same amount of freshwater is discharged to the ocean for all three models; however, more seawater is recirculated in Case 1, resulting in a much larger total. Upon closer analysis of the water budget, the fresh recharge applied to the top of the model is discharged either to the general-head boundary cells on the left, or to the constant-head cells representing the ocean. In Case 1, about 79% of the freshwater entering the model discharges to the ocean, whereas, approximately 73% of the freshwater applied discharges to the ocean in Cases 2 and 3. This is why the cumulative discharge from Figure 41B is slightly higher for Case 1, than for Cases 2 and 3.

The average annual rate of SGD was calculated for each constant-head cell representing the ocean (Figure 42) and revealed that the geology (or type of hydraulic connection between the aquifer and the ocean) has an effect on the location of SGD (in relation to the shoreline). In Case 1, most of the SGD is into the first ocean cell. Case 1

also shows large components of recirculated seawater, observed as negative SGD rates farther offshore (Figure 41C and Figure 42). The low hydraulic conductivity layer in Case 2 impedes SGD, forcing terrestrially-derived groundwater to discharge as far as 1.8 km from the shoreline. For Case 3, most of the SGD is concentrated into the cell representing the submarine spring and relatively low discharge rates are observed near the shoreline. Results from Byrne's (1999) research in Biscayne Bay supports the model results indicating that sediment characteristics and distance from shore affect the location and amount of discharge. The highest groundwater discharge is relatively close to shore and decreases with distance. Byrne's thesis (1999) also reveals that areas of the ocean floor with thick, low hydraulic conductivity sediments decrease the amount of discharge.

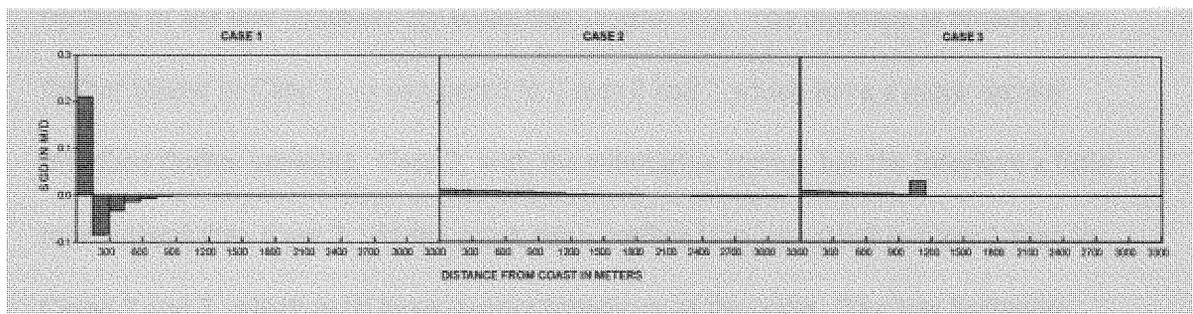


Figure 42: Model results showing the annual average discharge with distance from the coast.

Discharge rates calculated in the 3 cases compare reasonably well with field data. Electromagnetic seepage meter deployments in Biscayne Bay by Swarzenski (Swarzenski and others, 2004b) show that discharge rates from the Biscayne aquifer to the bay vary between 10-50 cm/day with an average of 23.2 cm/day. Figure 41C shows that total discharge is between 9 cm/day in Case 2 to 35 cm/day in Case 1. Byrne (1999) calculates an average discharge from the Biscayne aquifer into Biscayne Bay to be 20.6 m³/day per meter of shoreline (from seepage meter results). Byrne's results compare well to model results. There are often errors associated with seepage meter measured fluxes due to the

seepage meter only representing a small area, while aquifer heterogeneity can cause seepage to spatially vary over larger areas (Cable and others, 2003). However, Byrne's number is based on the deployment of 15 seepage meters in different locations on the floor of Biscayne Bay, which should average out some of the spatial variability. A water budget analysis reveals that Case 2 results in a total discharge of about 13 m³/day per meter of shoreline, and this increases to approximately 57 m³/day per meter of shoreline in Case 1. These values are also in the range of calculations by Byrne (1999).

4.3.2.2 *Salinity*

The shape, thickness, and location of the interface varies between Cases 1 to 3 because of the low conductivity sediments (Figure 43). The interface is broader and farther inland in Case 1, as compared to Cases 2 and 3 which have a more narrow interface farther seaward. Case 3, with the submarine spring, has the interface a little more inland than Case 2. At the coast, the interface is more mixed in Case 1 than in Cases 2 and 3, which both have sharper interfaces at the coast. The low hydraulic conductivity sediments on the ocean floor in Cases 2 and 3 decrease the mixing between the ocean water and groundwater, causing the interface to be sharper and slightly seaward.

The changes in salinity with time for each case appear to be caused by fluctuations in ocean stage as shown by an inverse correlation (Figure 44); a higher ocean stage corresponds with a smaller difference in salinity between the aquifer and ocean in all three cases. However, the average salinity difference is only about 2 g/L TDS in Case 1, indicating that most of the SGD for this case has near-seawater salinities. This is

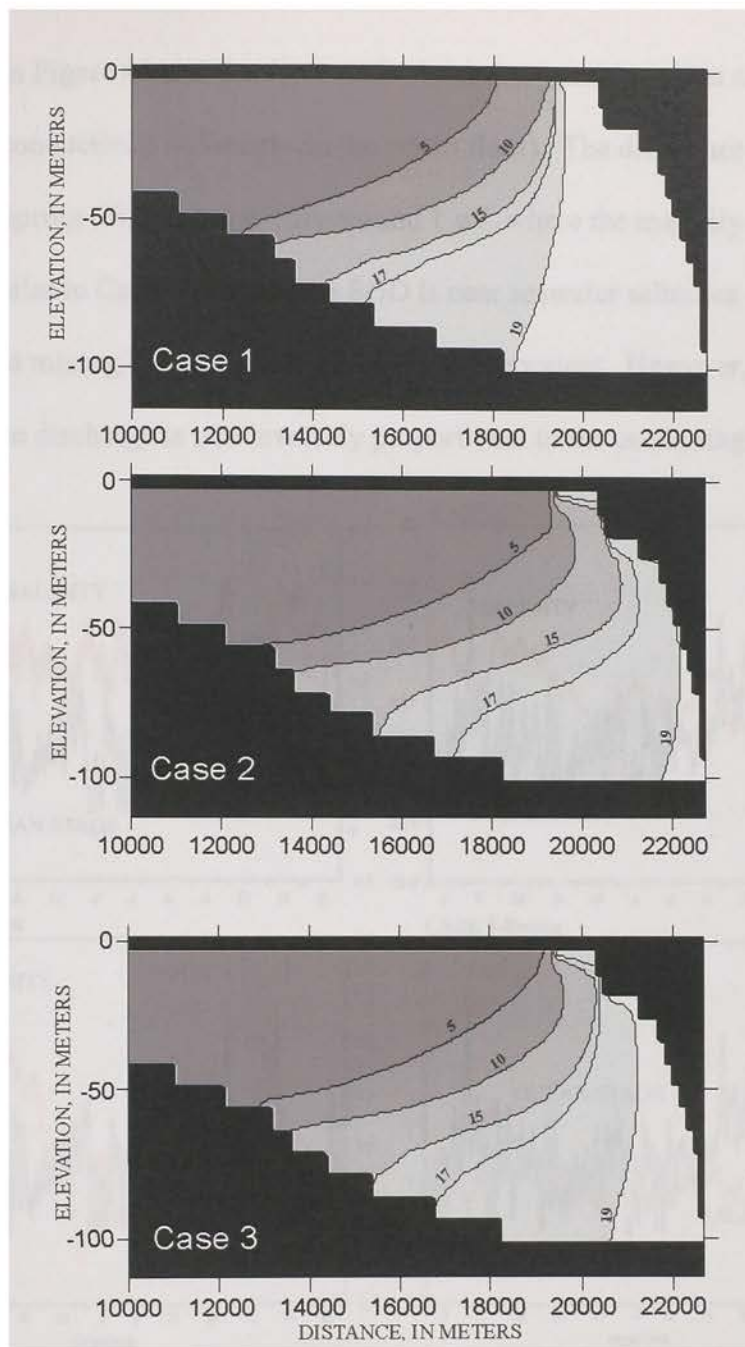


Figure 43: Cross section of three different cases showing salinity contours in g/L of total-dissolved solids.

because SGD at the coast has a large portion of recirculated seawater (Figure 41C and Figure 42) due to the open connection between the ocean and aquifer. The inverse correlation is also seen in Cases 2 and 3; however, at the coast the difference in salinity is around 20 g/L and higher. The large difference in salinity correlates with the sharp

interface seen in Figure 43 and the decreased mixing between the ocean and aquifer (from the low conductivity sediments on the ocean floor). The difference in salinity at the submarine spring (Figure 44) is only around 1 g/L where the majority of SGD is occurring. Similar to Case 1, most of the SGD is near seawater salinities at the spring due to increased mixing between the ocean and aquifer waters. However, the salinity difference of the discharge is still inversely proportional to the ocean stage in all cases.

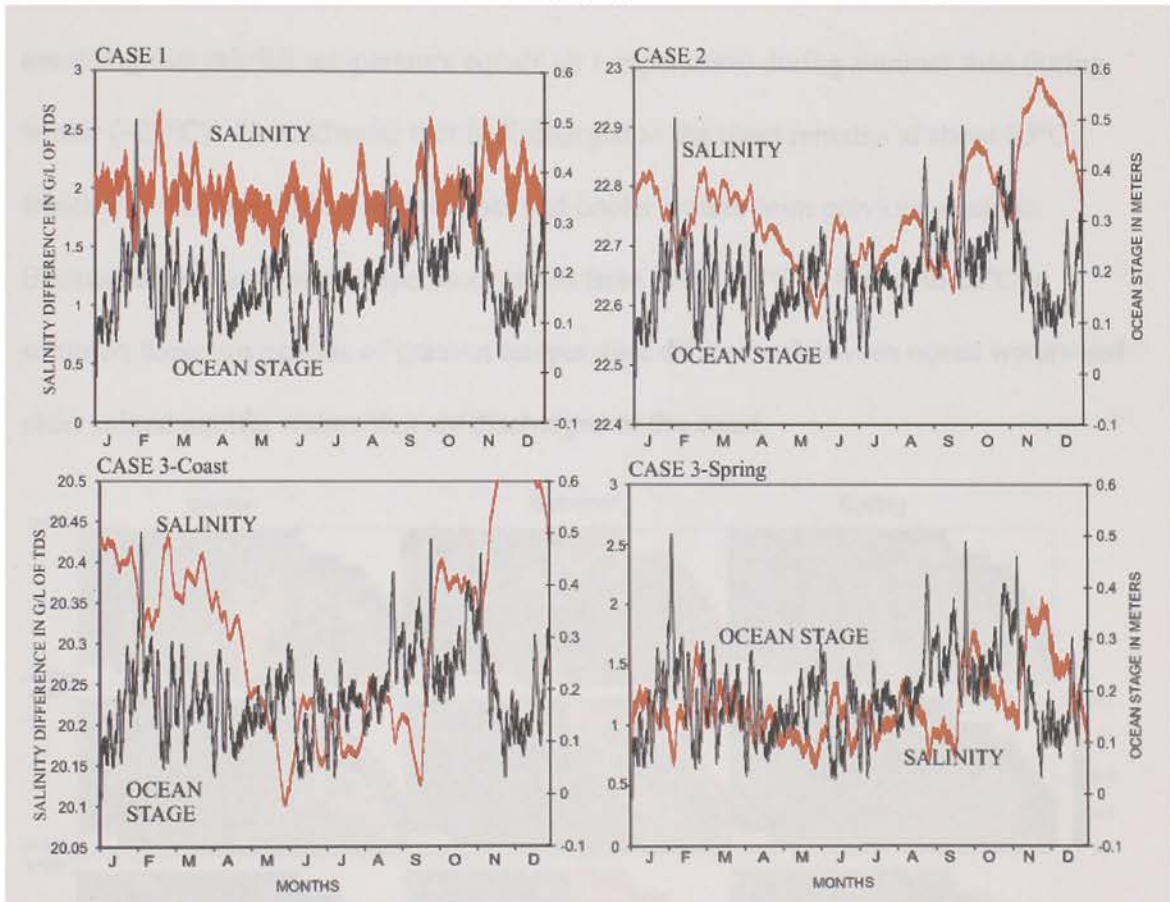


Figure 44: Graphs showing the difference in salinity between the aquifer and ocean (in red, ocean-aquifer salinity) and the ocean stage (in black) with time at the coast for Cases 1, 2, and 3. The difference in salinity and the ocean stage at the submarine spring for Case 3.

4.3.2.3 Temperature

The model simulates a seasonal fluctuation between the ocean and SGD, with warmer groundwater discharging into the colder saline ocean in the winter (Figure 45). During late summer, cooler groundwater discharges into the warmer ocean waters. Temperature differences between groundwater and the ocean are minimal during the spring and fall. In southern Florida, the ocean and rainfall are both warmer ($\sim 28^{\circ}\text{C}$, assuming that rainfall temperature equals air temperature) during summer than during winter ($\sim 22^{\circ}\text{C}$). Groundwater that is discharged to the coast remains at about 25°C , which is a mixture of the older warmer and cooler waters from previous seasons. Because the ocean water temperature varies from about 22°C in winter to 28°C in summer, these are periods of greatest temperature difference between ocean waters and older mixed aquifer waters that are discharged to the coast.

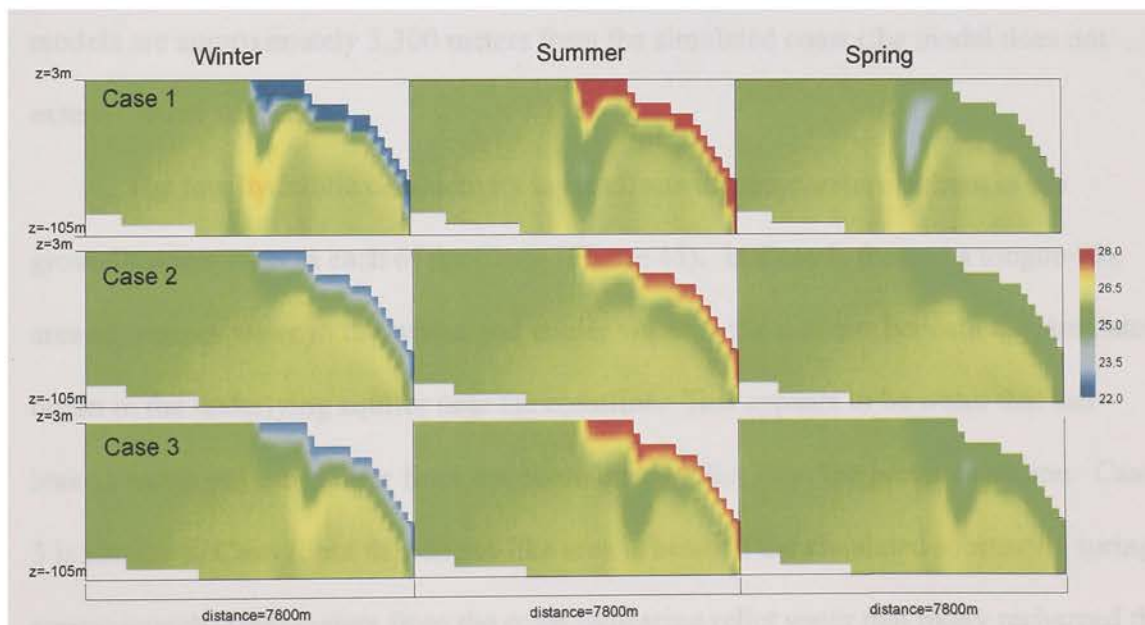


Figure 45: Temperature (in degrees Celsius) for the three cases in the winter, summer, and spring.

The simulated seasonal change between the ocean and aquifer is verified with observation data collected at the coast of Miami-Dade County and in Biscayne Bay (Figure 38 and Figure 46), revealing temperature differences in winter and summer as high as 10°C. Temperature differences simulated at the coast of all three cases compare well to data collected by René Price and Jeremy Stalker from FIU at observation sites A1A and BP1 at the coast (Figure 38). Data collected at groundwater wells in the field were subtracted from data from surface water sites that correspond with the location of the groundwater wells; the data were then graphed with simulated differences in temperature (Figure 46). Chris Reich from the USGS collected surface water and groundwater data from a site in Biscayne Bay called *midbay* approximately 7,000 meters from the Miami-Dade coast (Figure 38 and Figure 46B). Reich's data compare relatively well to simulated data from all three models, despite the fact that the observations in the models are approximately 3,300 meters from the simulated coast (the model does not extend farther seaward).

The low hydraulic conductivity layer affects the temperature pattern in the groundwater system in each of the Cases (Figure 45). In Case 1, there is a tongue-like area of warmer water in the winter and cooler water in the summer beneath the simulated ocean in the underlying aquifer near the coastline. This appears to be water that has leaked/recharged the aquifer from the ocean and is relict from the previous season. Case 3 is similar to Case 1, but the tongue-like area is beneath the simulated submarine spring approximately 1000 meters from the coast indicating relict water that likely recharged the aquifer in an earlier season. Case 2, with the low hydraulic conductivity sediments, has

no specific area where water appears to have recharged the aquifer, but a constant temperature gradient between the ocean and aquifer.

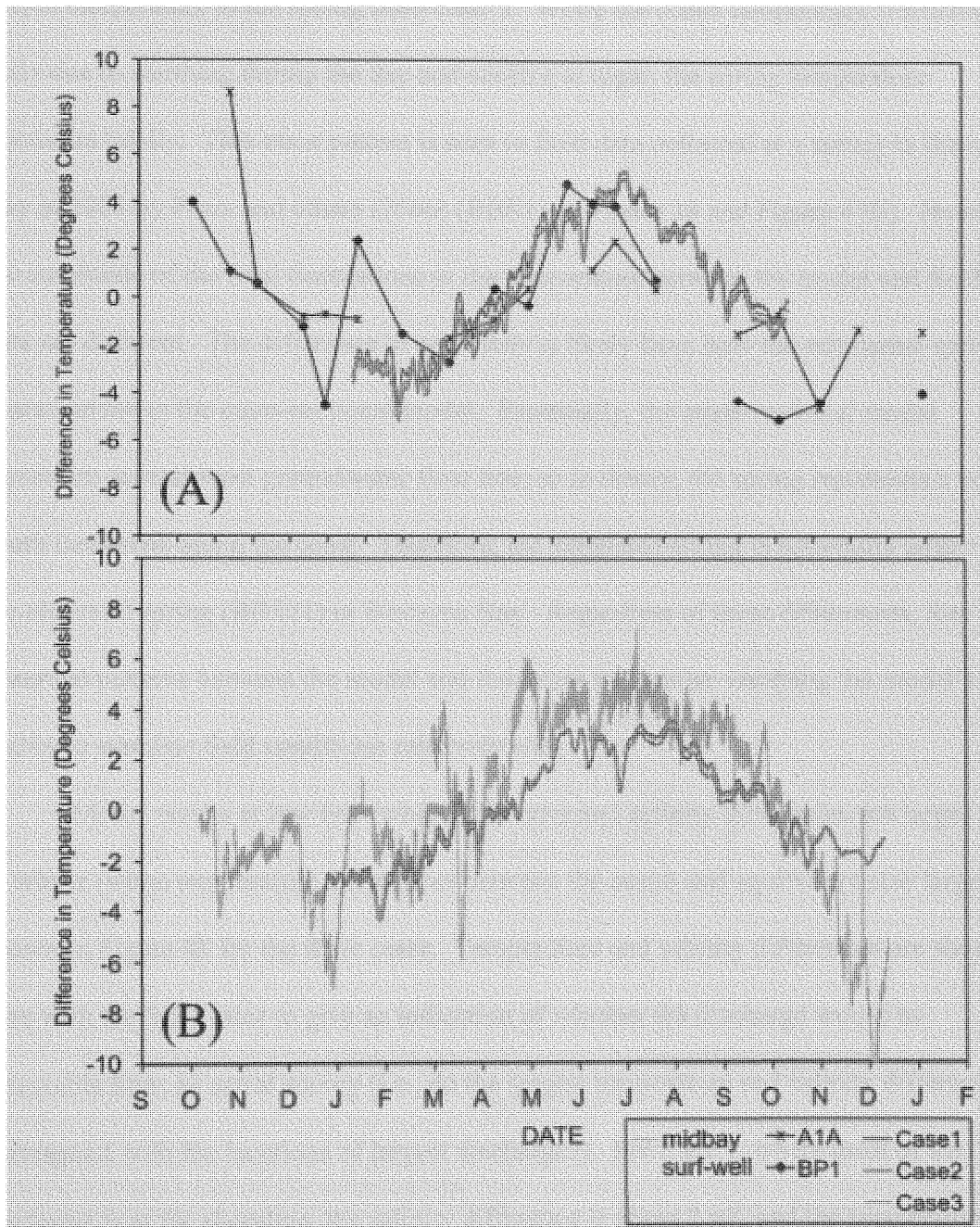


Figure 46: Graphs showing the difference between the ocean temperature and the groundwater temperature with time. (A) Field data (Figure 38) collected at the coast (A1A and BP1) compared to the difference in temperature at the simulated coast in Cases 1-3 (column 130 minus column 129 in layer 1), and (B) Field data collected at the *midbay* surf-well (Figure 38) compared with simulated data approximately 3,000 meters from the simulated coast (column 151 in layer 12 minus column 151 in layer 13).

Figure 47A shows a graph of the temperature of the ocean in the model with the output temperature of the spring from Case 3. While the ocean temperature fluctuates daily due to warming during the day and cooling at night, the spring temperature fluctuates tidally. This same pattern is seen in field data collected at a spring in Biscayne Bay in 2005 by Proni and others (2006) (BBS21 in Figure 38 and Figure 47B). However, the amplitude of the tidal fluctuations in the temperature between the model and field data are different. The difference in amplitude is likely from how the submarine spring is characterized in the cross-sectional model. Essentially, the cross-sectional model represents an east-west groundwater flow line, so in theory, the spring represents a north-south line/break along the coast. Therefore, the simulated spring is notionally larger than the observed spring (BBS21) in Biscayne Bay. Regardless of these differences, the observed patterns between the model and field data are similar verifying the model's ability to simulate field conditions relatively well.

Model results at low tide (when SGD rates and salinity differences are large) and in winter (when temperature differences between the ocean and aquifer are also large) are shown in Figure 48 for the three cases. Temperature and salinity differences are shown here with the SGD rates to give an indication of whether the discharge would be detectable from an aerial survey (i.e., do the largest temperature and salinity differences correspond with the locations of largest discharge?). For Case 1, where most of the discharge is at the shoreline, the salinity difference is about 2 g/L and the temperature difference is about 3°C. In Case 2, the fresh SGD is not concentrated near the shoreline, but discharged over an outflow face extending over 1 km from the coast. The low

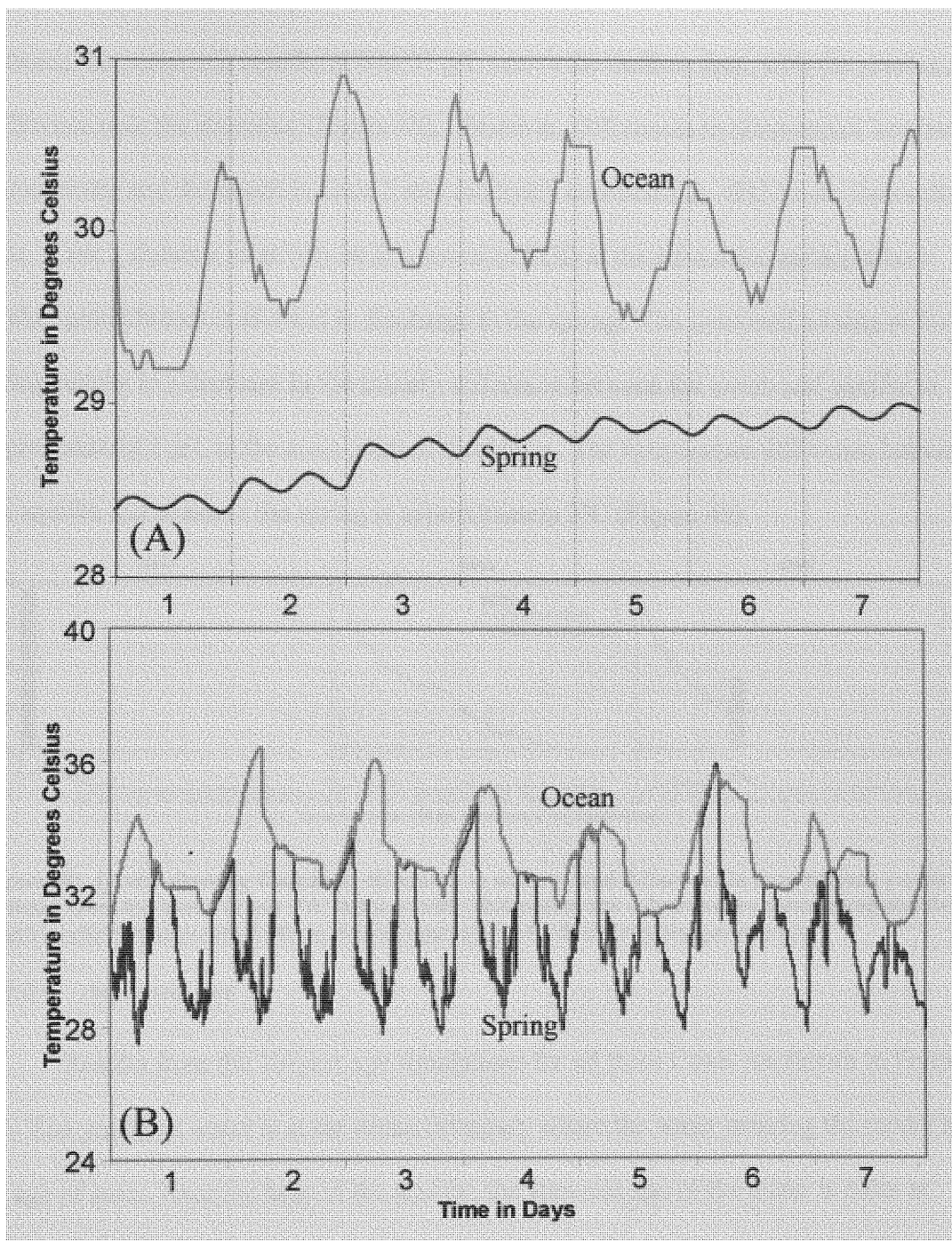


Figure 47: Temperature of the ocean showing daily fluctuation in temperature with the temperature of the spring showing tidal fluctuations. (A) Model output from Case 3, and (B) Data collected from spring BBS21 in Biscayne Bay (Prioni and others, 2006).

hydraulic conductivity layer in Case 2 impedes the flow of SGD and reduces the mixing of the aquifer and ocean waters. The reduced mixing results in a salinity difference

between the ocean and aquifer of 6 to 23 g/L across the outflow face, with the greatest difference near the shoreline (Figure 48). However, differences in temperature between groundwater and the ocean in Case 2 stay relatively consistent at ~6°C across the outflow face. Case 3 shows a relatively large amount of SGD at the submarine spring, where fresher groundwater is allowed to discharge to the spring. The increased mixing at the spring results in a decrease in the salinity difference between the ocean and aquifer to approximately 3 g/L at the main point of discharge. The temperature difference between the aquifer and ocean at the spring is approximately 3°C (Figure 48).

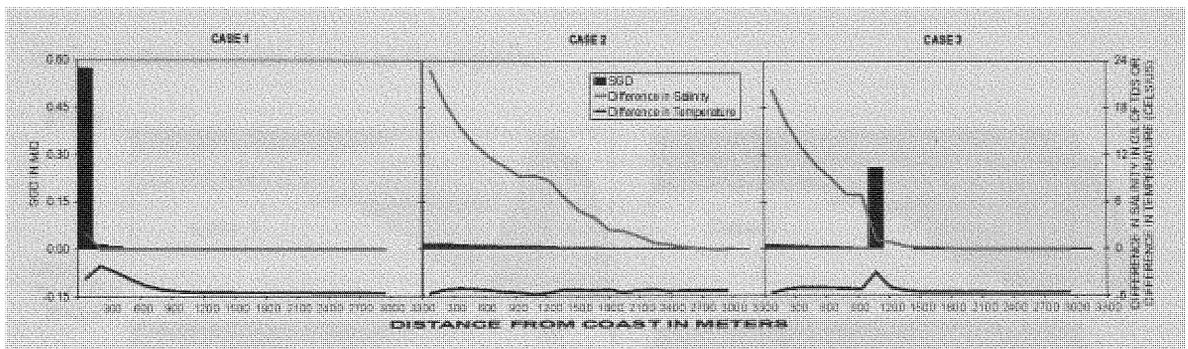


Figure 48: Graph showing discharge, difference in salinity, and difference in temperature versus distance from the coast, at low tide in the winter (differences are calculated by subtracting simulated aquifer salinity/temperatures from ocean/constant-head cell salinity/temperatures).

4.3.2.4 Apparent Age

Results from the 10-year age simulations for all three Cases are shown in Figure 49. The youngest water is at the ocean boundary where the water entering the model has an age of zero. Near the base of the aquifer, the apparent age of the water is older at approximately 10 years in all three Cases. The recharge applied to the top of the model also has an age of zero years; however it mixes with older waters giving an age of approximately 5 years. Cases 1 and 3 have tongue-like areas of young saline water that recharge the aquifer. However, upon comparing Figure 45 and Figure 49, the younger

water from the age simulations (the blue tongue-like area) is slightly seaward of where the relict temperature from previous seasons occurs in Cases 1 and 3. It appears the younger water is recharged (at the temperature of the ocean), then recirculated in the aquifer to be discharged at a later time (and different temperature, relict of previous seasons). The locations of the younger aquifer waters in Cases 1 and 3 are dependent upon the hydraulic connection to the ocean and location of the submarine spring. The water from Case 3 comes from the simulated spring and the water from Case 1 is leaking downward at the coast. Case 2 has a relatively constant age gradient from younger water in the ocean to older water in the aquifer.

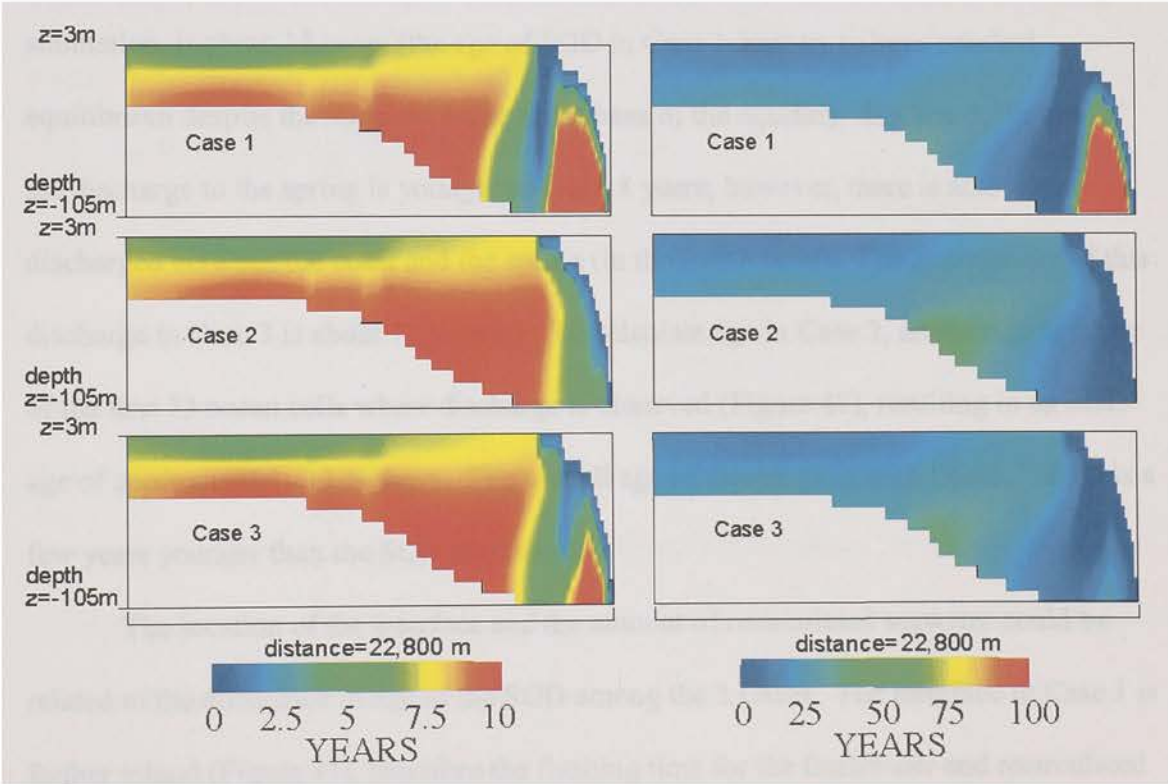


Figure 49: Age of water for each case after 10 years (repeating the one year simulation 10 times) and after 100 years (repeating the one year simulation 100 times).

The 100-year age simulation shown in Figure 49 reveals that for a longer-term simulation, age at the base of Case 1 is older than both Cases 2 and 3. Case 1 has a stagnant area of water near the base of the aquifer where the age is 100 years; essentially revealing that age at the base has not reached equilibrium. However, the oldest waters simulated in Cases 2 and 3 are approximately 50 years, revealing that these two simulations have reached equilibrium in regards to age.

Apparent age of the main locations of discharge (Figure 42) in each Case was extracted from the model after the 100-year simulations to get approximate residence times of SGD. In Case 1 the age of the discharge to the first ocean cell, after a 100-year simulation, is about 15 years (the age of SGD in Case 1 appears to have reached equilibrium despite the stagnant water at the base of the aquifer). In Case 3, the age of the discharge to the spring is younger at about 8 years; however, there is also water discharged between the coast and the spring (in the first 8 cells). The average age of this discharge in Case 3 is about 12 ½ years. To calculate age in Case 2, an average is taken of the first 13 ocean cells where discharge is observed (Figure 42), resulting in an SGD age of approximately 13 ½ years. The overall age of discharge in both Cases 2 and 3 is a few years younger than the SGD for Case 1.

The location of the interface and the amount of recirculated seawater could be related to the difference in age of the SGD among the 3 Cases. The interface in Case 1 is farther inland (Figure 43), therefore the flushing time for the freshwater and recirculated seawater is likely longer than Cases 2 and 3. The longer flushing times are confirmed by the stagnant older water at the base of the aquifer in Case 1, where the water is a minimum of 100 years in the simulation. Whereas, in Cases 2 and 3, the oldest simulated

water is around 50 years. The older SGD in Case 1 could also result from a higher amount of older recirculated seawater, compared to Cases 2 and 3, as observed in Figure 41C.

4.4 Discussion

Variable-density groundwater flow models can be used to understand the complex nature of a coastal groundwater system. This analysis illustrates how the salinity, temperature, rate, and age of SGD are affected by the hydraulic character of the coastal system from the geological setting to the ocean stage. The results from this type of analysis can be used to help guide data collection efforts for studies of SGD as well as understand the nature of the system, quantify the residence times of water, and potentially give insight into the amount of nutrients in the SGD.

4.4.1 Model Calibration

This study shows how various types of data (tidal to seasonal salinity, water-level, and temperature data) can be used in model calibration and verification. It also shows that short-term tidal fluctuations, to longer-term seasonal fluctuations, can not only be observed in the data, but represented in a model and used to obtain important information about model parameters. Research has shown that tides are pertinent when studying SGD (Robinson and others, 2006a, 2006b); therefore, it is important to include tides in a numerical simulation to accurately represent SGD. Even though a model may only be representative of a system, the model can still be developed, verified, and used to give insight into a complicated coastal system.

4.4.2 *Implications for Data Collection*

Geophysical surveys, such as EM resistivity, have the ability to detect salinity variations at depth (beneath the ground surface/ocean floor). Electromagnetic resistivity has successfully been used to map the location of the saltwater-freshwater interface; therefore, can potentially be used to detect fresh SGD above the saltwater-freshwater transition zone (Becker, 1988; Fitterman and Deszcz-Pan, 1998, 2002a, 2002b; Swarzenski, 2004b, 2007; Kontar and Ozorovich, 2006). While geophysical techniques have been used to identify rock formations and the presence of saltwater versus freshwater below land surface; Becker (1988) was one of the first scientists to show that *aerial* resistivity mapping could be used to map the location of the saltwater-freshwater interface. Later, Fitterman and Deszcz-Pan (1998, 2002a, 2002b) used aerial EM resistivity surveys to map the location of the freshwater-saltwater interface in the Everglades in southern Florida. The success of the resistivity surveys depended upon borehole logs to identify the relationship between the water quality and resistivity results, as well as a large enough difference in salinity with depth to identify the interface. Miyaoka (2007) used electrical conductivity in groundwater wells, as well as streaming resistivity profiles to show that groundwater-seawater interactions are affected by the geology and tidal conditions in Japan. Having the ability to successfully map the location of the interface can then potentially be used to give insight to estimating locations of SGD above the saltwater-freshwater transition zone (Kontar and Ozorovich, 2006).

During all times of the year, fresher groundwater is discharged to the ocean in southeastern Florida above this transition zone. However, the salinity difference between the aquifer and ocean is affected by the hourly and monthly ocean stage variations

(Weinstein and others, 2007). The modeling for this research reveals that aerial EM surveys (or other geophysical surveys) may be best conducted at low tide and when ocean stages are at a relative low. This is when the difference in salinities between the aquifer and ocean are greatest (Figure 44 and Figure 48). Therefore, the results from an aerial survey could potentially be improved by including expected ocean stage variations for the specific target area as part of the data collection plan. Similar results were found off the southeastern coast of Sicily by Kontar and Ozorovich (2006), where geo-electromagnetic surveys along with seepage meter and Radon data were used to map the freshwater-saltwater interface and give insight to SGD. Results from Kontar and Ozorovich (2006) also revealed that tides affected the location of the interface and amount of SGD.

Modeling as part of the research presented in this dissertation show that an aerial survey using EM resistivity may or may not be successful depending upon the geology of the aquifer. An aquifer in direct hydraulic connection with the ocean, such as Case 1, may not have large enough salinity differences between the aquifer and ocean for an aerial survey to detect (a difference of only 2 g/L at the shoreline, decreasing to 0 g/L with distance from the shore). Case 2 contains a low hydraulic conductivity layer of sediments across the ocean floor. Although the sediments impede SGD and increase the zone of discharge over a larger area of the ocean floor, the difference in salinity between the ocean and aquifer waters is relatively high in this environment (up to 23 g/L), enabling likely detection by EM resistivity (Figure 48). If there is a fracture in the low conductivity layer, resulting in a submarine spring, as in Case 3, the SGD across the ocean floor and at the spring may be high enough for detection by the survey as long as the salinity differences between the aquifer and ocean are relatively high, as in Figure 48.

Data collection methods utilizing thermal imagery to quantify SGD are successful in calm waters where the temperature difference between the SGD and ocean waters is greater than 0.08°C at the ocean surface. Thermal imagery cannot detect temperature variations below the surface; therefore, a large temperature difference between the SGD and the ocean and a relatively large amount of SGD are necessary for detection. Thermal images should be collected at low tide when SGD is relatively high and at a location where SGD rates would be large enough to reach the ocean surface and affect the temperature (Mulligan and Charette, 2006). According to the model results presented, in southern Florida thermal imagery surveys are best conducted during the late summer or late winter when temperature differences between SGD and the ocean waters are the largest, $\sim 3^{\circ}\text{C}$ (Figure 45 and Figure 46). During the spring and fall, SGD is about the same temperature as the ocean and would probably not be detected. This is confirmed by data collected on Cape Cod, Massachusetts by Michael and others (2005), where seasonal temperature changes affected the temperature of submarine groundwater discharge as compared to the ocean water.

Model results suggest that the success of a survey using thermal imagery is affected by the geology of the aquifer. When the aquifer is in direct hydraulic connection to the ocean, as in Case 1, a narrow zone of high discharge exists at the shoreline close to the surface. In this environment, the temperature difference of $\sim 3^{\circ}\text{C}$ between the SGD and the ocean would probably be detected by an aerial survey using thermal imagery (Figure 48). If there is a low conductivity layer of marine sediments producing a wide zone of discharge across the sea floor and a decreased amount of SGD (Case 2), thermal imagery will likely not work. Even though the temperature difference is $\sim 6^{\circ}\text{C}$, the lack of

concentrated discharge reaching the ocean surface would make SGD undetectable (Figure 48). However, if there is a submarine spring in this environment (Case 3), it would likely be identified by thermal imagery as long as the spring exists in shallow waters, there is an increased amount of SGD (i.e., at low tide; Shaban and others, 2005), and the temperature difference is greater than 0.08°C (Figure 48). If the submarine spring is too deep, thermal imagery will likely not detect the spring.

The conclusions from the modeling presented in this chapter appear to be reasonable when compared to successful collection of thermal imagery and temperature data in other areas around the world. Thermal imagery was successfully used off the coast of Lebanon to identify submarine springs, submarine groundwater discharge, as well as geologic features (Shaban and others, 2005). The thermal imagery data was collected when the temperature differences between a carbonate aquifer and ocean were greatest, in the late summer in early morning and late evening. Shaban and others (2005) were also able to correlate the SGD with geologic and karstic features by comparing the thermal imagery data with satellite images. Mulligan and Charette (2006) were also able to successfully collect thermal imagery data in Waquoit Bay in the late summer where groundwater temperatures were much cooler than temperatures in the bay. They also revealed that at low tide and when ocean waters are at a relative low (as compared to the rest of the year) were the best time to collect the thermal imagery data because SGD rates from a sandstone aquifer were at a maximum. Thermal imagery data was used in the Waquoit Bay study with seepage meter data and pressure transducers in monitoring wells to detail SGD rates and locations. Taniguchi and others (2003) were also able to use groundwater temperature to estimate SGD rates from a limestone aquifer in Australia.

4.4.3 Implications for SGD Residence Times and Potential Nutrient Transport

Modeling of variable-density systems, which include the apparent age of the water, could potentially be used by geochemists and ecologists in the analysis of SGD groundwater residence times and nutrient transport. Swarzenski and others (2004a) as well as Price and others (2003, 2006) were able to successfully use geochemical techniques to quantify nutrients and age in SGD/CGD. Oberdorfer (2003) was also able to show how modeling can be used in SGD estimates; however, pointing out that numerical models often neglect the important part of recirculated seawater portion of SGD. Simulations from research in this dissertation reveal that the recirculated seawater, as well as estimates of age, can be successfully simulated in numerical models if the model is designed properly. It also appears that age and residence time of SGD can be affected by the aquifer geology/marine sediments. The geology affects not only the amount of fresh SGD, but also the location of the interface and amount of recirculated seawater, which in turn affects the residence time of the SGD. Weinstein and others (2007) use seepage meter data, radon, and sea level to study SGD rates on the coast of Israel, pointing out that recycled seawater is an important part of quantifying SGD.

An area with no marine sediments on the ocean floor impeding SGD could contain more nutrients because of the longer groundwater residence times, likely from an interface farther inland with longer flushing times. In areas where there are marine sediments that impede SGD, the amount of freshwater discharge and recirculated seawater is reduced, the interface is farther seaward, and the groundwater residence times are less. Therefore, the amount of nutrients discharged to the coastal system could be less.

Tritium/helium data can be used to date groundwaters with ages of less than 50 years. Price and others (2003) successfully dated groundwaters beneath Everglades National Park, just west of Miami-Dade County in southeastern Florida, in the surficial aquifer system. Results from that research revealed that at depths of less than 30 meters, groundwater ages were less than 30 years. Whereas, depths of greater than 30 meters revealed groundwater ages greater than 30 years (however, the older groundwaters were not specifically dated, only known to be older than 30 years because of the lack of tritium). Resulting ages from the 100-year simulations do not contradict the age dating performed by Price and others (2003). Simulations result in SGD ages from 12-15 years, as well as ages of less than 30 years in the top 30 meters of the aquifer. At depths greater than 30 meters, all three Cases result in ages of greater than 30 years.

Results from the age simulations are preliminary, only providing a first step towards demonstrating that apparent age can be successfully simulated with SEAWAT. However, the modeling results are encouraging because the age simulations appear to be consistent with research done in the southeastern Florida area. Therefore, the potential for using age to calibrate a model or guide geochemists in data collection appears reasonable.

4.5 Chapter Summary and Conclusions

Numerical modeling can help enhance knowledge of SGD and guide SGD data collection efforts by providing estimates of expected salinity, temperature, and age variations. Aerial surveys using EM resistivity are more appropriate for some coastal environments, whereas, thermal imagery is likely more successful in others. Results

from this research indicate that modeling of a coastal environment prior to data collection can reveal the potential for success using either type of aerial surveys. This investigation also reveals that ignoring short-term temporal changes on the system, such as tides, could hinder modeling efforts to guide data collection.

This modeling effort shows that not only temperature and salinity, but age can also be simulated using SEAWAT. Simultaneously modeling these three species can give insight to groundwater residence times and potentially nutrient transport in SGD, which could aid geochemists and ecologists. The data from geochemists (particularly age), as well as other types of temperature and concentration field data, could also aid modelers in the calibration process if multiple species such as salinity, temperature, and age are simulated.

Although the results presented here appear to be representative for southeastern Florida, the general conclusions may also be valid for other environments with similar hydrogeological and ocean characteristics.

5 SUMMARY AND CONCLUSIONS

This dissertation reveals how multiple species can be practically included in a variable-density flow and transport model. Simulating species such as salinity, heat, and age can enable better model calibration where data are available. At the same time, this research shows how a model can be used to guide data collection. Hopefully, this dissertation can be used to aid scientists in multiple fields (such as hydrology, geology, geochemistry, etc...) by revealing how different types of data can be pragmatically used

in numerical modeling and how numerical modeling can aid scientists in their data collection efforts.

In conclusion, this dissertation reveals how the most recent version of SEAWAT accurately simulates variable-density flow resulting from multiples species, including concentration and temperature. This research presents successful and innovative use of the code in two hydrologic analyses: (1) to utilize a new linear method to quantify the worth of temperature and salinity data in a nonlinear model, and (2) to present a novel way in which a variable-density model can be utilized to guide data collection. Results from this research will enable a broader audience to use SEAWAT in hydrologic studies, as well as provide original methods to use variable-density models to guide data collection. This could potentially aid scientists in saving time and money in research projects that combine a data collection effort with modeling.

5.1 Benchmarking of SEAWAT Version 4

SEAWAT Version 4 supports equations of state for fluid density and viscosity and can be used to simultaneously simulate salinity and temperature effects on variable-density flow in liquid through a porous medium. Variations in viscosity from changes in temperature or concentration are included, as well as the ability to implement distinct diffusion coefficients for each species.

This research documents verification of SEAWAT by benchmarking the code against six previously published numerical modeling, analytical, or laboratory problems. Results from the benchmark problems reveal that the following equations and/or processes have been implemented correctly in the code: (1) density-dependent flow due

to changes in heat and/or concentration of one or more species, (2) variations in viscosity from differences in temperature using multiple equations, and (3) diffusion of multiple species (including solute or heat). Results from the benchmark problems also show that SEAWAT can be used to simulate convective versus conductive transport of heat/energy through a porous medium. In the process of exploring the effects of viscosity on convection versus conduction, it is apparent that the critical Rayleigh number could change by implementing the variable viscosity mechanism.

In summary, the newest version of SEAWAT has been expanded to simulate liquids such as oil or water with concentrations from fresh to brine. Included in the new version is the ability to simulate the temperature and concentration effects on density and viscosity. This research shows how the expanded version of the code could be used to aid in solving multiple field problems such as water supply and waste disposal.

5.2 Using a linear method to quantify the worth of salinity and temperature data in a nonlinear variable-density model

Results from the method presented in this paper, though linear, provide a first step in showing that relative data contributions toward reducing predictive uncertainty could potentially be applicable to a nonlinear variable-density groundwater flow and transport model. The research here takes into account multiple, highly variable, parameter fields, in testing the linear applicability to a nonlinear model; however, the degree of nonlinearity of the numerical model is not defined. This research has shown how the linear method can be used in an underdetermined model (more parameters than observations). The analysis done in this study reveals how scientific information on the

aquifer system supplied by hydrogeologists (through the $C(\mathbf{p})$ matrix) could be used in modeling to guide additional data collection.

This dissertation shows how an innovative linear method provides similar results for quantifying the worth of data in a nonlinear model in regards to the relative rank of salinity and temperature observations. The relative ranking of the salinity observations employed in this study (in terms of their effectiveness in reducing the variance of the prediction of interest) was unchanged regardless of whether sensitivities were computed using uniform or heterogeneous hydraulic property fields. The locations of some of the more effective measurements for salinity varied from case to case. However, what remained constant were the locations of effective measurements relative to the location of the interface. In general, salinity measurements taken closer to the interface were most effective in reducing the predictive uncertainty of movement of the saltwater-freshwater interface. Overall, salinity data contributes more worth to reducing predictive uncertainty in interface movement than temperature data, with salinity data reducing uncertainty an order of magnitude more than temperature in most cases for this particular problem. However, if collecting temperature data to predict interface movement, an area where the change in temperature with distance is relatively sharp, in the warmest area beneath the surface, will be the best location to acquire the data.

The linear analysis is appealing because it only requires calculation of observation and prediction sensitivities to individual parameters based on the model; therefore, no calibration or field data are necessary. The linear analysis is also attractive because the computationally intensive model runs necessary for a nonlinear analysis are not required. However, caution must be taken before applying this linear method to other nonlinear

models. The linearity assumption likely would not hold up in certain models depending on the degree of nonlinearity. The author recommends future research to develop guidelines in application of this linear method to numerical models by quantifying the degree of nonlinearity in a numerical model in which the linear method would still apply.

5.3 Simulation of submarine groundwater discharge salinity and temperature variations: Implications for data collection

Variable-density groundwater flow models can be used to understand the complex nature of a coastal groundwater system. This research presents an original way to study the salinity, temperature, rate, and age of SGD. Modeling results show how the salinity, temperature, rate, and age of SGD are affected by the hydraulic character of the coastal system from the geological setting to the ocean stage. The results from this research show how this type of modeling analysis can be used to help guide data collection efforts for studies of SGD as well as understand the nature of the system, residence times of water, and potentially give insight to the amount of nutrients in the SGD.

This study shows how various types of data (salinity, water level, and temperature) can be used in model calibration and verification. It also shows that short-term tidal fluctuations, to longer-term seasonal fluctuations, can not only be observed in the data, but represented in a model and used to obtain important information about model parameters. Even though a model may be representative of a system, the model can still be developed, verified, and used to give insight into a complicated coastal system.

The modeling in this research reveals that aerial EM surveys are best conducted at low tide and when ocean stages are at a relative low. This is when the difference in salinities between the aquifer and ocean are greatest. Therefore, the results from an aerial survey could potentially be improved by including expected ocean stage variations for the specific target area as part of the data collection plan. An aerial survey using EM resistivity may or may not be successful depending upon the geology of the aquifer. An aquifer in direct hydraulic connection to the ocean may not have large enough salinity differences between the aquifer and ocean for an aerial survey to detect. Whereas, an aquifer that contains a low hydraulic conductivity layer of sediments across the ocean floor appears to have a large enough difference in salinity between the ocean and aquifer to enable likely detection by EM resistivity. If there is a fracture in the low conductivity layer, resulting in a submarine spring, the SGD across the ocean floor and at the spring may be high enough for detection by the aerial survey as long as the salinity differences between the aquifer and ocean are relatively high.

Thermal imagery data should be collected at low tide when SGD is relatively high and at a location where SGD rates would be large enough to reach the ocean surface and affect the temperature. In southern Florida, thermal imagery surveys are best conducted during the late summer or late winter when temperature differences between SGD and the ocean waters are the largest $\sim 3^{\circ}\text{C}$. During the spring and fall, SGD is about the same temperature as the ocean and would probably not be detected.

The success of a survey using thermal imagery can also be affected by the geology of the aquifer. When the aquifer is in direct hydraulic connection to the ocean a narrow zone of high discharge exists at the shoreline close to the surface. In this

environment, the temperature difference of $\sim 3^{\circ}\text{C}$ between the SGD and the ocean would probably be detected by an aerial survey using thermal imagery. If there is a low conductivity layer of marine sediments producing a wide zone of discharge across the sea floor and a decreased amount of SGD, thermal imagery will likely not work. However, if there is a submarine spring in this environment, it would likely be identified by thermal imagery as long as the spring exists in shallow waters, there is an increased amount of SGD (i.e., at low tide), and the temperature difference is greater than 0.08°C . If the submarine spring is too deep, thermal imagery will likely not detect the spring.

Modeling of variable-density systems that include the age of the water could potentially be used by geochemists and ecologists in the analysis of SGD groundwater residence times and nutrient transport. Simulations reveal the apparent age and residence time of SGD can be affected by the aquifer geology/marine sediments. The geology affects not only the amount of fresh SGD, but also the location of the interface and amount of recirculated seawater, which in turn affects the residence time of the SGD. An area with no marine sediments on the ocean floor (i.e., direct connection between the aquifer and ocean) could contain more nutrients because of the longer groundwater residence times, likely from an interface farther inland with longer flushing times. In areas where there are marine sediments that impede SGD, the amount of freshwater discharge and recirculated seawater is reduced, the interface is farther seaward, and the groundwater residence times are less. Therefore, the amount of nutrients discharged to the coastal system could be less.

Numerical modeling can help enhance knowledge of SGD and guide SGD data collection efforts by providing estimates of expected salinity, temperature, and age

variations. Aerial surveys using EM resistivity are more appropriate for some coastal environments, whereas, thermal imagery is likely more successful in others. Results from this research indicate that modeling of a coastal environment prior to data collection can reveal the potential for success using either type of aerial survey. This investigation also reveals that ignoring short-term temporal changes on the system, such as tides, could hinder modeling efforts to guide data collection. This modeling effort also shows that age can be simulated using SEAWAT, giving insight to groundwater residence times and potentially nutrient transport in SGD, which could aid geochemists and ecologists.

LIST OF REFERENCES

- Afify, A.A., 2007, Effects of Temperature-Dependent Viscosity with Soret and Dufour Numbers on Non-Darcy MHD Free Convective Heat and Mass Transfer Past a Vertical Surface Embedded in a Porous Medium. *Transport in Porous Media*, v. 66, p. 391-7401.
- Al-Maktoumi, A., Lockington, D.A., and Volker, R.E., 2007, SEAWAT 2000: modeling unstable flow and sensitivity to discretization levels and numerical schemes. *Hydrogeology Journal: Earth and Environmental Science*. DOI: 10.1007/s10040-007-0164-2.
- Anderson, M.P., 2005, Heat as a ground water tracer. *Ground Water*, v. 43, no. 6, p. 951-968.
- Aster, R.C., Borchers, B., and Thurber, C.H., 2005, *Parameter Estimation and Inverse Problems*. Elsevier Academic Press Publications, Burlington, MA.
- Ataie-Ashtiana, B., and Aghayi, M.M., 2006, A note on benchmarking of numerical models for density dependent flow in porous media: *Advances in Water Resources*, 29(2006), p. 1918-1923.
- Barry, D.A., Li, L., Stagnitti, F., and Parlange, J.Y., 1999, Submarine groundwater discharge and associated chemical input to a coastal sea. *Water Resources Research*, 35(11), p. 3253-3259.
- Becker, A., 1988, Airborne resistivity mapping. *IEEE Transactions on Antennas and Propagation*, v. 36, Issue 4, p. 557-562.
- Bejan, A., 1987, Convective heat transfer in porous media, in: S Kakac/ Shah R.K./ Aung W. (eds), *Handbook of Single-Phase Convective Heat Transfer*, Wiley, New York.
- Bayes, T., 1763/1958, *Studies in the History of Probability and Statistics: IX. Thomas Bayes' Essay Towards Solving a Problem in the Doctrine of Chances*, *Biometrika*, 45:296–315. (Bayes' essay in modernized notation)
- Beven, K. J., and Binley, A., 1992, The future of distributed models: model calibration and uncertainty prediction, *Hydrol. Process.*, 6, p. 279-298.
- Bird, R.B., Stewart, W.E., and Lightfoot, E.N., 2006, *Transport Phenomena* (2nd Edition). John Wiley & Sons, Inc., New York.
- Bokuniewicz, H., Buddemeier, R., Maxwell, B., and Smith, C., 2003, The typological approach to submarine ground-water discharge (SGD). *Biogeochemistry* 66, p. 145–158.

- Breier J. A., 2006, The impact of groundwater flows on estuaries, In *Aquifers of the Gulf Coast of Texas*, Report 365, Texas Water Development Board, Austin, Texas, p. 165-172.
- Broward County Department of Planning and Environmental Protection, 2000, Delineation of saltwater intrusion: Accessed on July 21, 2002, at <http://www.broward.org/moi00612.pdf>
- Byrne, M.J., 1999, Groundwater Nutrient Loading in Biscayne Bay, Biscayne National Park, Florida. A thesis submitted to Environmental Studies at Florida International University.
- Cable, J.E., Corbett, D.R., Shinn, E.A., Reich, C.D., Hickey, D.T., and Martin, J.B., 2003, Factors influencing ground water discharge measurements using seepage meters. IUGG 2003 Abstract. Retrieved on 8/17/2007 from: www.olympus.net/IAPSO/abstracts03/JSP03/02/016177-1.html.
- Camp, Dresser, and McKee, Inc., 1980, Prospect well field impact analysis: City of Fort Lauderdale, 96 pp.
- Carrera, J., Alcolea, A., Medina, A., Hidalgo, J., and Sooten, L.J., 2005, Inverse problem in hydrogeology. *Hydrogeology Journal*, 13:206–222, DOI 10.1007/s10040-004-0404-7.
- Carter, J.N., Ballester, P.J., Tavassoli, Z., and King, P.R., 2006, Our calibrated model has poor predictive value: An example from the petroleum industry. *Reliability Engineering and System Safety*, 91 (2006) p. 1373-1381.
- Castendyk, D.N., and Webster, J., 2004, The effects of groundwater on the physical limnology of a future pit lake predicted using Dyresm, Martha Mine, New Zealand. *Geological Society of America: Abstracts with Programs*, Vol. 36, No. 5, p. 466.
- Christensen, S., and Cooley, R.L., 1999, Evaluation of prediction intervals for expressing uncertainties in groundwater flow model predictions, *Water Resources Research*, 35(9), p. 2627–2640.
- Christensen, S., and Doherty, J. D., 2008, Predictive error dependencies when using pilot points and singular value decomposition in groundwater model calibration. *Advances in Water Resources*, 31(2008) p. 674-700.
- Constantz, J., Stewart, A.E., Niswonger, R., and Sarma, L., 2002, Analysis of temperature profiles for investigating stream losses beneath ephemeral channels: *Water Resources Research*, v. 38, no. 12, p. 52-1 to 52-13.
- Cooley, R. L., 2004, A theory for modeling ground-water flow in heterogeneous media, U.S. Geological Survey Professional Paper: 1679, 220 pp.

- Cooley, R.L. and Christensen, S., 2006, Bias and uncertainty in regression-calibrated models of groundwater flow in heterogeneous media, *Advances in Water Resources*, 29(5), p. 639-656.
- Cooper, H. H., Jr., 1959, A hypothesis concerning the dynamic balance of fresh water and salt water in a coastal aquifer. *Journal of Geophysical Research*. v. 64, p. 461-467.
- Cordier, E., and Goblet, P., 1991, Contribution to the analysis of the RIVM brine migration experiments. INTRAVAL level 1, Commissariat a l'Energie Atomique, Report LHM/RD/91/8, 12 pp.
- Dausman, A.M. and Langevin, C. D., 2005, Movement of the saltwater interface in the surficial aquifer system in response to hydrologic stresses and water-management practices, Broward County, Florida: U.S. Geological Survey Scientific Investigations Report 2004-5256.
- Diersch, H.J.G., and Kolditz, O., 2002, Variable-density flow and transport in porous media: Approaches and Challenges: *Advances in Water Resources*, v. 25, p. 899-944.
- Doherty, J., 2004, Model-Independent Parameter Estimation User Manual: 5th Edition, Watermark Numerical Computing.
- Doherty, J., 2007a, Addendum to the PEST Manual, Watermark Numerical Computing.
- Doherty, J., 2007b, Groundwater Data Utilities Part B: Program Descriptions, Watermark Numerical Computing.
- Draper, N. R., and Smith, H., 1981, *Applied Regression Analysis* (2nd ed.), 709 pp., John Wiley, New York.
- Elder, J.W., 1967, Transient convection in a porous medium. *Journal of Fluid Mechanics*, v. 27, no. 3, p. 609-623.
- Fetter, C. W., 1994, *Applied Hydrology*; Robert A. McConnin, Prentice Hall, Upper Saddle River, N. J., 691 pp.
- Finkl, C. W. and Krupa, S. L., 2003, Environmental impacts of coastal-plain activities on sandy beach systems: hazards, perception and mitigation. *Journal of Coastal Research*, 35, p. 132-150.
- Fish, J.E., 1988, Hydrogeology, aquifer characteristics, and ground-water flow of the surficial aquifer system, Broward County, Florida: U.S. Geological Survey Water-Resources Investigations Report 87-4034, 92 pp.

- Fitterman, D.V., and Deszcz-Pan, M., 1998, Helicopter EM mapping of saltwater intrusion in Everglades National Park, Florida: *Exploration Geophysics*, v. 29, p. 240-243.
- Fitterman, D.V., and Deszcz-Pan, 2002a, Helicopter electromagnetic mapping of water quality in coastal aquifers of south Florida. 17th Salt Water Intrusion Meeting, Delft, The Netherlands, 6-12 May, 2002.
- Fitterman, D.V., and Deszcz-Pan, M., 2002b, Helicopter electromagnetic data from Everglades National Park and surrounding areas: Collected 9-14 December 1994: U.S. Geological Survey Open-File Report 02-101 (on CD-ROM).
- Frolovic, P., and De Schepper, H., 2000, Numerical modeling of convection dominated transport coupled with density driven flow in porous media, *Advances in Water Resources*, 24 (1), p. 63-72.
- Gary, J., Kassory, D.R., Tadjeran, H. and Zebib, A., 1982, The effect of significant viscosity variation on convective heat transport in water-saturated porous media, *Journal of Fluid Mechanics*, v. 117, p.233–249.
- Ghyben, W.B., 1888, Nota in verband met de voorgenomen putboring nabij Amsterdam, *Tijdschrift van het Koninklijk Inst. Van Ing.*
- Glover, R.E., 1959, The pattern of fresh-water flow in a coastal aquifer. *Journal of Geophysical Research*. v. 64, p. 457-460.
- Goode, D. J., 1996, Direct simulation of groundwater age, *Water Resources Research*, 32(2): p. 289-296.
- Guo, W., and Bennett, G.D., 1998, Simulation of saline/fresh water flows using MODFLOW, in Poeter, E., and others, MODFLOW '98 Conference, Golden, Colorado, 1998, Proceedings: Golden, Colorado, v. 1, p. 267-274.
- Guo, W., and Langevin, C.D., 2002, User's guide to SEAWAT: A computer program for simulation of three-dimensional variable-density ground-water flow: U.S. Geological Survey Techniques of Water-Resources Investigations, book 6, chap. A7, 77 pp.
- Guo, Z., and Zhao, T.S., 2005, Lattice Boltzmann simulation of natural convection with temperature-dependent viscosity in a porous cavity: *Progress in Computational Fluid Dynamics* v. 5, nos. 1/2: p. 110-117.
- Harbaugh, A.W., Banta, E.R., Hill, M.C., and McDonald, M.G., 2000, MODFLOW-2000, the U.S. Geological Survey modular ground-water model—User guide to modularization concepts and the ground-water flow process: U.S. Geological Survey Open-File Report 00-92, 121 pp.

- Henry, H.R., 1964, Effects of dispersion on salt encroachment in coastal aquifers, in Cooper, H.H., Sea Water in Coastal Aquifers: U.S. Geological Survey Water-Supply Paper 1613-C, p. C71-C84.
- Henry, H.R., and Hilleke, J.B., 1972, Exploration of multiphase fluid flow in a saline aquifer system affected by geothermal heating: University of Alabama Bureau of Engineering Research Contract No. 14-08-0001-12681, submitted to U.S. Geological Survey, Washington D.C., 105 pp.
- Herzberg, A., 1901, Die Wasserversorgung einiger nordseebader: J. Gasbeleucht. Wasserversorg., 44, p. 815-819.
- Hill, M.C., and Tiedeman, C.R., 2007, Effective Groundwater Model Calibration: With Analysis of Data, Sensitivities, Predictions, and Uncertainty. John Wiley and Sons, Inc., Hoboken, New Jersey.
- Holzbecher, E.O., 1998, Modeling density-driven flow in porous media: principles, numerics, software: Berlin Heidelberg New York, Springer-Verlag, 286 pp.
- Horne, R.N., 1975, Transient Effects in Geothermal Convective Systems, Phd. Thesis, University of Auckland.
- Horton, C.W., and Rogers Jr., F.T., 1945, Convection currents in a porous medium. Journal of Applied Physics. 16:367-70.
- Hubbert, M.K., 1940, The theory of ground-water motion. Journal of Geology. v. 48, p. 785-944.
- Hughes, J.D., and Sanford, W.E., 2004, SUTRA-MS a version of SUTRA modified to simulate heat and multiple-solute transport: U.S. Geological Survey Open-File Report 2004-1207, 141 pp.
- Hughes, J.D., Sanford, W.E., and Vacher, H.L., 2005, Numerical simulation of double-diffusive finger convection, Water Resources Research, v. 41, 16 pp.
- Hunt, R. J., Doherty, J. E., and Tonkin, M. J., 2007, Are models too simple? Arguments for increased parameterization. Ground Water, 45(3), p. 254-262.
- Kim, J. Park, Y., and Harmon, T.C., 2005, Real-time model parameter estimation for analyzing transport in porous media: Ground Water Monitoring & Remediation 25, p. 78-86.
- Kipp, K.L., Jr., 1987, HST3D—A computer code for simulation of heat and solute transport in three-dimensional ground-water flow systems: U.S. Geological Survey Water-Resources Investigations Report 86-4095, 517 pp.

- Kipp, K.L., Jr., 1997, HST3D—Guide to the Revised Heat and Solute Transport Simulator: HST3D—Version2: U.S. Geological Survey Water-Resources Investigations Report 97-4157, 149 pp.
- Koch, K.R., 1987, Parameter Estimation and Hypothesis Testing in Linear Models. Berlin: Springer-Verlag.
- Kohout, F.A., 1965, A hypothesis concerning cyclic flow of salt water related to geothermal heating in the Floridan Aquifer: N.Y. Acad. Sci. Trans., ser. 2, v. 28, p. 249-271.
- Kohout, F.A., 1966, Submarine Springs: A Neglected Phenomenon of Coastal Hydrology. Central Treaty Organization's Symposium on Hydrology and Water Resources Development, February 5-12, 1966.
- Konikow, L.F., and Bredehoeft, J.D., 1992, Ground-water models cannot be validated. *Advances in Water Resources*, 15(1992), p. 75-83.
- Konikow, L.F., and Reilly, T.W., 1999, Seawater intrusion in the United States, in Bear, A.H., and others (eds), *Seawater intrusion in coastal aquifers-Concepts, methods, and practices*: Dordrecht, Kluwer Academic Publishers, p. 463-506.
- Kontar, E.A., and Ozorovich, Y.R., 2006, Geo-electromagnetic survey of the fresh/salt water interface in the coastal southeastern Sicily. *Continental Shelf Research* 26: 843-851.
- Langevin, C.D., 2001, Simulation of Ground-Water Discharge to Biscayne Bay, Southeastern Florida. Water-Resources Investigations Report 00-4251.
- Langevin, C. D., 2003, Simulation of submarine ground water discharge to a marine estuary: Biscayne Bay, Florida. *Ground Water* 41(6), p. 758-771.
- Langevin, C.D., Shoemaker, W.B., and Guo, W., 2003, MODFLOW-2000, the U.S. Geological Survey Modular Ground-Water Model—Documentation of the SEAWAT-2000 Version with the Variable-Density Flow Process (VDF) and the Integrated MT3DMS Transport Process (IMT): U.S. Geological Survey Open-File Report 03-426, 43 pp.
- Langevin, C.D., Thorne, D.T., Jr., Dausman, A.M., Sukop, M.C., and Guo, W., 2008, SEAWAT Version 4: A Computer Program for Simulation of Multi-Species Solute and Heat Transport: U.S. Geological Survey Techniques and Methods Book 6, Chapter A22, 39 pp.
- Lapwood, E.R., 1948, Convection of a fluid in a porous medium, *Proc. Cambridge Phil. Soc.* A 225, p. 508-521.

- Laroche, J., Nuzzi, R., Waters, R., Wyman, K., Falkowski, P. G., and Wallace, D. W. R., 1997, Brown tide blooms in Long Island's coastal waters linked to interannual variability in groundwater flow: *Global Change Biology*, v. 3, p. 397–410.
- Lerner, D.N., and Ockelford, A., 2006, Assessing the origin and age of groundwater with depth- a modeling approach. *Geophysical Research Abstracts*, Vol. 8, 06771. SRef-ID: 1607-7962/gra/EGU06-A-06771.
- Martin, R.J., Bender, S.F., Gaulke, S.W., and Wallace, J., 2001, Simulation of groundwater flow and heat transport on Grand Cayman Island. In: Seo, S., Poeter, E.P., Zheng, C. Poeter, O., (Eds) *MODFLOW 2001 and Other Modeling Odysseys*, Conference Proceedings, International Ground Water Modeling Center, Colorado School of Mines, Golden, CO. p. 776-782.
- Miyaoka, K., 2007, Seasonal changes in the groundwater-seawater interaction and its relation to submarine groundwater discharge, Ise Bay, Japan. In Sanford, W., Langevin, C.D., Polemio, M., and Povinec, P., eds., 2007, *A new focus on groundwater-seawater interactions: IAHS Publication 312*, Oxfordshire, United Kingdom, p. 68-74.
- McDonald, M. G. and Harbaugh, A.W., 1988, A modular three-dimensional finite-difference ground-water flow model. *US Geol. Survey Techniques of Water Resources Investigations*, Book 6.
- Merritt, M.L., 1996, Assessment of saltwater intrusion in southern coastal Broward County, Florida: *U.S. Geological Survey Water-Resources Investigations Report 96-4221*, 133 pp.
- Michael, H. A., Mulligan, A. E. and Harvey, C. F., 2005, Seasonal oscillations in water exchange between aquifers and the coastal ocean. *Nature*, 436(6054), p. 1145-8.
- Moore, C., and Doherty, J. E., 2005, Role of the calibration process in reducing model predictive error. *Water Resources Research*, 41(5), W05050.
- Moore, C., and Doherty, J. E., 2006, The cost of uniqueness in groundwater model calibration. *Advances in Water Resources*, 29(4), p. 605-623.
- Moore, W.S., 1996, Large groundwater inputs to coastal waters revealed by 226Ra enrichments. *Nature* 380:612–614.
- Moore, W.S., 1999, The subterranean estuary: a reaction zone of ground water and sea water, *Mar. Chem.* 65 (1999), p. 111–125.
- Moore, W.S., Blanton, J.O., and Joye, S.B., 2006, Estimates of flushing times, submarine groundwater discharge, and nutrient fluxes to Okatee Estuary, South Carolina. *Journal of Geophysical Research*, Vol. 111, C09006, 14 pp.

- Moore, W.S., and Church, T.M., 1996, Submarine groundwater discharge – Moore and Church reply, *Nature* 382 (1996), p. 122.
- Mulligan, A.E., and Charette, M.A., 2006, Intercomparison of submarine groundwater discharge estimates from a sandy unconfined aquifer. *Journal of Hydrology*, 327: 411-425.
- Nield, D.A., and Bejan, A., 1999, *Convection in Porous Media* (2d ed): New York, Springer-Verlag.
- Nusselt, W., 1944, *Technische Thermodynamik II (Theorie der Wärmekraftmaschinen)*, Sammlung Goschen, Bd. 1151, 144 pp.
- Oberdorfer, J.A., 2003, Hydrogeologic modeling of submarine groundwater discharge: comparison to other quantitative methods. *Biogeochemistry*, 66: 159-169.
- Parker, G.G., Ferguson, G.E., Love, S.K., and others, 1955, *Water resources of southeastern Florida: Geological Survey Water-Supply Paper 1255*, 965 pp.
- Pasa, G., and Titaud, O., 2005, A Class of Viscosity Profiles for Oil Displacement in Porous Media or Hele-Shaw Cell. *Transport in Porous Media*, v. 3, No. 3, p. 269-286.
- Pawlowski, J., 1991, *Veränderliche Stoffgrößen in der Ähnlichkeitstheorie*, Satté+Sauerländer, Frankfurt a. M., 108 pp.
- Prasad, A., and Simmons, C.T., 2003, Unstable density-driven flow in heterogeneous porous media: A stochastic study of the Elder [1967b] “short heater” problem: *Water Resources Research*, 39(1), 1007.
- Prasad, A., and Simmons, C.T., 2005, Using quantitative indicators to evaluate results from variable-density ground-water flow models: *Hydrogeology Journal* v13, p. 905-914.
- Price, R.M., Top, Z., Happell, J.D., and Swart, P.K., 2003, Use of tritium and helium to define groundwater flow conditions in Everglades National Park. *Water Resources Research*, 39(9), 1267.
- Price, R.M., Swart, P.K., and Fourqurean, J.W., 2006, Coastal groundwater discharge – an additional source of phosphorus for the oligotrophic wetlands of the Everglades: *Hydrobiologia* 569:23-36.
- Pringle, S.E., Glass, R.J., and Cooper, C.A., 2002, Double-diffusive finger convection in a Hele-Shaw cell—An experiment exploring the evolution of concentration fields, length scales and mass transfer: *Transport in Porous Media*, V. 47, no. 2, p. 195-214.

- Proni, J.R., Casanova, H.L., and Featherstone, C.M., 2006, Detection, mapping, and characterization of groundwater discharges to Biscayne Bay, South Florida Water Management District, Contract C-15870: Expanded Final Report.
- Ramsing, N., and Gundersen, J., 2007, Seawater and Gases: Tabulated physical parameters of interest to people working with microsensors in marine systems. Accessed on September 15, 2008 on: <http://www.unisense.com/Default.aspx?ID=117>.
- Rayleigh, Lord, 1916, On convection currents in a horizontal layer of fluid when the higher temperature is on the under side. *Philos Mag.*, Vol. XXXII, p. 529-546.
- Reilly, T.E., Plummer, L.N., Phillips, P.J., and Busenberg, E., 1994, The use of simulation and multiple environmental tracers to quantify flow in a shallow aquifer. *Water Resources Research*, 30(2), p. 421-433.
- Robinson, C., Givves, B., and Li, L., 2006a, Driving mechanisms for groundwater flow and salt transport in a subterranean estuary. *Geophysical Research Letters*, Vol. 33, L03402.
- Robinson, C., Li, L., and Barry, D.A., 2006b, Effect of tidal forcing on a subterranean estuary. *Advances in Water Resources*. Doi: 10.1016/j.advwatres.2006.07.006.
- Sanford, W.E., and Konikow, L.F., 1985, A two-constituent solute-transport model for ground water having variable density: U.S. Geological Survey Water-Resources Investigations Report 85-4279, 88 pp.
- Segol, G., Pinder, G.F., and Gray, W.G., 1975, A Galerkin-finite element technique for calculating the transient position of the saltwater front. *Water Resources Research*, 11(2), p. 343-347.
- Sengpiel, K.P., Siemon, B., 1998. Examples of 1-D inversion of multifrequency HEM data from 3-D resistivity distributions. *Exploration Geophysics* 29, 133-141.
- Shaban, A., Khawlie, M., Abdallah, C., and Faour, G., 2005, Geologic controls of submarine groundwater discharge: application of remote sensing to north Lebanon. *Environmental Geology*, 47: 512-522.
- Shellenbarger, G.G., Monismith, S.G., Genin, A., and Paytan, A., 2006, The importance of submarine groundwater discharge to the nearshore nutrient supply in the Gulf of Aqaba (Israel). *Limnol. Oceanogr.*, 51(4), p. 1876-1886.
- Shoemaker, W.B., and Edwards, K.M., 2003, Potential for saltwater intrusion into the lower Tamiami aquifer near Bonita Springs, southwestern Florida: U.S. Geological Survey Water-Resources Investigations Report 03-4262, 74 pp.

- Simpson, M.J., and Clement, T.P., 2004, Improving the worthiness of the Henry problem as a benchmark for density-dependent ground-water flow models. *Water Resources Research*, 40(1), 1504.
- Smith, L. and Zawadski, W., 2003, A hydrogeologic model of submarine groundwater discharge: Florida intercomparison experiment. *Biogeochemistry* 66, p. 95–110.
- Stonestrom, D.A., and Blasch, K.W., 2003, Appendix A, Determining temperature and thermal properties for heat-based studies of surface-water ground-water interaction, in Stonestrom, D.A., and Constantz, J., eds., *Heat as a tool for studying the movement of ground water near streams: U.S. Geological Survey Circular 1260*, p. 73-80.
- Strack, O.D.L., 1995, A Dupuit-Forchheimer model for three-dimensional flow with variable density: *Water Resources Investigation*, v. 12, p. 3,007-3,017.
- Stuyfzand, P.J., 1989, An accurate relatively simple calculation of the saturation index of calcite for fresh to salt water. *Journal of Hydrology*, v. 105, p. 95-107.
- Swarzenski, P.W., Bratton, J.F., and Crusius, J., 2004a, Submarine ground-water discharge and its role in coastal processes and ecosystem, U.S. Geological Survey Open File Report 2004-1226.
- Swarzenski, P.W., Burnett, B., Reich, C., Dulaiova, H., Peterson, R., and Meunier, J., 2004b, Novel geophysical and geochemical techniques used to study submarine groundwater discharge in Biscayne Bay, Florida. U.S. Geological Survey Fact Sheet 2004-3117.
- Swarzenski, P.W., Kruse, S., Reich, C., and Swarzenski, W.V., 2007, Multi-channel resistivity investigations of the freshwater-saltwater interface: a new tool to study an old problem, in Sanford, W., Langevin, C.D., Polemio, M., and Povinec, P.I., eds., 2007, *A new focus on groundwater-seawater interactions: IAHS Publication 312*, Oxfordshire, United Kingdom, p. 272-280.
- Taniguchi, M., Burnett, W. C., Cable, J. E. and Turner, J. V., 2002, Investigation of submarine groundwater discharge. *Hydrol. Processes* 16, p. 2115–2129.
- Taniguchi, M., Turner, J.V., and Smith, A.J., 2003, Evaluations of groundwater discharge rates from subsurface temperature in Cockburn Sound, Western Australia. *Biogeochemistry* 66: 111-124.
- Thiesen/ Scheel/ Distelhorst, 1900, *Wiss. Abhandlungen phys. techn. Reichsanstalt* 3, 67.
- Thorne, D., Langevin, C.D., and Sukop, M.C., 2006, Addition of simultaneous heat and solute transport and variable fluid viscosity to SEAWAT: *Computer and Geosciences* v. 32, p. 1758-1768.

- Thorne, D.T. and M.C. Sukop, 2004, Lattice Boltzmann model for the Elder problem, *in* Computational Methods in Water Resources, Proceedings of the XVth International Conference on Computational Methods in Water Resources (CMWR XV), June 13-17, 2004, Chapel Hill, NC, USA. C.T. Miller, M.W. Farthing, W.G. Gray, and G. F. Pinder Eds. Elsevier, Amsterdam.
- Tilton, L.W., and Taylor, J.K., 1937, Accurate representation of the refractivity and density of distilled water as a function of temperature. *Journal of Research Nat. Bur. Stand.* 18, Paper RP971, p. 205-214.
- Tonkin, M. and Doherty, J., 2005, A hybrid regularized inversion methodology for highly parameterized models. *Water Resources Research*, 41(2005), W10412, doi:10.1029/2005WR003995.
- Tonkin, M. J., and Doherty, J. E., 2008, Calibration-constrained Monte Carlo analysis of highly-parameterized models using subspace techniques. *Water Resources Research* (submitted).
- Tonkin, M. J., Doherty, J. E., and Moore, C., 2007, Efficient nonlinear predictive error variance for highly parameterized models. *Water Resources Research*, 43, W07429.
- Tonkin, M.J., Tiedeman C. R., Ely D.M., and Hill M.C., 2007, OPR-PPR, a Computer Program for Assessing Data Importance to Model Predictions Using Linear Statistics: Reston Virginia, U.S. Geological Survey Techniques and Methods Report TM-6E2, 115 pp.
- Vecchia, A.V. and Cooley, R.L., 1987, Simultaneous confidence and prediction intervals for non-linear regression models with application to a groundwater flow model, *Water Resources Research*, 23(7), p. 1237-1250.
- Voss, C.I., 1984, A finite-element simulation model for saturated-unsaturated, fluid-density-dependent ground-water flow with energy transport or chemically-reactive single-species solute transport: U.S. Geological Survey Water-Resources Investigations Report 84-4369, 409 pp.
- Voss, C.I., 1984, A finite-element simulation model for saturated-unsaturated, fluid-density-dependent ground-water flow with energy transport or chemically-reactive single-species solute transport: U.S. Geological Survey Water-Resources Investigations Report, 84-4369, 409 pp.
- Voss, C.I., and Souza, W.R., 1987, Variable density flow and solute transport simulation of regional aquifers containing a narrow freshwater-saltwater transition zone: *Water Resources Research*, 23(10), p. 1851-1866.

- Walker, G.R., and Cook, P.G., 1991, The importance of considering diffusion when using carbon-14 to estimate groundwater recharge to an unconfined aquifer. *Journal of Hydrology*, 128, p. 41-48.
- Weatherhill, D., Simmons, C.T., Voss, C.E., and Robinson, N.I., 2004, Testing density-dependent ground-water models: two-dimensional steady state unstable convection in infinite, finite and inclined porous layers: *Advances in Water Resources*, 27(2004), p. 547-562.
- Weber, J.E., 1975, The boundary layer regime for convection in a vertical porous layer. *International Journal of Heat Mass Transfer*, v. 18, p.569–573.
- Weinstein, Y., Shalem, Y., Burnett, W.C., Swarzenski, P.W. and Herut, B., 2007, Temporal variability of submarine groundwater discharge: assessments via radon and seep meters, the southern Carmel Coast, Israel. In Sanford, W., Langevin, C.D., Polemio, M., and Povinec, P., eds. A new focus on groundwater-seawater interactions: IAHS Publication 312, Oxfordshire, United Kingdom, p. 125-133.
- Weiss, M., Kruse, S., Burnett, W. C., Chanton, J., Greenwood, W., Murray, M., Peterson, R. and Swarzenski, P., 2005, Evaluation of geophysical and thermal methods for detecting submarine groundwater discharge (SGD) in the Suwannee River Estuary. American Geophysical Union, Fall Meeting 2005, abstract #H43F-0554.
- Wilson, A. M., 2005, Fresh and saline groundwater discharge to the ocean: a regional perspective. *Water Resources Research* 41(2), p. 1–11.
- Wooding, R.A., 1957, Steady state free thermal convection of liquid in a saturated permeable medium. *Journal of Fluid Mechanics*, vol. 13, p. 129-144.
- Younger, P.L., 1996, Submarine groundwater discharge. *Nature* 382:121–122.
- Zektser, I.S., Ivanov, V.A., Meskheteli, A.V., 1973, The problem of direct groundwater discharge to the Seas. *J Hydrol* 20:1–36.
- Zheng, C., 1990, MT3D: A modular three-dimensional transport model for simulation of advection, dispersion and chemical reactions of contaminants in groundwater systems. Report to the US Environmental Protection Agency, Ada, Oklahoma, USA.
- Zheng, C., and Wang, P.P., 1999, MT3DMS—A modular three-dimensional multispecies transport model for simulation of advection, dispersion and chemical reactions of contaminants in ground-water systems; documentation and user's guide: U.S. Army Corps of Engineers Contract Report SERDP-99-1.
- Zheng, C., 2006, MT3DMS v5.2 Supplemental user's guide: Technical Report to the U.S. Army Engineer Research and Development Center, Department of Geological Sciences, University of Alabama, 24 pp.

Zimmerman, D. A., 1998, A comparison of seven geostatistically based inverse approaches to estimate transmissivities for modeling advective transport by groundwater flow. *Water Resources Research* 34(6), p. 1373–1414.

VITA

ALYSSA MARIE DAUSMAN

1974	Born, Jackson, Mississippi
1996	B.S., Geology Tulane University New Orleans, Louisiana
2000	M.S., Geology University of New Orleans New Orleans, Louisiana
2000-2008	Hydrologist U.S. Geological Survey Ft. Lauderdale, Florida

PUBLICATIONS AND PRESENTATIONS

Dausman, A.M., Doherty, J., Langevin, C.D., and Sukop, M.C. (2008) Quantifying Data Contributions toward Reducing Predictive Uncertainty in a Variable-Density Flow and Solute/Heat Transport Model. Conference paper published in *MODFLOW and More: Ground Water and Public Policy*.

Dausman, A.M., Langevin, C.D., Sukop, M.C., and Walsh, V. (2008) Saltwater/Freshwater Interface Movement in Response to Deep-Well Injection in a Coastal Aquifer. Conference paper published in the *Program and Proceedings of the 20th Salt Water Intrusion Meeting*.

La Licata, I., Langevin, C. D., Dausman, A.M., and Alberti, L. (2008) Tidal Effects on Transient Dispersion of Simulated Contaminant Concentrations in Coastal Aquifers. Conference paper published in the *Program and Proceedings of the 20th Salt Water Intrusion Meeting*.

Langevin, C.D., Thorne, D.T., Jr., Dausman, A.M., Sukop, M.C., and Guo, Weixing (2008) SEAWAT Version 4: A Computer Program for Simulation of Multi-Species Solute and Heat Transport: U.S. Geological Survey Techniques and Methods Book 6, Chapter A22, 39 p.

Dausman, A.M., Langevin, C.D., and Sukop, M.C. (2007) Simulation of submarine groundwater discharge salinity and temperature variations: implications for remote detection. In Sanford, W., Langevin, C.D., Polemio, M., and Povinec, P., eds., 2007, A new focus on groundwater-seawater interactions: IAHS Publication 312, Oxfordshire, United Kingdom, p. 272-280.

- La Licata, I., Langevin, C.D., Dausman, A.M. (2007) Effect of tidal fluctuations on contaminant transfer to the ocean. In Sanford, W., Langevin, C.D., Polemio, M., and Povinec, P., eds., 2007, A new focus on groundwater-seawater interactions: IAHS Publication 312, Oxfordshire, United Kingdom, p. 334-341.
- Dausman, A.M., Langevin, C.D., Doherty, J., Sukop, M.C., and Walsh, V. (2007) A Unique Approach to Calibrating a Variable-Density Flow and Transport Model. GSA, Vol. 39, No. 6. ISSN 0016-7592.
- Dausman, A.M., C.D. Langevin, M.C. Sukop, and Walsh, V. (2006) Development and Calibration of a Variable-Density Numerical Model of a Deep-well Injection Site near the Southeastern Florida Coast, Eos Trans. AGU, 87(52), Fall Meet. Suppl., Abstract H33D.
- Dausman, A.M., Langevin, C.D., Walsh, V., and Sukop, M.C. (2006) Modeling the Potential for Plume Migration from a Deep Well Injection Site. Abstract Book of the 2006 Ground Water Summit. National Ground Water Association.
- Dausman, Alyssa and Langevin, Christian. (2005) Movement of the saltwater interface in the Surficial Aquifer System in response to hydrologic stresses and water-management practices, Broward County, Florida: USGS Scientific Investigations Report: SIR 2004-5256.
- Langevin, C. and Dausman, A. (2005) Numerical simulation of saltwater intrusion in response to sea-level rise: In Proceedings of the Water & Environmental Resources Congress 2005—Impacts of Global Climate Change, Anchorage, Alaska.
- Dausman, A.M., and Langevin, C.D. (2003) Relationship among water levels, canal stage and saltwater intrusion, Southeastern Florida, USA. In Proceedings of the Second International Conference on Saltwater Intrusion and Coastal Aquifers—Monitoring, Modeling, and Management. Merida, Mexico, March 27 – April 2, 2003.
- Easley, D.H., Gaubert, A., Dausman, A., and Stoessell, R.K. (2003) Modeling of Salinity and Temperature Effects upon Ground Water in the Surficial Carbonate Aquifer, Yucatan Peninsula, Mexico. In Proceedings of the Second International Conference on Saltwater Intrusion and Coastal Aquifers—Monitoring, Modeling, and Management. Merida, Mexico, March 27 – April 2, 2003.
- Dausman, A.M., Easley, D.H., and Stoessell, R.K. (2002) Ground Water Model of the Northeastern Yucatan Peninsula, Mexico. American Water Resources Association: Annual Water Resources Conference., extended abstract.
- Dausman, A.M., and Langevin, C.D. (2002) Representing hydrodynamic dispersion in saltwater intrusion models of different temporal scales: American Water Resources Association. Spring Specialty Conference: Coastal Water Resources, extended abstract.